WAGENINGEN UNIVERSITY & RESEARCH CENTRE | DELTARES GROUNDWATER MANAGEMENT

Which input to care about?

A sensitivity analysis in variable density groundwater flow modeling

MIEKE HULSHOF

UTRECHT - WAGENINGEN, AUGUST 2013

Which input to care about?

A sensitivity analysis in variable density groundwater flow modeling

By *Mieke Hulshof*
Student Registration Number: 870206-376-130

Code HWM 80436

Master Thesis Hydrology and Quantitative Water Management submitted in partial fulfillment of the degree of Master of Science in Hydrology and Water Quality at Wageningen University, The Netherlands.

Supervision & Examination:
Ph.D. G.M.C.M. Janssen, Deltares
Dr. ir. G.H.P. Oude Essink, Deltares
Ing. G. Bier, Wageningen University and Research Centre
Drs. P.J.J.F. Torfs, Wageningen University and Research Centre

Utrecht-Wageningen, August 2013

“a work of fiction”
Nancy Cartwright

PREFACE

The present report is submitted in partial fulfillment of the degree of Master of Science in Hydrology and Water Quality at Wageningen University, and is the result of eight months of research at Deltares' Groundwater Management department in Utrecht.

It was a challenging research. In the beginning, I had no clue. Peclet? Neumann? Courant? Variable density groundwater flow modeling at Deltares: for me, it was just a leap of faith. However, in retrospective, it was a right one. It was great to get the opportunity to delve into the fresh-salt physics, to discover modelling by trial and error and to experiment the creative and innovative environment at Deltares. Therefore, I also hope that, although it was not always easy to combine fundamental research (University) with the request for practical output (Deltares), the results are to the contentment of all and that they will provide some useful handles in future studies.

Though this is an individual thesis, it is by no means an individual achievement; during the past eight months many people contributed to and supported its development. I want to thank all of them here. First, I want to thank my supervisors at Deltares; Gijs Janssen for his practical advices and unconditional support, and Gu Oude Essink for the possibility to join his fresh-salt group and for the elaborated and critical, though always constructive, feedback. A special thanks also to Paul Torfs and George Bier (Wageningen University and Research Centre). Besides providing me with lots of tips and tricks and very detailed feedback, it was only thanks to their flexibility that it was possible for me to hand in this report in time. Thanks also for the many interesting in-depth discussions we had on the reliability, validity and value of groundwater modelling in general. Last, but not least, thanks to all others that in some way contributed to this assignment; be it for providing me with interesting books and articles, having fruitful discussions, helping me out with software issues, listening to my thesis-complaints, having fun, or just for making me feel welcome in Utrecht and Wageningen

Dear reader, I hope you will find in this report what you are looking for. Enjoy reading!

Mieke Hulshof

Utrecht-Wageningen, The Netherlands
August 2013

CONTENTS

LIST OF FIGURES

LIST OF TABLES

ABSTRACT

The Waterdunen variable density groundwater flow model simulates a fresh-salt coastal groundwater system in Zeeland, The Netherlands. A sensitivity analysis on physical and numerical parameters was performed to provide modellers valuable information on the parameters to prioritize when model accuracy is to be improved and resources (e.g. time and budget) are limited. However, this research shows there exists no clear-cut list of 'priority parameters'; the parameters to focus on depend on the location and output the modeller is interested in. However, the analysis does shine a light on the locations that are, in general, most sensitive to changes in the parameterization and the type of response the parameters induce on the model output. Regarding the location, the study shows that the 1km-band along the lateral model boundaries, the shoreline, the vicinity of rivers & ditches, the bottom & edges of large freshwater lenses and the sandy creek ridges are most influenced by parameter adjustments. Besides, it turns out that there are parameters that have an overall negligible effect on the model output, parameters to which the output shows a monotone response and parameters that do not change the model output anymore above or below a certain threshold value. In addition, it is shown that because of difficulties to convert electrical conductivities into chloride concentrations and the use of a threshold value it is not straightforward to use freshwater lens thickness to compare modeled with observed values. Altogether, solute-transport adds a lot of extra complexity to the modeling of groundwater flow because of, amongst others, the heterogeneity of the chloride field, the limited amount of measurements and the difference in time scales regulating groundwater flow and solute-transport.

ABBREVIATIONS & SYMBOLS

AHN	Algemeen Hoogtebestand Nederland (Dutch surface level database)
CFL-Condition	Courant-Friedrichs-Lewy Condition
ECPT	Electrical Cone Penetration Test GHB = General Head Boundary
FDA	Finite Differences Approach
MAE	Mean Absolute Error
MOC	Method-of-Characteristics
NAP	Normaal Amsterdams Peil, Dutch ordinance stratum, corresponds to mean sea level (m)
RDS	Rijksdriehoekcoördinaten, Dutch Cartesian coordinate system
RMSE	Root Mean Square Error
TOP10-database	digital TOPographic database
TDS	Total amount of Dissolved Solids
tfwl	Freshwater lens thickness (m)
pers. comm.	Personal communication

$V_i = average\ effective\ pore\ groundwater\ velocity\ (LT^{-1})$
$V_x, V_y, V_z = average\ effective\ pore\ groundwater\ velocity\ in\ the\ x, y\ and\ z\ directions\ (LT^{-1})$
$C^*_{j,i,k} = averaged\ volumetric\ chloride\ concentration\ \ (ML^{-3})$
$x_i = Cartesian\ coordinates\ (L).$
$\Delta x, \Delta y, \Delta z = cell\ dimensions\ in\ the\ x, y\ and\ z\ directions\ (L).$
$\gamma = cell\ fraction\ that\ particles\ are\ allowed\ to\ travel\ within\ one\ time\ step\ (-)$
$D_{xx}, D_{yy}, D_{zz} = coefficients\ of\ hydrodynamic\ dispersion\ in\ the\ x, y, z\ directions\ (L^2T^{-1})$
$COND = conductance\ (L^2T^{-1}).$
$q_i = Darcian\ specific\ discharge\ (LT^{-1})$
$q_x, q_y, q_z = Darcian\ specific\ discharges\ along\ the\ x, y\ and\ z\ coordinate\ axes\ (LT^{-1})$
$\Delta x_i = dimensions\ grid\ block\ in\ the\ ith\ direction\ (L)$
$\Delta t = duration\ of\ the\ solute\ time\ step\ (T)$
$V_i = effective\ pore\ groundwater\ velocity\ in\ direction\ x_i (LT^{-1})$
$\varepsilon = effective\ porosity\ of\ the\ medium\ (-).$
$z = elevation\ head\ (L)$
$\phi_f = equivalent\ freshwater\ head\ (L)$
$\rho_f = fresh\ groundwater\ density\ (1\ 000\ kg/m^3)\ (ML^{-3})$
$\rho_i = groundwater\ density\ (ML^{-3})$
$D_{ij} = hydrodynamic\ dispersion\ coefficient\ (L^2T^{-1})$
$D_h = hydrodynamic\ dispersion\ coefficient\ (L^2T^{-1})$
$K_{xx}, K_{yy}, K_{zz} = \ hydraulic\ conductivity\ along\ the\ x, y\ and\ z\ coordinate\ axes\ (LT^{-1})$
$K_{ij} = \ hydraulic\ conductivity\ of\ the\ porous\ media\ (LT^{-1})$
$H = hydraulic\ head\ (L).$
$\overline{K}_{xx}, \overline{K}_{yy}, \overline{K}_{zz} = \ interblock\ hydraulic\ conductivity\ in\ the\ x, y\ and\ z\ directions\ (LT^{-1})$
$C^t_{j,i,k} = initial\ volumetric\ chloride\ concentration\ \ (ML^{-3})$
$L = length\ of\ the\ ditch\ or\ river\ within\ the\ cell\ (L)$
$D_L, D_{Th}, D_{Tv} = longitudinal, transversal\ horizontal\ and\ transversal\ vertical\ dispersion\ (L^2T^{-1})$
$\alpha_L, \alpha_{Th}, \alpha_{Tv} = longitudinal, transversal\ horizontal\ and\ transversal\ vertical\ dispersion\ factor\ (L)$
$D_m = mechanical\ dispersion\ coefficient\ (L^2T^{-1})$
$D_d = molecular\ diffusion\ coefficient\ (L^2T^{-1}).$
$h_f = pressure\ head\ expressed\ in\ freshwater\ (L)$
$c = resistance\ of\ the\ river\ bed (T)$
$t = time\ (T)$
$C = volumetric\ chloride\ concentration\ \ (ML^{-3})$
$C^{t+adv}_{j,i,k} = volumetric\ chloride\ concentration\ after\ advection\ alone\ \ (ML^{-3}).$
$C' = volumetric\ chloride\ concentration\ in\ the\ sink/source\ fluid\ (ML^{-3})$
$W = volumetric\ fluid\ sink\ (W < 0)\ or\ source\ (W > 0)\ rate\ per\ unit\ volume\ of\ aquifer\ (T^{-1})$
$Q = volumetric\ inflow\ or\ ouflow\ per\ unit\ of\ volume\ (T^{-1})$
$W = width\ of\ the\ ditch\ within\ a\ cell\ (L)$

CHAPTER 1: INTRODUCTION

1.1 Waterdunen

In 2012, a consortium of local and regional governments, private investors and NGOs started with the development of the nature and recreational area 'Waterdunen' in Zeeuws-Vlaanderen (uttermost south-west of the Netherlands) (Project Waterdunen 2013). A major element of the project is the re-implementation of a nature area with a tidal regime –see Figure 1- to the east of the village of Breskens (idem). However, the higher water level and higher density of saline water associated with the creation of such a tidal plane leads to a higher effective groundwater pressure in the upper aquifer (Figure 2). This pressure, in combination with the artificially maintained drainage levels in the surrounding polders, in theory, might lead to a decrease or even disappearance of freshwater lenses (Buma 2010). Especially farmers are highly reluctant: a decrease in fresh water availability and an increase of brackish-salt water in the capillary zone pose a significant threat to crop growth and, thus, agricultural production (Janssen and Oude Essink 2012). Therefore, in 2012, a group of stakeholders asked Deltares to assess the probability of the mentioned salinization to occur.

Figure 1. Project Waterdunen. On the left hand side figure the current agricultural fields in Waterdunen; on the right hand side a drawing of the nature and recreational plans that are being implemented (including an indication of the location in The Netherlands).

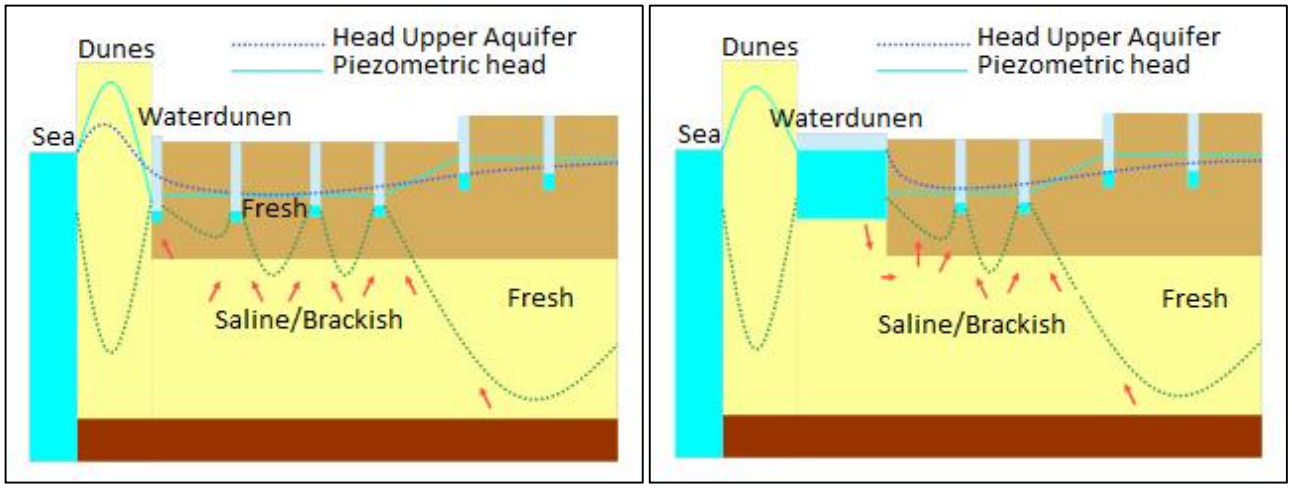

Figure 2. Schematization of the changes in the groundwater system due to the implementation of Project Waterdunen; on the left hand side the current situation, on the right hand side the situation after implementation of Project Waterdunen. The higher heads and concentrations induced by the project lead to higher heads in the first aquifer. As a consequence, seepage fluxes increase and freshwater lenses are 'pushed' upward. Adapted from Buma (2010).

In response to the mentioned request, Deltares set-up the variable density groundwater flow model 'Waterdunen' (a so-called childmodel of the much larger Zeeland model). This model was then used for a series of scenario studies to evaluate the impact of the project on the surrounding agricultural fields. Despite the fact that the model satisfied the

requirements it was built for, the modellers state that they would like to further improve its accuracy (Janssen and Oude Essink 2012). Unfortunately, it remains unclear which factors are determinant for the misfit and, thus, on which parameters the modellers should focus to improve model performance.

Just arbitrarily augmenting the detail of the physical input is not an option. Measurements are expensive, laborious and time consuming. Consequently, a more detailed physical characterization of the model area is not straightforward. Especially, if it is unknown to what extent it will improve modelling performance. Besides, more physical and numerical detail leads to an increase in model runtime, while also in this case the effect on the model performance is unknown.

1.2 Problem description

The problem the modellers of the Waterdunen model were confronted with is in no way an isolated problem. In the report on the Zeeland model, Van Baaren, Oude Essink et al. (2011) state that "when building [a] groundwater model almost all [physical] parameter values are uncertain. In some cases uncertainty is small, for example when a parameter value can be measured directly and accurately in the field. However, often uncertainties are high either because direct measurements in the field are not possible or because values are highly variable in space and/or time. Consequently, the –per definition finite- amount of measurements can only represent the parameter field to a limited extent." Konikow (2011), Clement (2011) and Dam (1996) underline this statement; moreover, they stress that, regarding the physical parameters, it is often unclear how reliable the available data is, how uncertain the parameters are, how they vary in time and space, what they actually represent and how they can be meaningfully measured.

The computational time, speed of computers and memory allocation are major constraints to the implementation of more numerical detail (Oude Essink and Boekelman 1996). In most cases there is little time for model development, but even less for running models with extra fine numerical discretizations. Also, when many simulations are needed, it is very impractical to have extremely long runtimes. At the same time, the impact of the numerical parameters on the model output is hardly known. As a consequence, in day-to-day modelling, numerical parameters are often chosen based on experience, but without a detailed justification.

Notice that, to a certain extent, the above mentioned difficulties also apply for groundwater modelling in general. However, the costs by of solute accurate and precise solute measurements and the very long runtimes are especially problematic in the field of variable density groundwater flow modelling.

Although it is difficult to overcome the mentioned problems, it would already be very useful if it were known to which parameters variable density groundwater flow models are most sensitive. Such knowledge could help to decide which parameters to prioritize during fieldwork, to determine when input parameters are good enough and, consequently, to balance the high costs of boreholes, pumping tests and geophysical exploration techniques (Dam 1996; Langevin, Swain et al. 2005; Clement 2011; Konikow 2011).

1.3 Objective

The aim of this research is, therefore, to determine the sensitivity of the Waterdunen model to changes –within a realistic range- in a series of physical and numerical input parameters. In this, the focus will be on those parameters that are most uncertain. In this, the objective is to identify the physical and numerical parameters that have the largest impact on the overall characterization of fresh-salt groundwater systems; the overall result would then be a kind of 'priority list' of most sensitive parameters. This list should provide modellers with reliable data to decide which parameters they should focus on.

1.4 Research questions

Based on the previous paragraphs the following main research question and sub-research questions have been formulated:

"How sensitive is the variable density groundwater flow model 'Waterdunen' to changes in physical and numerical input parameters that are most uncertain?"

a) Which physical parameters used to model variable density groundwater flow are quite uncertain, but have not been thoroughly studied until today?
b) Which numerical input parameters are questioned most in variable density groundwater flow modeling?
c) How does the output of the Waterdunen model change in function of the identified parameters?

1.5 Organization of the thesis

To answer these research questions first a thorough understanding of the physics involved in fresh-salt groundwater flow is needed. Furthermore, the assumptions and set-up of the numerical modelling code need to be well understood. Both the physics and the numerical code are described in the theoretical background in Chapter 2. Chapter 3 describes the set-up of the Waterdunen model, and the parameterization used in the reference simulation. Chapter 4 deals with the methodology that was applied to be able to answer the main research question. The results are described in Chapter 5, followed by a discussion in Chapter 6, conclusions in Chapter 7 and recommendations in Chapter 8.

CHAPTER 2: THEORETICAL BACKGROUND

In this chapter the theoretical background to the research is provided. First, a general description of the fresh-salt groundwater systems under consideration is given. Thereafter, the equations governing groundwater flow and solute-transport are presented in Subchapter 2.2, while Subchapter 2.3 deals with their numerical solution.

2.1 Fresh-salt groundwater systems

2.1.1 Chemical composition of groundwater

The research site 'Waterdunen' is located near the coastal village of Breskens (Zeeuws-Vlaanderen) in the south-west of The Netherlands. There, as in most deltaic areas, marine intrusion is the major determinant of the chemical composition of groundwater (Table 2). As a consequence, chloride is the dominant solute and a good proxy to the total amount of dissolved solids (TDS) (Pauw 2011). The Dutch standard classification of groundwater types -Table 1- is also based on chloride concentrations.

Table 2. Average chemical composition of sea water (Oude Essink 2001a). Chloride is the dominant solute.

Ions		mg/l
negative ions	Cl^-	19 000
	SO_4^{-2}	2 700
	HCO_3^-	140
	Br^-	65
total negative ions		21 905
positive ions	Na^+	10 600
	Mg^{+2}	1 270
	Ca^{+2}	400
	K^+	380
total positive ions		12 650
Total Dissolved Solids		34 555

Table 1. Classification of groundwater types, after Stuyfzand (1993). Water up to a concentration of 300 mgCl$^-$/l is suitable for drinking water; the average concentration of seawater along the coast of Zeeland has been set to 18630 mgCl$^-$/l; the average concentration of rainfall is 20 mgCl$^-$/l.

Type of groundwater	[Cl$^-$] (mgCl$^-$/l)	Density (kg/m^3)
oligohaline	0 – 5	1 000.00 – 1 000.01
oligohaline-fresh	5 – 30	1 000.01 – 1 000.04
fresh	30 – 150	1 000.04 – 1 000.21
fresh-brackish	150 – 300	1 000.21 – 1 000.42
brackish	300 – 1 000	1 000.42 – 1 001.39
agricultural fresh (Zeeland, NL)	≤ 1 500	≤ 1 002.08
brackish-saline	1 000 – 10 000	1 001.39 – 1 013.89
saline	10 000 – 20 000	1 013.89 – 1 027.78
hyperhaline or brine	≥ 20 000	≥1 027.78

2.1.2 Density and freshwater lenses

Depending on the TDS, temperature and viscosity, water density can assume very different values. According to Reilly and Goodman (1985), worldwide, the density of natural aquifer systems at 20°C ranges from 998 kg/m^3 for pure fresh water to 1 345 kg/m^3 for the Salado brine in New Mexico. The average concentration of ocean water is estimated to be in-between 1 022 and 1 028 kg/m^3 (Chow 1964; Meinardi 1983). In The Netherlands, seawater density is typically equalled to 1 025 kg/m^3 for practical reasons.

In the system under consideration, variations in temperature and viscosity are negligible (e.g. Figure 4 on page 15) and, therefore, not considered. Groundwater density is, therefore, linearly correlated with chloride concentration. As at islands (see Figure 3 on page 15) in the research area freshwater lenses float on top of brackish to highly saline water. This brackish to highly saline water is a mixture of water stored in the subsoil during Holocene transgressions, current marine intrusion and a deep freshwater flux that infiltrates several hundreds of kilometres southwards in Belgium and flows towards the Dutch coast (Post 2004; Janssen and Oude Essink 2012; Sommeijer 2013).

The floating freshwater lenses are formed by natural recharge and uphold by buoyancy forces. What is the explanation beyond this system? On the short term, fresh and saline water tend to keep more or less separated; so, rainfall does not immediately mix with the earlier described saline water. The chloride concentration, and thus density, of the incoming rainwater is much lower (20 mgCl$^-$/l) than that of brackish to saline water (1 000 to 20 000 mgCl$^-$/l). As such, and in agreement with the Archimedes' Principle, 'lighter' fresh water accumulates in lenses and floats on top of the 'heavier' saline water due to buoyancy forces. In between these lenses, seepage of saline water occurs toward drainage ditches (Figure 5 on page 15).

Coming back to the 'fresh and saline water tend to keep more or less separated' from the previous paragraph, sharp interface and equilibrium situations as depicted in Figure 3 on page 15 are rare in The Netherlands. In most situations

there is a gradual transition from fresh to saline water (Figure 5). As a consequence, the concept *freshwater lens* is not as straightforward as it seems; one has to define a threshold value up to which water is considered 'freshwater lenses-fresh'. In this research this threshold value is set at 1 000 mgCl$^-$/l following Dutch academics in this field of study[1]. The thickness of the transition zone depends on transient hydrogeological processes (i.e. regression and transgression), circulation of fresh, brackish and saline water, tidal regime and human activities (Reilly and Goodman 1985).

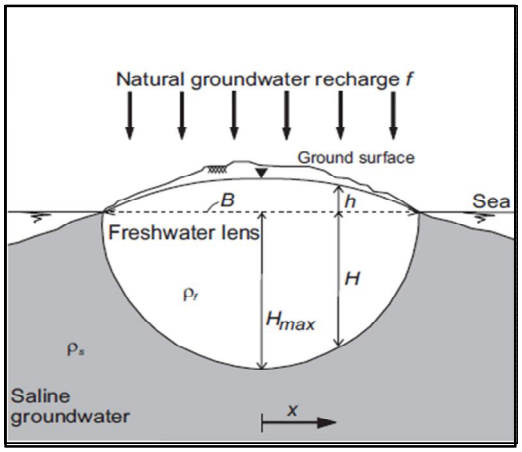

$$h = \frac{\rho_s - \rho_f}{\rho_f} H \quad (1)$$

$h = phreatic\ groundwater\ level\ (L)$
$\rho_s = salt\ groundwater\ density\ (ML^{-3})$
$\rho_f = fresh\ groundwater\ density\ (ML^{-3})$
$H = depth\ fresh - saline\ interface\ (L).$

Figure 3. Schematization of a sharp interface freshwater lens below an elongated island (Oude Essink 2001a), and formula to calculate the phreatic groundwater level assuming a hydrostatic equilibrium (Badon Ghijben and Drabbe 1889; Herzberg 1901).

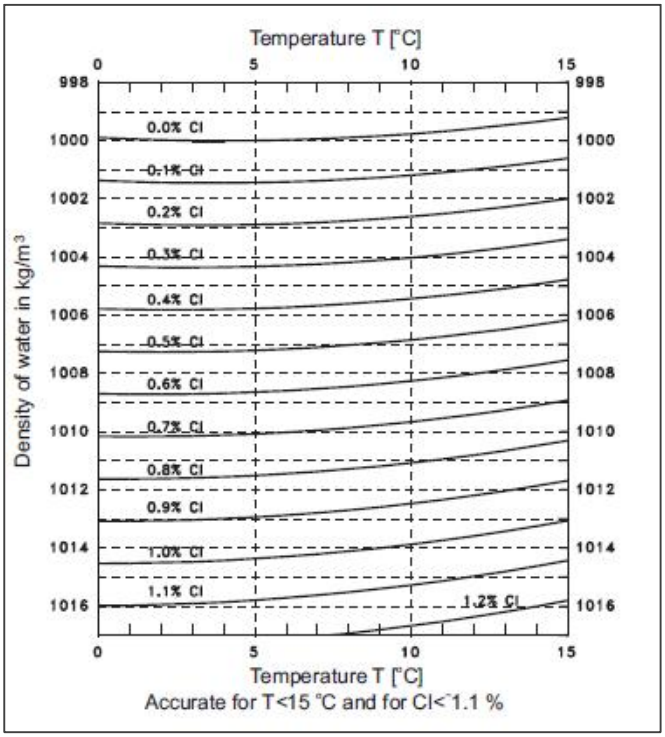

Figure 4. Water density as a function of chlorinity and temperature.ILRI (1972) in: Oude Essink (2001a).

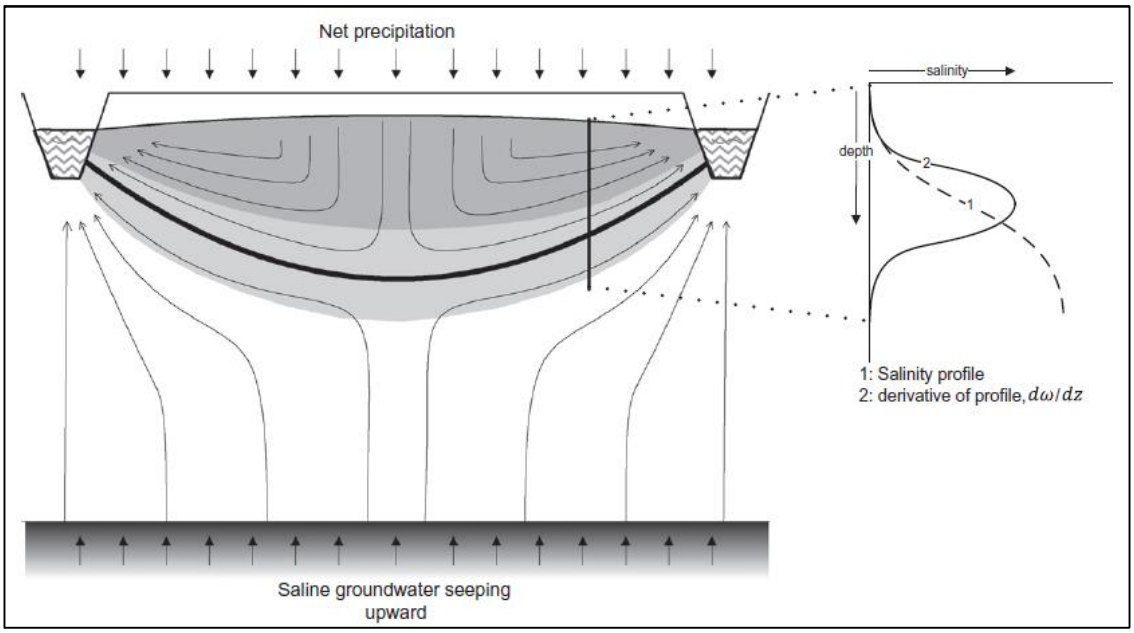

Figure 5. A steady state freshwater lens (in grey) on top of saline upward flowing groundwater (white) with arrows that illustrate flow lines. The mixing zone is (light grey) lies in between. The thick black line indicates the position of the 'interface'. On the right hand side a visualization of the salt mass fraction profile and its first derivative. Source: Eeman, Leijnse et al. (2011).

[1] NB: In the Province of Zeeland, also the 1 500 mgCl$^-$/l agricultural fresh value (Table 1) is used to determine the thickness of freshwater lenses.

To characterize the transition zone, Eeman, Leijnse et al. (2011) propose to use the spatial moment method, i.e. to determine the depth of the bottom (BMix), the centre (DMix) and the half-width (WMix) of the transition zone[2]; herein:

- Bmix is shallowest depth at which the chloride concentration is equal to that of the underlying seepage water;
- DMix is depth at which the chloride concentration is half that of seepage water; and,
- Wmix stands for the distance between BMix and DMix.

In this thesis, these indices are complemented by an analysis of the location and distance between the 30 $mgCl^-/l$, 1 000 $mgCl^-/l$ and 1 500 $mgCl^-/l$ isohalines to have an indication on the mixing around the threshold value used to determine freshwater lens thickness (1 000 $mgCl^-/l$).

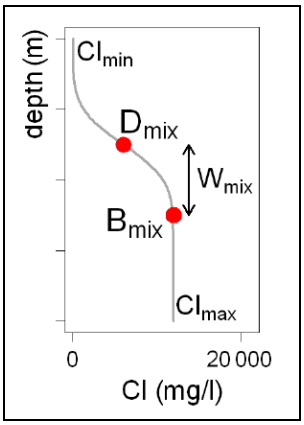

Figure 6. Characteristics of a rainwater lens Dmix, BMix and WMix. Adapted from Louw, Eeman et al. (2011).

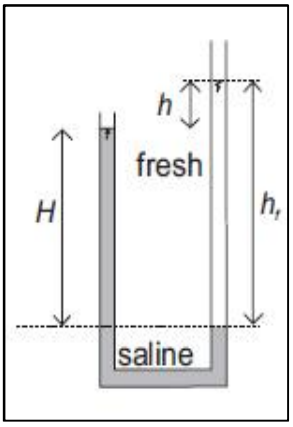

Figure 7. The pressure head expressed in freshwater (h_f) is equal to H+h. Source: Oude Essink (2001a).

2.2 Governing equations

In this subchapter, the governing groundwater flow and solute-transport (chloride) equations are introduced. First, the conversion to equivalent freshwater heads is explained. Then, the groundwater flow equation is presented as a function of equivalent freshwater heads. Finally, in Section 2.2.3 the solute-transport equation is discussed.

2.2.1 Equivalent freshwater heads

In most situations, hydraulic heads are used to calculate groundwater flow. However, in coastal areas, where chloride concentrations are highly variable, heads first have to be corrected for density differences (i.e. buoyancy forces). Under these conditions, equivalent freshwater heads should be used (Figure 7) (Langevin and Guo 2006);(Lusczynski 1961; Oude Essink 1996b):

$$\phi_f = z + h_f = z + \frac{\rho_i}{\rho_f} H \tag{2}$$

$\phi_f = equivalent\ freshwater\ head\ (L)$
$z = elevation\ head\ (L)$
$h_f = pressure\ head\ expressed\ in\ freshwater\ (L)$
$\rho_i = groundwater\ density\ (ML^{-3})$
$\rho_f = fresh\ groundwater\ density\ (1\,000\ kg/m^3)\ (ML^{-3})$
$H = hydraulic\ head\ (L).$

If density only depends on chloride concentrations than the following (linear) equation of state applies (Oude Essink 2001a):

$$\rho_i = \rho_f \left(1 + \alpha \frac{C_i}{C_s}\right) = \rho_f \left(1 + \frac{\rho_s - \rho_f}{\rho_f} * \frac{C_i}{C_s}\right) \tag{3}$$

$\rho_s, \rho_i = salt\ groundwater\ density\ (1\,025\ kg/m^3)\ and\ fresh\ groundwater\ density\ (1\,000\ kg/m^3)\ \ (ML^{-3})$
$C_i = chloride\ concentration\ (ML^{-3})$
$C_S = chloride\ concentration\ of\ salt\ water\ (ML^{-3})$
$\alpha = relative\ density\ difference\ (-).$

[2] NB: The method was originally developed to characterize shallow freshwater lenses, and not the thick lenses that are central in this research. However, it was assumed that in the situation of thick freshwater lenses the method might also provide important insights.

2.2.2 Groundwater flow equation

A general form to describe saturated constant density groundwater flow is obtained by combining Darcy's Law with the continuity equation. Using hydraulic heads and the Cartesian tensor notation this results in (adapted from McDonald and Harbaugh (1988)):

$$\frac{\partial}{\partial x_i}\left(K_{ij}\frac{\partial H}{\partial x_i}\right) = S_s\frac{\partial H}{\partial t} + Q \tag{4}$$

$K_{ij} = hydraulic\ conductivity\ of\ the\ porous\ media\ (LT^{-1})$
$H = hydraulic\ head\ (L)$
$t = time\ (T)$
$Q = volumetric\ inflow\ or\ ouflow\ per\ unit\ of\ volume\ (T^{-1})$
$x_i = Cartesian\ coordinates\ (L).$

Although fluid sources and sinks may be variable in time and space, these have been lumped into one term, Q, for practical reasons. Since the solution of the equation only depends on the net flux as a function of time there is no problem in adding up, for example, well extraction, rainfall and evapotranspiration (Konikow, Goode, et al. 1996).

In the situation of saturated variable density groundwater flow, the equation has to be rewritten in terms of equivalent freshwater heads (see also Appendix A). If then the principal axes of the hydraulic conductivity tensor are aligned with the x-y-z coordinate axes the groundwater flow equation can be rewritten as:

$$\frac{\partial}{\partial x}\left(K_{xx}\frac{\partial \phi_f}{\partial x}\right) + \frac{\partial}{\partial y}\left(K_{yy}\frac{\partial \phi_f}{\partial y}\right) + \frac{\partial}{\partial z}\left(K_{zz}\frac{\partial \phi_f}{\partial z} + \frac{\rho_i - \rho_f}{\rho_f}\right) = S_s\frac{\partial \phi_f}{\partial t} + Q \tag{5}$$

or, in Darcian specific discharges, as

$$-\frac{\partial q_x}{\partial x} - \frac{\partial q_y}{\partial y} - \frac{\partial q_z}{\partial z} = S_s\frac{\partial}{\partial t} + Q \tag{6}$$

$$q_x = -K_{xx}\frac{\partial \phi_f}{\partial x} \tag{7}$$

$$q_y = -K_{yy}\frac{\partial \phi_f}{\partial y} \tag{8}$$

$$q_z = -K_{zz}\left(\frac{\delta \phi_f}{\delta z} + \frac{\rho_i - \rho_f}{\rho_f}\right) \tag{9}$$

$K_{xx}, K_{yy}, K_{zz} = hydraulic\ conductivity\ along\ the\ x, y\ and\ z\ coordinate\ axes\ (LT^{-1})$
$\phi_f = equivalent\ freshwater\ head\ (L)$
$t = time\ (T)$
$Q = volumetric\ inflow\ or\ outflow\ per\ unit\ of\ volume\ (T^{-1})$
$q_x, q_y, q_z = Darcian\ specific\ discharges\ along\ the\ x, y\ and\ z\ coordinate\ axes\ (LT^{-1})$
$\rho_i = groundwater\ density\ (ML^{-3})$
$\rho_f = fresh\ groundwater\ density\ (1\ 000\ kg/m^3)\ (ML^{-3}).$

According to Verruijt (1980), Bear and Verruijt (1987) and Vandenbohede (2008), the effect of viscosity and density differences on hydraulic conductivity are negligible. These differences are, therefore, not taken into account.

Because the movement and mixing of solutes is highly affected by the velocity of the flowing groundwater to calculate the effective groundwater velocity, one must account for the effective porosity of the medium:

$$V_i = \frac{q_i}{\varepsilon} \tag{10}$$

$V_i = average\ effective\ pore\ groundwater\ velocity\ (LT^{-1})$
$q_i = Darcian\ specific\ discharge\ (LT^{-1})$
$\varepsilon = effective\ porosity\ of\ the\ medium\ (-).$

2.2.3 Solute-transport equation

The principle of conservation of mass requires the net difference between the solute mass entering and leaving the model to be equal to the accumulation or loss of mass stored during a certain time interval in a particular volume of aquifer (Konikow, Goode et al. 1996). Because only chloride –a conservative solute- is looked at, neither sorption nor (radioactive) decay takes place; therefore, the following partial differential solute-transport equation can be written down (adapted from Konikow, Goode et al. 1996):

$$\frac{\partial C}{\partial t} = -\frac{\partial}{\partial x_i}(CV_i) + \frac{\partial}{\partial x_i}\left(D_{ij}\frac{\partial C}{\partial x_j}\right) + \frac{\sum C'W}{\varepsilon} \qquad (11)$$

$C = volumetric\ chloride\ concentration\ (ML^{-3})$
$t = time\ (T)$
$D_{ij} = hydrodynamic\ dispersion\ coefficient\ (L^2T^{-1})$
$V_i = effective\ pore\ groundwater\ velocity\ in\ direction\ x_i (LT^{-1})$
$C' = volumetric\ chloride\ concentration\ in\ the\ sink/source\ fluid\ (ML^{-3})$
$W = volumetric\ fluid\ sink\ (W < 0)\ or\ source\ (W > 0)\ rate\ per\ unit\ volume\ of\ aquifer\ (T^{-1})$
$\varepsilon = effective\ porosity\ of\ the\ medium\ (-).$

This solute-transport equation is also known as advection-dispersion equation. The first right hand side term represents changes in chloride concentration due to advection, the second changes due to hydrodynamic dispersion (mechanical dispersion + molecular diffusion) and the third due to sources and sinks (see also Figure 8).

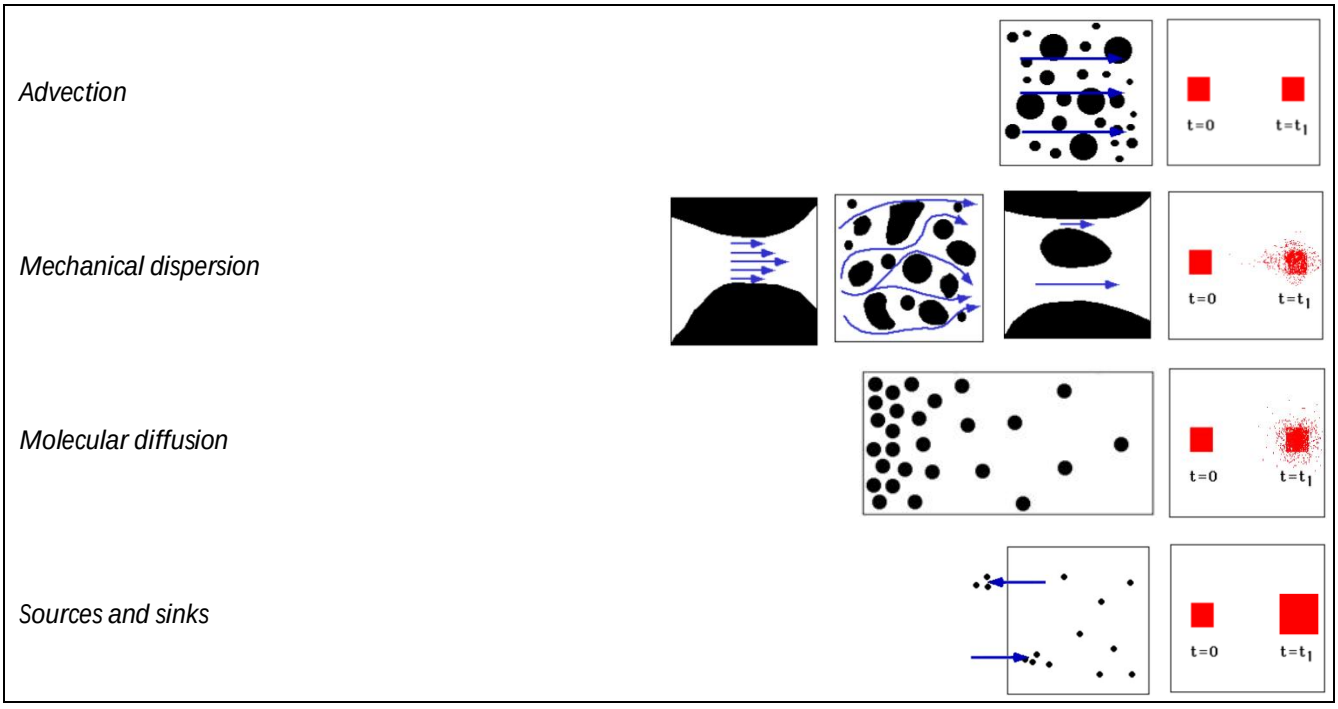

Figure 8. Solute-transport mechanisms: advection, mechanical dispersion, molecular diffusion and sources & sinks. Blue-black figures are graphical representations of the process; red block-figures show the effect on a group of solute particles.

Advection refers to the movement of particles by means of the fluid's bulk motion. Hydrodynamic dispersion is a measure for the spreading away of solute particles from the mean flow path and their movement toward lower concentration areas. Hydrodynamic dispersion is made up by mechanical dispersion and molecular diffusion (Meinardi 1983):

$$D_h = D_m + D_d \qquad (12)$$

$D_h = hydrodynamic\ dispersion\ coefficient\ (L^2T^{-1})$
$D_m = mechanical\ dispersion\ coefficient\ (L^2T^{-1})$
$D_d = molecular\ diffusion\ coefficient\ (L^2T^{-1}).$

Mechanical dispersion of solute particles occurs due to variations in magnitude and direction of velocity. Inhomogeneity of an aquifer (e.g. permeability and porosity) and the variety in flow paths chosen by droplets when encountering a soil particle lead to these (small) variations. The resulting spatially variable velocity field is one of the reasons why solute particles stray away from the mean flow path (Figure 8 on page 18). Since mechanical dispersion is not uniform in all directions it is represented as a tensor (Scheidegger 1958). In 3D-problems, the tensor is made up of three components: longitudinal, transversal horizontal and transversal vertical dispersion. Longitudinal dispersion refers to the process parallel to the flow path, wherein particles get 'behind' or 'ahead' mean groundwater flow. In transversal horizontal and transversal vertical dispersion, solute particles get 'aside' the pure advective groundwater flow. Dispersion is calculated by multiplying the absolute effective groundwater velocity with the respective dispersivity factor:

$$D_L = \alpha_L |V_i| \quad (13)$$
$$D_{Th} = \alpha_{Th} |V_i| \quad (14)$$
$$D_{Tv} = \alpha_{Tv} |V_i| \quad (15)$$

$D_L, D_{Th}, D_{Tv} = longitudinal, transversal\ horizontal\ and\ transversal\ vertical\ dispersion\ (L^2T^{-1})$
$\alpha_L, \alpha_{Th}, \alpha_{Tv} = longitudinal, transversal\ horizontal\ and\ transversal\ vertical\ dispersion\ factor\ (L)$
$V_i = effective\ pore\ groundwater\ velocity\ in\ direction\ x_i (LT^{-1})$.

Until today, the understanding of dispersion is rather limited and generic because of its mathematical complexity, spatial and temporal variability, and scale dependency; dispersion is hard to quantify (Eeman, Leijnse et al. 2011). According to Gelhar, et al. (1992), longitudinal dispersion ranges between 10^{-2} and 10^4 m. Little is known about transversal dispersion; yet, in general, it is assumed that transversal dispersion factors are at least one order of magnitude smaller than the longitudinal one. In addition, it has been shown that longitudinal dispersion is dominant at the start of lens formation, while later on transversal dispersion becomes increasingly important (Eeman, Leijnse et al. 2011).

Molecular diffusion. Meinardi (1983) ascribes the identification of molecular diffusion as central in the very long term (hundreds to thousands of years) transport of ions in stagnant water to Mazure and Volker (1961). They found that there are solute particles, here chloride ions, that move randomly through groundwater. The intensity and direction of this process depend on the variability in solute concentration, soil properties and the characteristics of the transporting water and is proportional to the square root of time. Molecular diffusion is effective under all circumstances, groundwater moving or not (Meinardi 1983). The relative effect of molecular diffusion, together with the earlier mentioned transversal dispersion, becomes more important when the steady state situation is approached.

To conclude this subchapter, it is appropriate to make a remark on the hydrodynamic dispersion theory presented here. To a certain extent, the less we know about a system the higher the hydrodynamic dispersion coefficient becomes. "At whatever scale we operate, some internal structure will be present at the smaller scale, and we will likely be ignorant of most of it and of the true velocity distribution" (Konikow 2011). Therefore, during model simulations, certain conceptualization and parameterization details are inherently averaged out.[3] These simplifications lead to an enlargement of the 'rest-term' mechanical dispersion. On the contrary, the more detail is incorporated, the more the total hydrodynamic dispersion value will resemble the value of molecular diffusion. Being an indicator of simplification, cell size should be considered in the application of the dispersion coefficient (Langevin, Swain et al. 2005).

2.3 Numerical methods

2.3.1 Introduction MOCDENS3D

Available codes. The objective of numerical variable density groundwater flow models is to simulate non-uniform density-driven flow. The codes available for these simulations include MOCDENS3D (Oude Essink 1996b), USGS SEAWAT (Guo and Langevin 2002; Langevin, Shoemaker et al. 2003), MODHMS (HydroGeoLogic Inc 2002), FEFLOW (Diersch 2005) and SUTRA (Voss and Provost 2008). Some of these codes are based on finite elements, others on finite differences; some simulate dispersive solute-transport, others use a continuity-flow approach. Codes are founded on different assumptions and approaches, in general not being better or worse. Instead, there is often added value in their

[3] For more information about the relation between model up scaling and dispersion refer to Bear, J. (1979). Hydraulics of groundwater. New York, McGraw-Hill.

differentiation. Some approaches might be a good choice in one situation, whereas in other cases it might be more appropriate to use another code. Assumptions beyond the code, computation time, access to interfaces, support availability, and so forth might play a role in deciding which code to use.

History MOCDENS3D. The Waterdunen model was developed in MOCDENS3D. MOCDENS3D is a diversion of MODFLOW-88, a 3D-finite-difference groundwater flow model (McDonald and Harbaugh 1988). In 1996, the USGS developed the MODFLOW plug-inn MOC3D-package to track solute-transport (Konikow, Goode et al. 1996). However, the MOC3D-package does not take into account the influence of solute concentrations on the physical characterization of the system. In large coastal aquifer systems, for example, fluid density differences caused by non-uniform chloride-concentration distributions are not considered when calculating groundwater flow. Since piezometric head differences are typically small in coastal plains, such simplification can have quite an impact on the output of the models (e.g. head distribution, velocity fields and flow lines). To correct for this problem, Oude Essink (1996c) developed MOCDENS3D. The MODENS3D-code applies the Strongly Implicit Procedure (SIP-solver) and consists of two fully integrated components: a solute-transport module (MOC) and a groundwater flow module adapted for transient density dependent groundwater flow (MODFLOW).

Over the past years, MOCDENS3D has been used to evaluate salinization in the following (Dutch) projects: 'Determination of future groundwater salinization in Zuid-Holland' (Oude Essink, Van Baaren et al. 2010), 'Calculation of the effects of surface level lowering in Barradeel II, Friesland' (Wetterskyp Fryslân 2005), 'Impact assessment of the Volkerak Zoommeer on the groundwater system' (Oude Essink, Baaren et al. 2008), 'The Netherlands: a climate proof water country' (Hoogvliet, Oude Essink et al. 2008), 'Hydrogeologic research in Texel' (Pauw, Louw et al. 2012) and 'NHI: the fresh-salt module' (Oude Essink and Verkaik 2010).

2.3.2 Groundwater flow equation (based on Konikow, Goode et al. (1996))

Because aquifers are heterogeneous and are limited by complex boundary conditions, it is not possible to solve the groundwater and solute-transport equations analytically. Instead, numerical methods are used. Therefore, the continuous aquifer is replaced by grid-cells (Figure 9) in which equivalent heads and concentrations are defined; time is divided into time steps. All variables are then defined in (i.e. averaged over) this discretized space and time. In MOCDENS3D flow can be steady or transient. Aquifer properties can vary spatially and hydraulic transmissivity can be anisotropic.

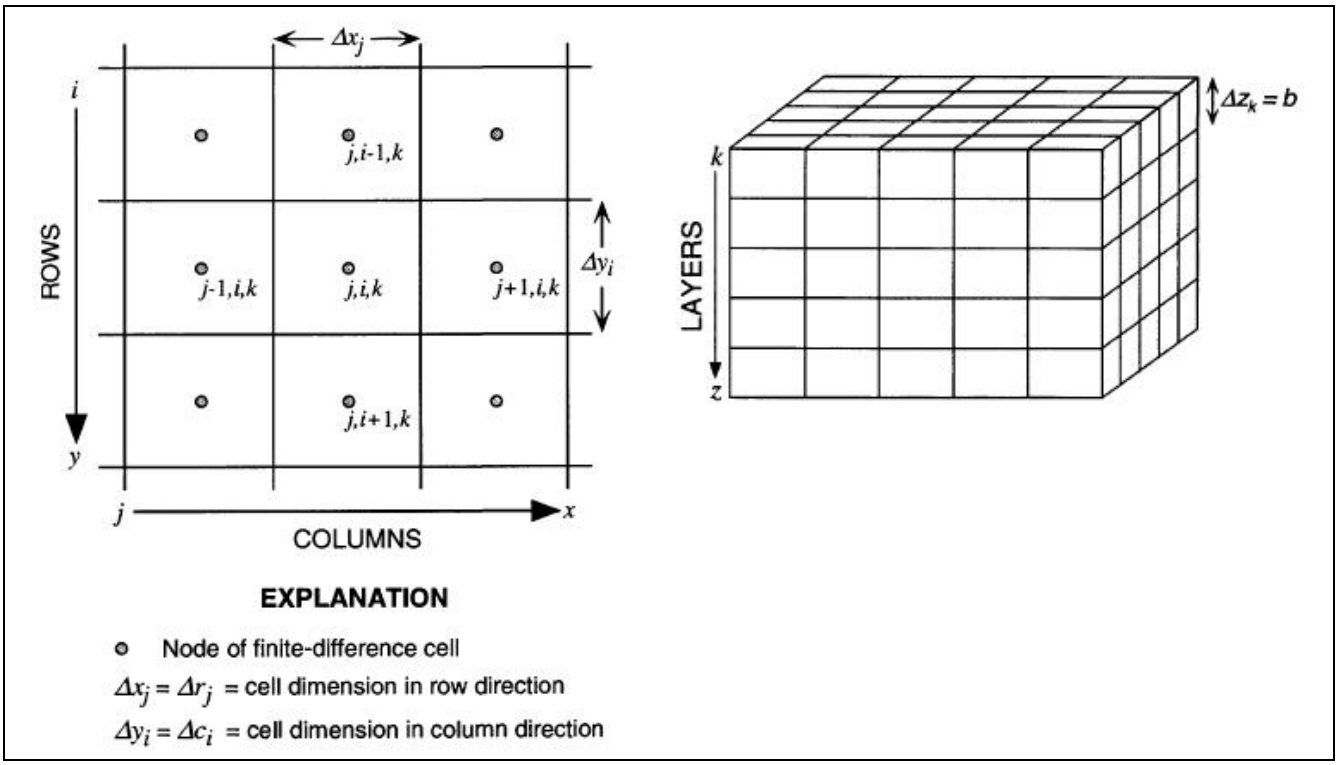

Figure 9. Left hand side: spatial discretization used in MOCDENS3D within layer (k) of a 3D, block-centered and finite-difference grid. Right hand side: representative 3D-grid for MOCDENS3D (Konikow, Goode et al. (1996)).

Since advection and mechanical dispersion depend on the velocity of groundwater flow, after the heads have been calculated for a given flow time step, the Darcian specific discharges across the cell boundaries and the effective groundwater velocity are calculated next. The specific discharges are calculated using a finite-difference form of Equations (7), (8) and (9):

$$q_{x(j+\frac{1}{2},i,k)} = -\overline{K}_{xx(j+\frac{1}{2},i,k)} \frac{\left(\phi_{f\,(\boldsymbol{j+1},\boldsymbol{i},\boldsymbol{k})} - \phi_{f\,(j,i,k)}\right)}{\Delta x} \tag{16}$$

$$q_{y(j,i+\frac{1}{2},k)} = -\overline{K}_{yy(j,i+\frac{1}{2},k)} \frac{\left(\phi_{f\,(\boldsymbol{j},\boldsymbol{i+1},\boldsymbol{k})} - \phi_{f\,(j,i,k)}\right)}{\Delta y} \tag{17}$$

$$q_{z(j,i,k+\frac{1}{2})} = -\overline{K}_{zz(j,i,k+\frac{1}{2})} \frac{\left(\phi_{f\,(\boldsymbol{j},\boldsymbol{i},\boldsymbol{k+1})} - \phi_{f\,(j,i,k)}\right)}{\Delta z} \tag{18}$$

$q_x, q_y, q_z = specific\ Darcian\ discharge\ along\ the\ x, y\ and\ z\ coordinate\ axes\ (LT^{-1})$
$\overline{K}_{xx}, \overline{K}_{yy}, \overline{K}_{zz} = \ interblock\ hydraulic\ conductivity\ in\ the\ x, y\ and\ z\ directions\ (LT^{-1})$
$\phi_f = equivalent\ freshwater\ head\ (L).$

Based on these Darcian specific discharges it is possible to calculate the effective pore groundwater velocity; note, once again, that this velocity is very important because it is one of the major factors controlling solute-transport. The effective pore groundwater velocity is calculated using the finite difference form of Equation (10):

$$V_{x(j,i,k)} = \frac{q_{x\left(j+\frac{1}{2},i,k\right)} - q_{x(j-\frac{1}{2},i,k)}}{2\varepsilon_{(j,i,k)}} \tag{19}$$

$$V_{y(j,i,k)} = \frac{q_{y\left(j,i+\frac{1}{2},k\right)} - q_{y(j,i-\frac{1}{2},k)}}{2\varepsilon_{(j,i,k)}} \tag{20}$$

$$V_{z(j,i,k)} = \frac{q_{z\left(j,i,k+\frac{1}{2}\right)} - q_{z(j,i,k-\frac{1}{2})}}{2\varepsilon_{(j,i,k)}} \tag{21}$$

$V_x, V_y, V_z = average\ effective\ pore\ groundwater\ velocity\ in\ the\ x, y\ and\ z\ directions\ (LT^{-1})$
$q_x, q_y, q_z = specific\ Darcian\ discharge\ along\ the\ x, y\ and\ z\ coordinate\ axes\ (LT^{-1})$
$\varepsilon = effective\ porosity\ of\ the\ medium\ (-).$

2.3.3 Solute-transport equation

The governing equation for solute-transport (Equation (11)) is much more difficult to solve than the groundwater flow equation because:

- the mathematical properties of the equation vary depending on the dominant solute-transport process;
- the dominant solute-transport process may vary from point to point due to the heterogeneity of the aquifer and the variability in velocities; and,
- in advection-dominated problems, it is numerically difficult to preserve a sharp concentration front when it is moving through the domain (Konikow Goode, et al., 1996).

In general, it is possible to accurately solve dispersion-dominated solute-transport by means of standard finite-differences or finite-elements approaches. However, the application of one of the previous approaches to advection-dominated problems leads to too much numerical dispersion. To overcome this problem, in MOCDENS3D the solute-transport equation is not solved directly, but split up in a system of two ordinary differential equations (Frolkovic 2001). Concentration changes due to hydrodynamic dispersion and due to fluid sources and sinks are computed using a standard finite-differences approach in a fixed-in-space finite difference-grid, while advection is solved by means of the method-of-characteristics (MOC), a particle tracking technique (Vandenbohede 2008).

Method-of-Characteristics. Equation (11) describes the change of concentration over time at fixed reference points within a stationary coordinate system (Eulerian framework). The MOC calculates the change in concentration over time, but in representative fluid parcels as they move with the groundwater flow (Lagrangian framework). Changes in concentration can, therefore, be calculated by introducing a set of so-called advection particles (i.e. the representative fluid parcels) that follow characteristic curves. These advection particles can be traced within the stationary coordinates of a finite-difference grid (Figure 10). At each moment in time, an advection particle has a position and concentration associated with it and moves through the model domain according to the local effective groundwater velocity (Konikow, Goode et al. 1996). At the end of each (solute) time step[4], the mean of the concentrations of all advection particles that ended up in a cell is calculated, hereby providing the start concentrations for the next (solute) time step. The MOC makes it possible to model large-scale geometries, even with coarse elements and large time steps, while preserving sharp fronts and avoiding oscillations (Chilakapati 1998).

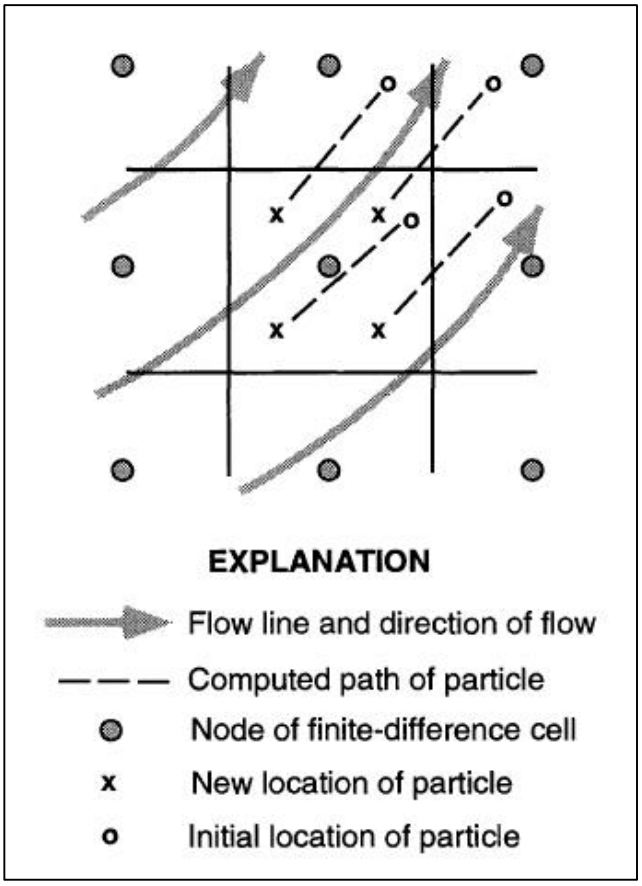

Figure 10. Part of a hypothetical finite-difference grid showing the relation between the flow field and the movement of the advection particles in MOCDENS3D to simulate advection. Modified from Konikow and Bredehoeft (1978) in: Konikow, Goode et al. (1996).

Although advection and hydrodynamic dispersion are occurring continuously and simultaneously (Konikow and Bredehoeft 1978), in MOCDENS3D these processes are solved sequentially for practical reasons. Yet, this order might influence the results because dispersion depends on the concentration gradient, which in turn can change significantly due to advection. To correct for this, dispersion is calculated using the average of the concentrations at each node before and after advection (Konikow, Goode et al. 1996). The averaged concentrations are calculated as:

$$C^{*}_{j,i,k} = \frac{C^{t}_{j,i,k} + C^{t+adv}_{j,i,k}}{2} \qquad (22)$$

$C^{*}_{j,i,k} = averaged\ volumetric\ chloride\ concentration\ \ (ML^{-3})$
$C^{t}_{j,i,k} = initial\ volumetric\ chloride\ concentration\ \ (ML^{-3})$
$C^{t+adv}_{j,i,k} = volumetric\ chloride\ concentration\ after\ advection\ alone\ \ (ML^{-3}).$

[4] Depending on the stability criteria, each flow time step might be further subdivided into solute time steps. See section 2.3.4.

2.3.4 Stability criteria

Flow time steps. The flow time step (time increment used to solve the groundwater flow equation) has to be chosen small enough to capture the variability of the velocity field and the pace of solute-transport. However, and unlike its importance, there is no clear-cut method to determine the duration[5] of a reasonable flow time step. In most cases, flow time discretization is based on experience and trial-and-error, e.g. if concentrations vary a lot and velocities are high, small flow time steps are required (Oude Essink 1996b).

Solute time steps. For numerical stability reasons, it might be necessary to further subdivide the flow time steps into smaller solute time steps. Whether or not this extra subdivision is necessary and in how many solute time steps each flow time step has to be subdivided is determined by three stability criteria: the Neumann Criterion, the Mixing Criterion and the Courant Friedrich Lewy Condition. If one or more of these criteria is not met, the flow time step is subdivided in as many solute time steps as necessary to meet this requirement.

The *Neumann Criterion* considers the dispersion process. It checks for the stability of the numerical difference schemes when solving partial differential equations, in this case applied to the dispersion process. To ensure numerical stability, dispersion has to be small enough or else either the grid size has to be increased or the solute time step has to be decreased. The following criterion has to be fulfilled (Konikow and Bredehoeft 1978)[6]:

$$\Delta t \leq \underset{overgrid}{\text{Min}} \left[\frac{0.5}{\frac{D_{xx}}{(\Delta x)^2} + \frac{D_{yy}}{(\Delta y)^2} + \frac{D_{zz}}{(\Delta z)^2}} \right] \tag{23}$$

$\Delta t = duration\ of\ the\ solute\ time\ step\ (T)$
$D_{xx}, D_{yy}, D_{zz} = coefficients\ of\ hydrodynamic\ dispersion\ in\ the\ x, y, z\ directions\ (L^2T^{-1})$
$\Delta x, \Delta y, \Delta z = cell\ dimensions\ in\ the\ x, y\ and\ z\ directions\ (L).$

The *Mixing Criterion* assesses whether the difference between injected and existing groundwater does not exceed the difference between the source concentration and the concentration in the aquifer. The maximum possible change occurs when a source completely flushes the cell content at the start of a time step:

$$\Delta t \leq \underset{overgrid}{\text{Min}} \left[\frac{\varepsilon}{W_{j,i,k}} \right] \tag{24}$$

$\Delta t = duration\ of\ the\ solute\ time\ step\ (T)$
$\varepsilon = effective\ porosity of\ the\ medium\ (-)$
$W_{j,i,k} = volumetric\ fluid\ sink\ (W < 0)\ or\ source\ (W > 0)\ rate\ per\ unit\ volume\ of\ aquifer\ in\ cell\ [j,i,k] (T^{-1}).$

The *Courant-Friedrichs-Lewy Condition* (CFL-Condition), finally, defines the maximum distance a particle is allowed to move during one time step. Because the position of advection particles is linearly extrapolated from one time increment to the next, errors are introduced when streamlines are curvilinear. Therefore, the time step should be limited as follows (wherein γ is set by the modeller):

$$\Delta t \leq \frac{\gamma \Delta x}{\underset{overgrid}{\text{Max}} [V_x]} \tag{25}$$

$$\Delta t \leq \frac{\gamma \Delta y}{\underset{overgrid}{\text{Max}} [V_y]} \tag{26}$$

$$\Delta t \leq \frac{\gamma \Delta z}{\underset{overgrid}{\text{Max}} [V_z]} \tag{27}$$

$\Delta t = duration\ of\ the\ solute\ time\ step\ (T)$
$\gamma = cell\ fraction\ that\ particles\ are\ allowed\ to\ travel\ within\ one\ time\ step\ (-)$
$\Delta x, \Delta y, \Delta z = cell\ dimensions\ in\ the\ x, y\ and\ z\ directions\ (L)$
$V_x, V_y, V_z = average\ effective\ groundwater\ velocity\ in\ the\ x, y\ and\ z\ directions\ (LT^{-1}).$

[5] NB: In MOCDENS3D the modeller is asked to set the number of flow time steps per stress period; the duration of each flow time step is then the quotient between the duration of the stress period and the number of flow time steps.

[6] Note that if the solute would react with the soil a retardation factor would have to be taken into account (Genuchten and Wieringa, 1986); since chloride is a conservative solute this is not necessary in this situation.

In MOCDENS3D the subdivision of the flow time steps into smaller solute time steps is automatized. In the output-file, the constraining criterion, the amount of solute time steps per flow time step and the duration of these solute time steps is given at the end of each stress period. In most model runs, these time criteria have a major influence on runtimes: the smaller the solute time steps, the more calculations are required and, consequently, the longer the model run lasts.

Peclet Number Condition. The physical system is continuous in space (and time). However, to numerically model a system, it is necessary to average out characteristics over a certain volume of space. This averaging can have a large influence on the output of the model. Consequently, the decision about the scale and detail of the modelling is an important one. In numerical solute-transport modelling, the Peclet Number Condition is usually used to assess whether the spatial discretization is fine enough. The Peclet number condition calculates the relative importance of advective over dispersive fluxes:

$$Pegrid = \left|\frac{V_i \Delta x_i}{D_h}\right| \tag{28}$$

$V_i = average\ effective\ pore\ groundwater\ velocity\ (LT^{-1})$
$\Delta x_i = dimensions\ grid\ block\ in\ the\ ith\ direction\ (L)$
$D_h = hydrodynamic\ dispersion\ coefficient\ (L^2T^{-1})$.

For most codes to converge the Peclet number should be smaller than two, meaning that dispersion predominates (Oude Essink and Boekelman 1996). However, because MOCDENS3D uses a particle tracking technique to model advection, numerical truncation and oscillation are less of a problem. For that reason, unlike codes founded on standard finite-element or finite-difference techniques, the limitations to spatial discretization are not strict and the Peclet Number Condition has not to be satisfied in MOCDENS3D.

Yet, there is an aspect of spatial discretization that *is* strict for MOCDENS3D. MOCDENS3D requires the effective cell volume to be equal for all cells because the particle tracking algorithm assumes the volume of water to be equal in all cells. If row, column, layer thickness and porosity (or at least the multiplication of the four) are not constant, the averaging of particle concentration in the arrival cell might introduce a bias (Konikow, Goode et al. 1996).

2.3.5 Coupling the groundwater flow equation with the solute-transport equation

At the end of each flow time step, the new heads have to be corrected for the buoyancy effects of the new concentration field. To that end, concentrations are translated into densities by means of the equation of state (Equation (3)). Thereafter, the obtained density field is used to calculate equivalent freshwater heads, which, in turn, are input to the calculation of groundwater flow during the following time increment (Figure 11).

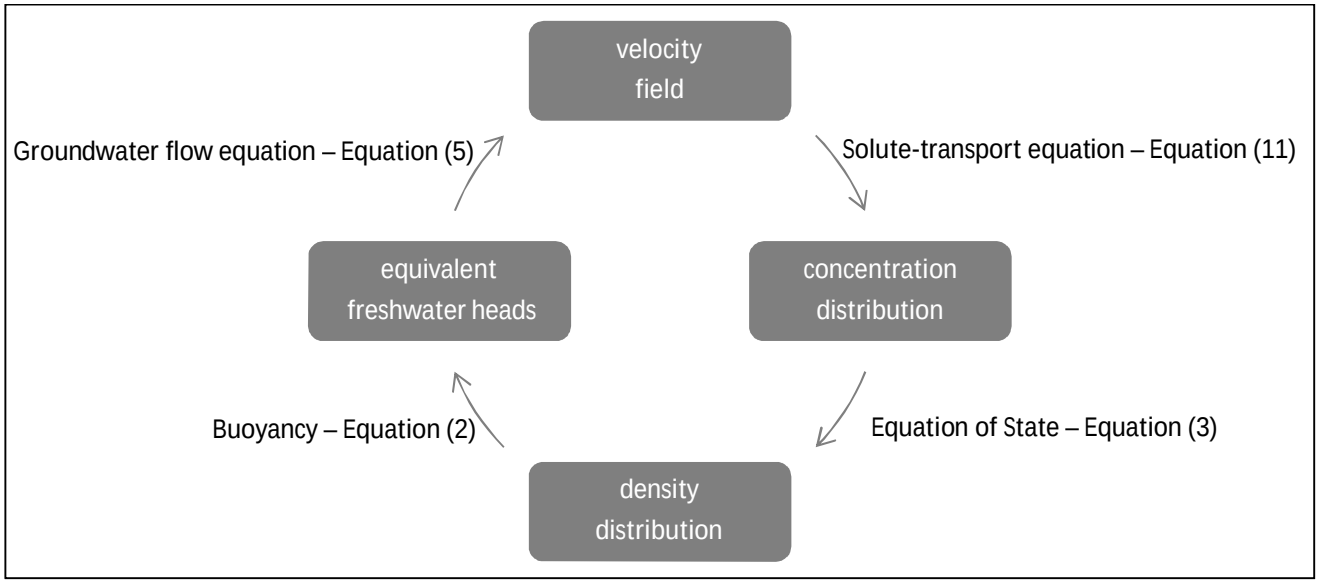

Figure 11. Scheme of the coupling between groundwater flow and solute-transport in MOCDENS3D. The governing and transformation equations are indicated next to the arrows.

2.3.6 Boundary conditions and external stresses

Model boundaries. In MOCDENS3D the model boundaries are established by head dependent flux boundary conditions (Cauchy-type) in the General Head Boundary (GHB)–package. When the GHB-package is used, the flux over the boundaries is proportional to the difference in equivalent heads. In this package, the modeller has to provide the chloride concentrations and equivalent freshwater heads that are expected to apply immediately outside the model domain, and the GHB-transmissivity, which determines how much influence the boundary concentrations and heads have on the model.

There are three major reasons why MOCDENS3D makes use of the GHB-package:

- in the past, the use of the GHB-package was less time consuming than the more standard Constant Head Boundary when solute-transport was to be simulated (G. Oude Essink, pers. comm. March 2013);
- the GHB-package makes it possible to incorporate the influence of important hydrogeological features situated at a larger distance of the modelling domain (Van Baaren, Oude Essink et al. 2011);
- the GHB-package is rather flexible compared to the Constant Head Boundary thanks to its adaptable transmissivities; these transmissivities enable the modeller to regulate the intensity of interaction between the model and the 'outside world' (G. Oude Essink, pers. comm. March 2013).

Top system. Rivers, ditches and drains are incorporated in MOCDDENS3D by means of a diffuse top system of the River and Drainage packages. The River package (RIV-package) is used to simulate rivers and ditches by means of head dependent flux boundaries; the flux from the river to the groundwater system, or vice versa, is calculated based on the stage of the river (water level), river bed resistance, river concentration and bottom of the river bed. This characterization and the location of the waterways have to be set by the modeller. The Drainage package also simulates head dependent boundaries, but does not allow infiltration. When the DRN-package is implemented in a cell, the package drains water from the groundwater system as long as the equivalent freshwater head in that cell is above a certain threshold level; when the equivalent freshwater head falls below that level, the flux from the drain to the model is equalled to zero. The modeller has to set the level and the resistance of the package (Harbaugh, Banta et al. 2000; U.S. Geological Survey 2013).

Groundwater recharge. During the development of the MOCDENS3D the modelling of chloride transport turned out not to be compatible with the Recharge package (RCH-package). To circumvent this problem, groundwater recharge (rainfall minus reference evapotranspiration) is applied to the domain by means of the Well package (WEL-package) (G. Oude Essink, pers. com. March 2013).

2.3.7 Review of assumptions

The physical systems studied using MOCDENS3D are highly complex. To come to a reasonable and tractable solution various assumptions and simplifications are required. In this paragraph, the main assumptions on which the MOCDENS3D-code is based are listed.

- The MOCDENS3D-code models three dimensional laminar saturated groundwater flow in an anisotropic porous medium.
- Unsaturated zones are thin to absent and, therefore, recharge is supplied directly to the groundwater reservoir.
- The system is incompressible; fluid density is assumed independent of fluid pressure (Oude Essink 1996a).
- The effect of temperature and pressure on viscosity are minimal and, therefore, considered insignificant (Verruijt 1980).
- As long as equivalent freshwater heads are used to correct for density differences, Darcy's Law is applicable (Oude Essink 1996a).
- Transversal dispersion, longitudinal dispersion and the retardation factor are assumed constant for the whole model domain.
- Porosity multiplied by cell volume should be kept constant over the whole domain because the particle tracking algorithm assumes an equal volume of water in all cells (Konikow, Goode et al. 1996).
- The head distribution at the end of each flow time step is assumed representative for the whole time interval.
- The input groundwater recharge should have already been corrected for increased concentration due to evaporation processes.

CHAPTER 3: THE WATERDUNEN MODEL

To answer the formulated research questions, the Waterdunen model was used. In this chapter, the set-up of the model and the parameterization as it was used in the reference run are described. The chapter starts with some background information. Thereafter, the model domain and the hydrogeological parameterization are described in Subchapters 3.2 and 3.3. Subchapter 3.4 is dedicated to the solute-transport parameters, whereas in Subchapter 3.5 the boundary conditions and external stresses are given. To conclude, a tabular synthesis is provided in Subchapter 3.6.

3.1 Background

The Waterdunen model was developed by Deltares in 2012 to assess the effects of the Waterdunen Project in Zeeuws-Vlaanderen, The Netherlands (www.waterdunen.com). More specifically, the model was used to assess whether the inlet of salt water, in combination with a higher (artificial) groundwater levels, will lead to higher chloride concentrations and thinner freshwater lenses near the project area (Janssen and Oude Essink, 2012). Note, however, that in the remainder of the research there is no link with the Waterdunen Project anymore. The reference model used in the sensitivity analysis, conceptualizes the current situation, without the implementation of the proposed plans.

The Waterdunen model (25*25 m^2 grid-cells) is a so-called child model of the much larger Zeeland model. The Zeeland model is a regional 3D-transient model that was developed to approximate the fresh-brackish saline interface in the Province of Zeeland. The Zeeland model is discretized on 100*100 m^2 grid-cells and its total surface is almost 30 times as large as that of the Waterdunen model. In order to improve the accuracy of the model, it was calibrated on equivalent freshwater heads (Van Baaren, Oude Essink et al. 2011); see Appendix B for details about this calibration.

In order to get more detailed information about the area of interest, the Waterdunen child model was extracted from the Zeeland model by means of a telescopic mesh refinement. The latter procedure allows for a local refinement of the spatial discretization (Figure 1), while the boundary conditions –in this case equivalent freshwater heads and chloride concentrations- are imposed by the larger model (Leake and Claar 1999). The vertical discretization is as in the Zeeland model.

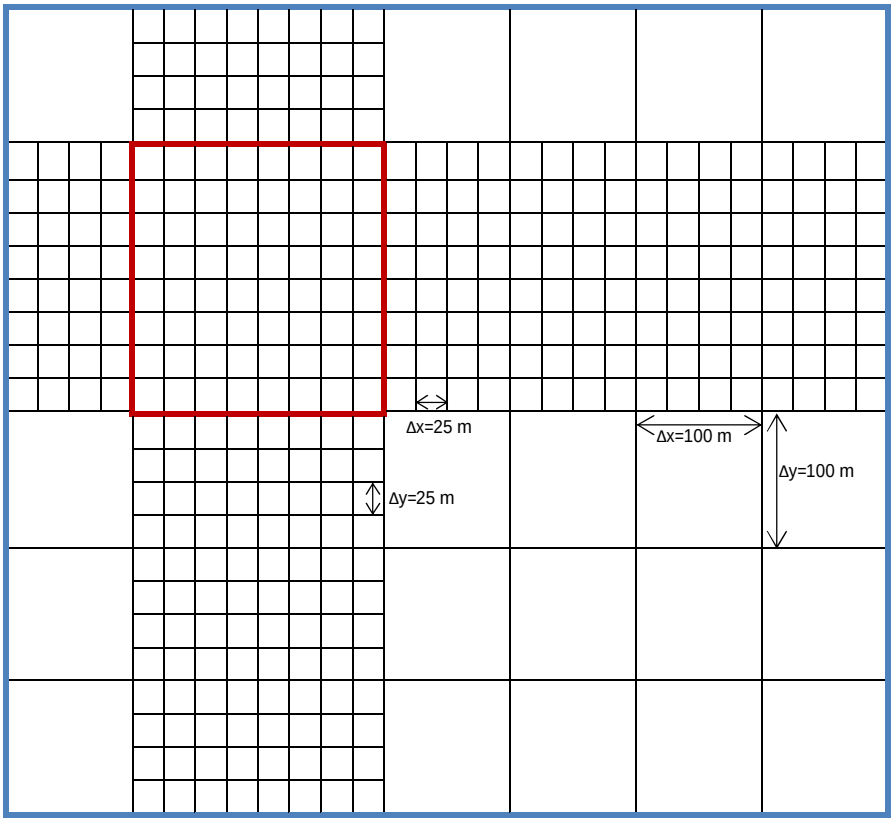

Figure 12. Example schematization of the procedure of a telescopic mesh refinement in which the grid is locally refined from a 100*100 m^2 to a 25*25 m^2 spatial discretization. In blue the boundaries of the mother model and in red the boundaries of the child model are indicated.

3.2 Model domain

Spatial discretization. Waterdunen is located in the uttermost south-west of The Netherlands, in Zeeuws-Vlaanderen. The model covers a total area of 8 km(EW)*7 km(NS)=56 km^2, and runs from RDS-coordinate[7] [21000; 29000] to [276000; 383000]. The bottom of the model is at -137 m+NAP. Cells are squared in the horizontal plane; column and row width are 25 m. The vertical discretization is taken from the Zeeland model. The model consists of 40 layers of variable thickness (Figure 14). Counting from top to bottom, the first layer, which contains only the higher landscape elements like dikes and dunes, has a thickness of 4.0 m[8]. Layers 2 to 11 are rather thin, 0.5 m-thick, to represent as accurately as possible the heterogeneous top system and the processes in the shallow subsurface. Thereafter, layer thickness increases stepwise: layers 12 to 21 are 1.0 m-, layers 22 to 32 4.0 m- and layers 33 to 40 10.0 m-thick.

Figure 13. The Waterdunen model domain with in the upper right corner its location in The Netherlands and delineated with red the lateral model boundaries. Source: modified from Google Maps (2013).

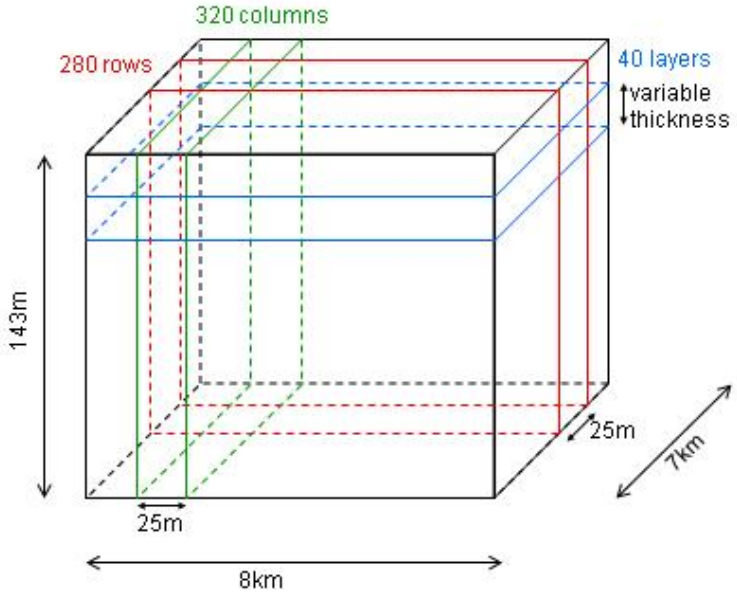

Figure 14. Spatial discretization of the Waterdunen model. The 8 km*7 km horizontal plane is subdivided in 320 columns and 280 rows, meaning the grid-cells are 25*25 m^2. In the vertical direction the model consists of 40 layers of variable thickness (set-up figure courtesy E. van Baaren).

[7] RDS stands for Rijksdriehoekscoördinaten and refers to the Dutch standard Cartesian coordinate system.

[8] Little is known about the exact vertical composition of the dikes, but it is assumed their characterization has little influence on the larger groundwater system (Pers. comm. G. Janssen, March 2013).

In Figure 15 the model domain is presented once again. The map is overlain by dashed arrows indicating the locations of the most important cross-sections and profiles used from here on. The east-west arrows run from x= 21 000 m to x=29 000 m (RDS-coordinates). On the contrary, the north-south profiles run against the coordinate system, that is to say, the slices start at y=383 000 m and end at y=376 000 m, the sea is, thus, depicted always at the left hand side.

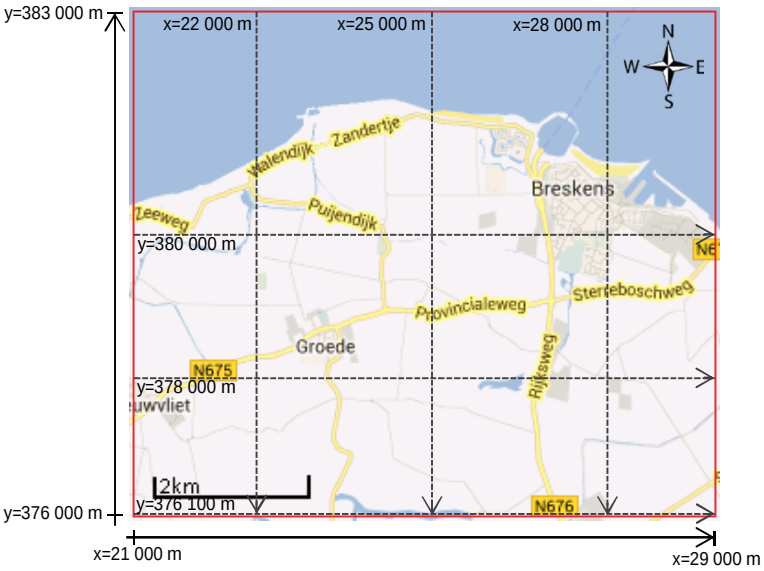

Figure 15. The dashed arrows indicate the location of the main cross-sections and profiles over the Waterdunen modelling domain used throughout this thesis. Note that the north-south arrows run against the coordinate system. Source: modified from Google Maps (2013).

Time discretization. Waterdunen is a stationary model in the sense that the stresses are kept constant in time on their long term averages. Output changes are, therefore, only the result of a changing chloride concentration (and, thus, density) field. The model is run for 100 stress periods of one year, each being subdivided in flow time steps of ten days (36 flow time steps per year). Depending on the stability criteria, MOCDENS3D further splits up these flow time steps into one to four solute time steps.

3.3 Hydrogeology

Geology. The hydrogeologic conceptualization of Waterdunen is based on the Dutch REGIS Zeeland 3D schematization (Regional Hydrogeological Information System)[9] and GEOTOP[10]. The hydrogeological base is at approximately -130 m+NAP. The Dongen and Tongeren Formations were deposited in a marine environment in the Eocene and Early Oligocene between 50 and 30 million years ago (Figure 16). These two formations consist of alternating layers of clay and sand. On top of the Tongeren Formation are the Pleistocene sands of Eem-Woudenberg and Boxtel. The Holocene deposits that follow are rather heterogeneous consisting of sand, peat and clay in variable composition. The system is topped by what in Dutch is called a *deklaag* ('cover layer'), a 4 m-thick confining layer of peat and clay deposited during alternating marine regressions and transgressions in the Holocene (Post 2004).

Deep aquifer. A comparison of Figure 16 and Figure 17 (page 29) shows that there are two major aquifers in the research area. The sands of the Dongen Formation form the deep aquifer. The aquifer has a rather low conductivity (0.1 – 1.0 m/d), but it is very extensive. Groundwater flows from the Belgian hinterlands, through this deep aquifer, to the Dutch coast. There, an upward groundwater flow forces a flux into the upper aquifer (Figure 17).

Upper aquifer. The upper aquifer dips slightly to the north-west and consists of fine to coarse Pleistocene sands (Eem Woudenberg and Boxtel Formations). Thanks to these sands the conductivity of this aquifer is high; depending on the location, the conductivity ranges between 5 and 25 m/d. The water in the upper aquifer is saline at the coast and

[9] REGIS is an open and interactive hydrogeological application system that includes data on distribution, depth, thickness and hydraulic properties of the subsoil (REGISII-DINOLoket 2008).

[10] GeoTOP is a 3D-model of the upper 30m of the Dutch subsurface that provides the user with a cell-based description of geologic, physical and chemical parameters (GeoTOP-DINOloket 2010).

becomes brackish more land inwards. The explanation for this variability is in the fact that groundwater recharge (rainfall-evapotranspiration), fresh water coming from Belgium, marine intrusion and ancient saline water mix up in this aquifer (Figure 17).

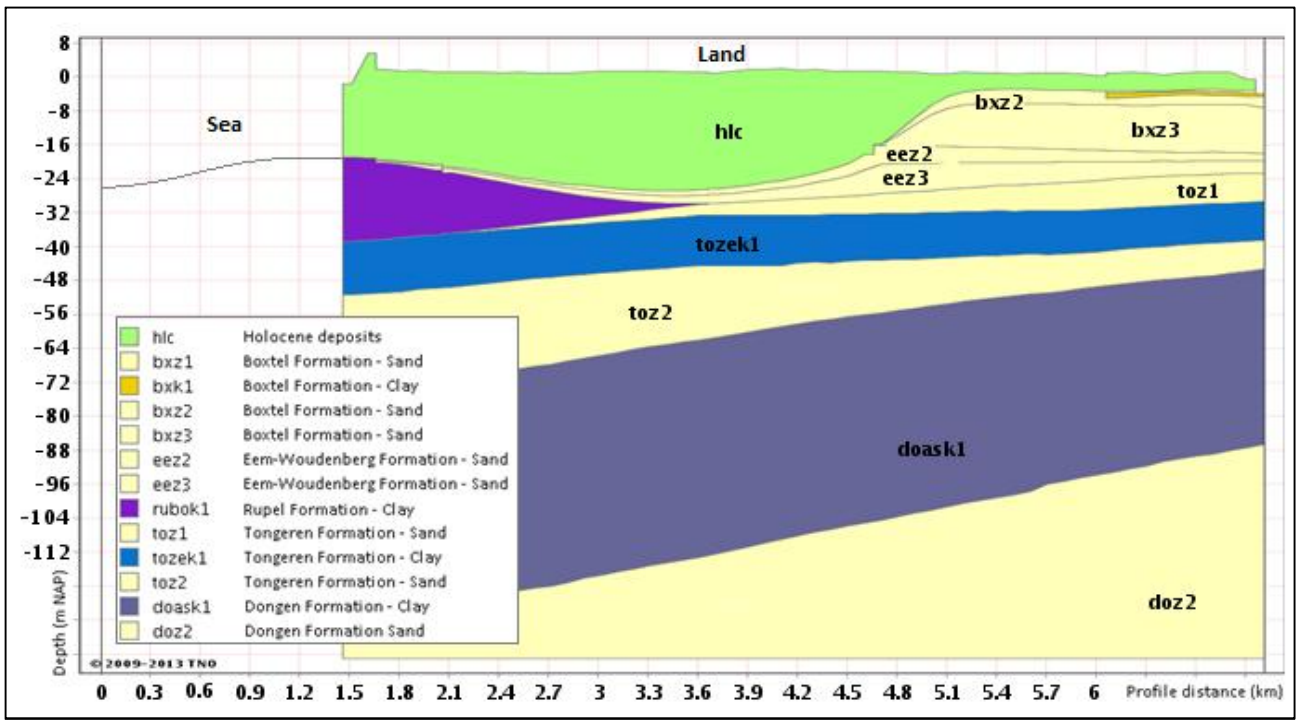

Figure 16. Geologic profile over x=25 000m (orientation map on page 28). At the research site there are two main sandy layers, Dongen Sand (doz2) and Eem-Woudenberg & Boxtel (toz2,eez3, eez2, bxz3, bxz2), separated by an alternation of thick clay formations with thin sandy layers (doask1, toz2, tozek1). Source: TNO-DinoLoket (2008).

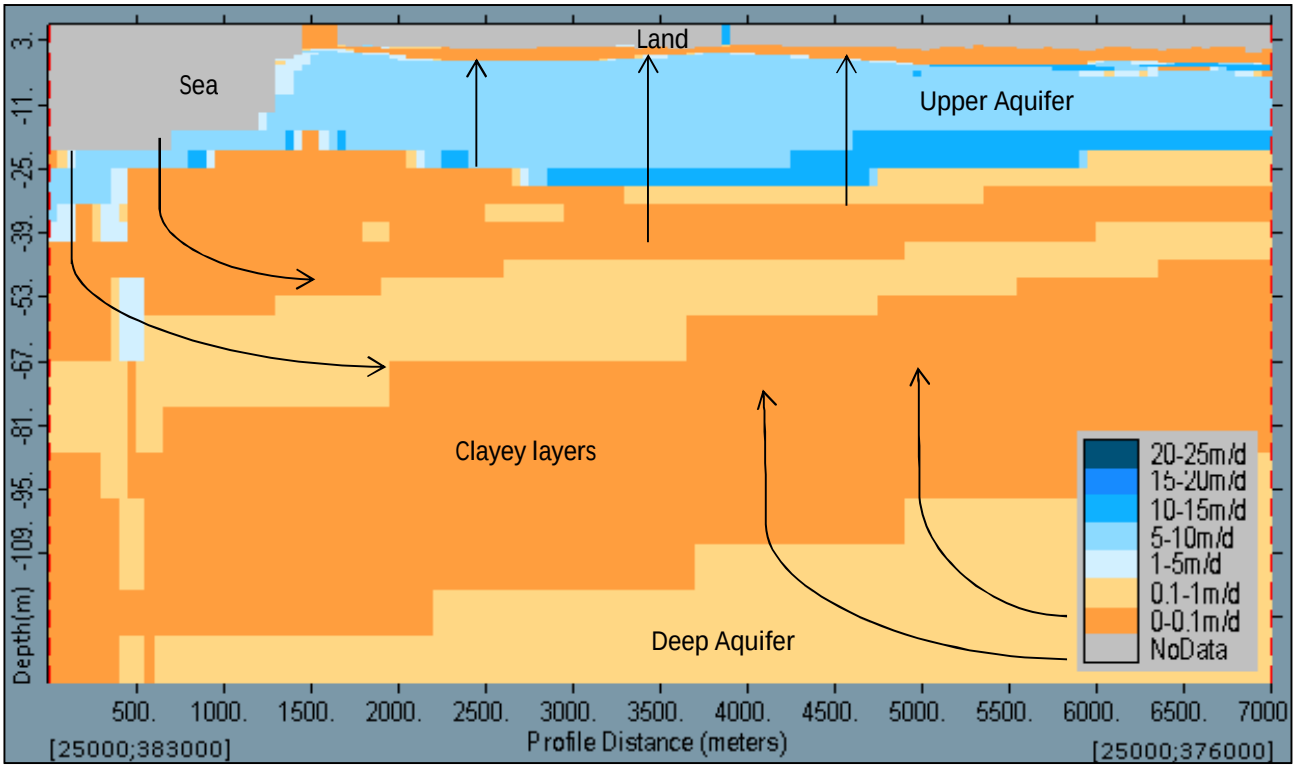

Figure 17. Horizontal hydraulic conductivity over cross-section x=25 000 m (orientation map on page 28). The so-called top layer (*deklaag* in Dutch) is almost impermeable. The upper aquifer has relatively high conductivities (5 to 20 m/d). Deeper in the model, very thick impermeable clay layers alternate with low-conductivity sandy layers. The arrows give an indication of the assumed major flow lines. There is no straightforward explanation for the 'fault' at the left hand side; it might be a numerical error in REGIS.

Tidal creeks. In the previous paragraphs the general hydrogeological characterization of the subsurface in Waterdunen was given. However, locally, highly permeable tidal creek ridge deposits have a very large influence on the groundwater system. How did these creek ridges develop? As mentioned already, Pleistocene sands were -at most places- covered by fairly impermeable clays and peat during the Holocene. However, at the location of the creek ridges, tidal channels were in place where coarse sand was deposited in. Unlike the surrounding peat and clayey marshes, these sand deposits did not subside due to drainage and poldering (Figure 18). Today, the ridges are easily recognisable in the landscape because surface elevations are up to 1.5 m higher than the surroundings (Louw, Eeman et al. 2011; Sommeijer 2013). Within the domain of the Waterdunen model, two of these creek ridges can be identified on the surface level map – see Figure 19.

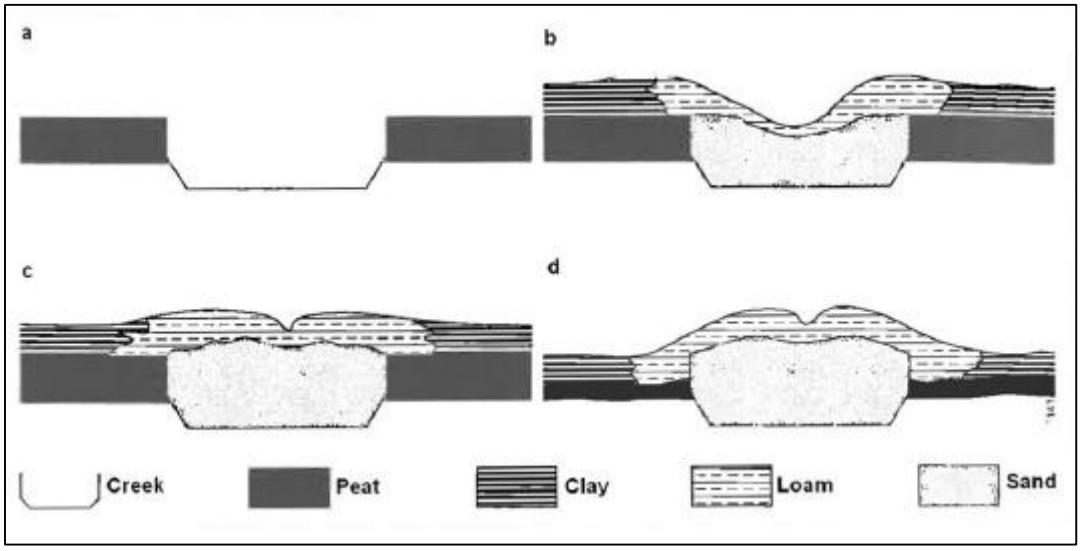

Figure 18. Development of a creek ridge, with a) incision of a tidal creek into a clayey peat layer, b) filling of the creek and covering of the top layer with new depositions, c) situation after regression of the sea, and d) situation after subsidence of the peat layer. Source: Berendsen (2005).

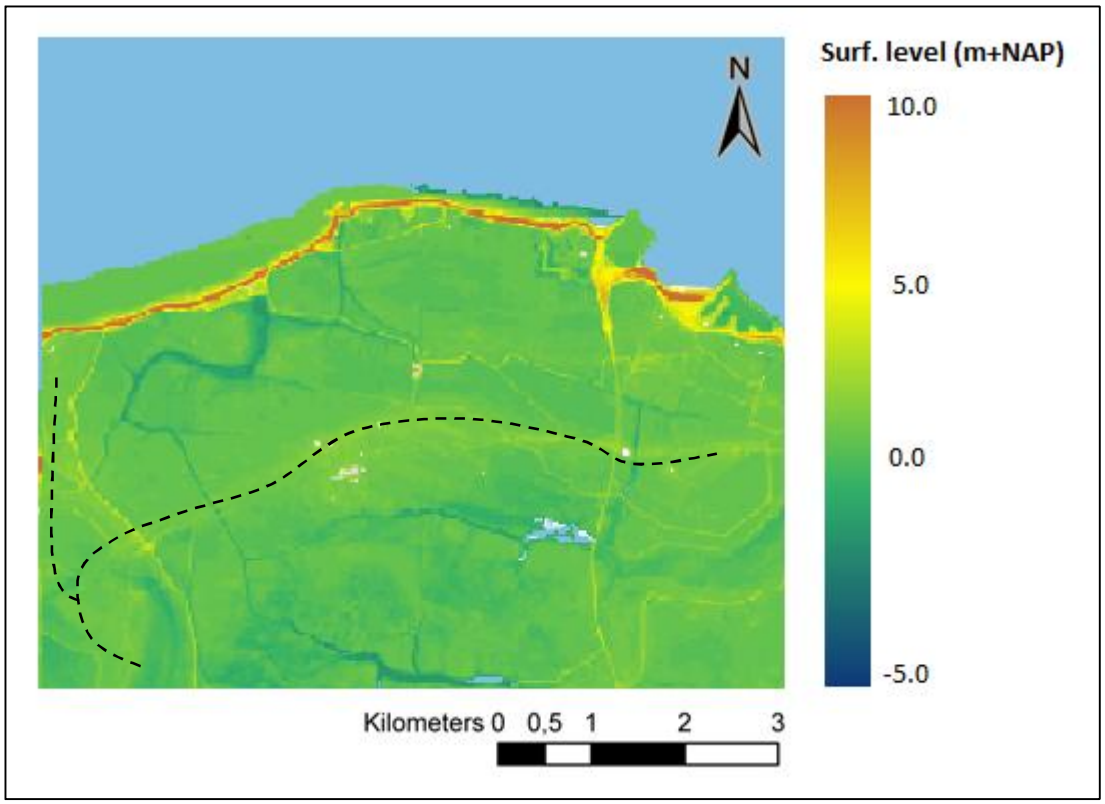

Figure 19. Hydrologic surface level (m+NAP), adapted from Geodan (2012). The yellowish-green areas indicate slightly higher altitudes and coincide with sandy creek ridges (dashed lines). In the rest of the domain, the top layers consist mainly of peat and clay.

3.4 Solute-transport

Transport parameters. In the Waterdunen model longitudinal dispersion, transversal dispersion and diffusivity were set to, respectively, 0.05, 0.005 and $8.64*10^{-4}$ m^2/d, following the findings by Stuyfzand (1993), Lebbe (1999), Oude Essink (2001b) and Vandenbohede, Houtte et al. (2009). The CFL-factor (γ), the maximum relative distance of cells to be travelled within one solute time step (see Equations (25), (26) and (27)), was set to four.

Initial concentrations. The initial concentrations are shown in Figure 20. Deep in the model water is saline with concentrations >10 000 $mgCl^-/l$. In blue are the floating freshwater lenses with concentrations similar to that of rainfall (see also Subchapter 2.1). As explained in the theoretical background, there is no sharp interface but a gradual transition between the lenses and the saline water. The lenses are separated from each other by the seepage fluxes toward (discharging) ditches and rivers. In the figure (some examples of) these separations are pointed to by black arrows; due to the upward fluxes, upconing of saline water occurs below the ditches and rivers.

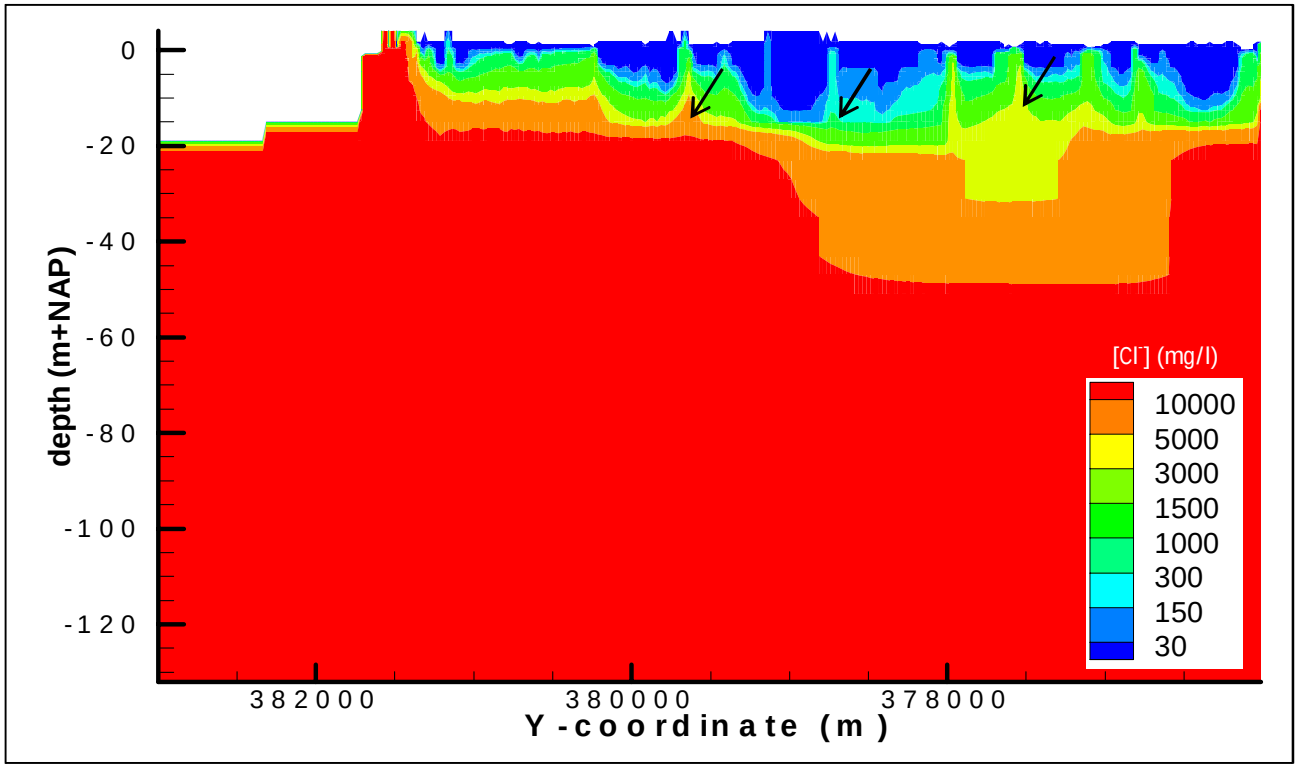

Figure 20. Initial concentrations for the Waterdunen model. Cross section over x=25 000 m (orientation map on page 28). On the left hand side is the sea, which is modelled with RIV-cells and, therefore looks 'empty'. The black arrows point to some of the locations with upconing of saline water.

3.5 Boundary conditions

GHB-package. The bottom of the Waterdunen model is a no-flux boundary. The lateral boundaries of the model are parameterized in the GHB-package with calibrated equivalent freshwater heads from the Zeeland model, output concentrations from the Zeeland model (corrected for what were considered unrealistic inversions) and a constant GHB-transmissivity of 500 m^2/d at the aquifers and 0 m^2/d at the aquitards (Janssen and Oude Essink 2012).

Top system. Following Van Baaren, Oude Essink et al. (2012), surface water bodies were classified into four types (rivers, ditches, tertiary ditches and sea), and modelled using MODFLOW's RIV-package. Location of these bodies is based on TOP10-vector data. Yearly average water levels are deducted from surface water level maps (NL: peilvakkenkaarten) provided by the local water board. The river bed resistances of the rivers, ditches and tertiary ditches was set to 2 days and the bottom of these water bodies to, respectively, 2.0 m, 0.5 m and 0.2 m below the average surface water level. Although it is known that chloride concentrations are highly variable in space and time (M. Sommeijer, pers. comm. January 2013), it is assumed that this parameter has little influence on the output of the model; the concentration of all rivers, ditches and tertiary ditches was set to 946 $mgCl^-/l$ (Table 3 on page 32).

The surface levels used to calculate the depth of the river bottoms with reference to NAP are based on AHN1 (Algemeen Hoogtebestand Nederland), the Dutch surface level database at 5*5 m^2-resolution that has been obtained by laser altimetry. To come to the hydrologic surface level, the data has been corrected for human interventions according to the TOP10-vector[11] database as described by Van Baaren, Oude Essink et al. (2011). To upscale the 5*5 m^2-data to 25*25 m^2 grid cells, the median of the related cells was calculated.

Note that the sea was also modeled with the RIV-package. The RIV-package was implemented to all sea floor cells; the cells representing the sea itself were deactivated (as was done with all cells above land surface level). The parameterization of sea floor cells was as follows: water level 0 m+NAP, sea floor resistance 208 days, concentration 18 000 mgCl^-/l and bottom according to the bathymetry (Table 3).

The characterization of the RIV-cells is defined as follows:

- Stage: average surface water level in a cell;
- Bottom: average surface water level minus the average height of the water column;
- Concentration: considered constant and equal to 946 mgCl^-/l;
- Conductance:

$$COND = \frac{wetted\ surface}{c} = \frac{(L * W + 2 * L * D)}{c} \quad (29)$$

$COND = conductance\ (L^2T^{-1})$
$L = lengthof\ the\ ditch\ or\ river\ within\ the\ cell\ (L)$
$W = width\ of\ the\ ditch\ within\ a\ cell\ (L)$
$c = resistance\ of\ the\ river\ bed\ (T).$

Herein, the wetted surface of the sea RIV-cells is equal to the area of the grid-cells. The stage, bottom, length of the rivers and (tertiary) ditches, and the width of the rivers depends on the spatial discretization.

Tile drainage. Tile drainage is applied in the model by means of the DRN-package. The presence of (agricultural) tile drainage was deducted from the map by Massop (2002); except for a ~100 m-wide strip along the coast and the village of Breskens, tile drainage was present everywhere. The depth of the drains was assumed to be 10 cm above winter water level to a maximum of -1.10 m+NAP. Please note the dependency of the average winter water level on the spatial resolution.

Groundwater recharge. A constant groundwater recharge of 186 mm/year (0.5 mm/day) with a concentration of 20 mgCl^-/l is applied to the model. These values are based upon calculations performed by Courtens, Vandenbohede et al. (2011), wherein reference evapotranspiration was subtracted from the average precipitation.

Table 3. Parameterization of the surface water bodies (rivers, ditches, tertiary ditches and sea) implemented by means of the RIV-package.

Surface water type	[Cl^-] (mg/l)	Resistance (days)	Width (meters)	Bottom (m below average water level)
rivers (NL: rivieren)	946	2	Based on the amount of 5*5 m^2-cells crossed by the river within the grid-cell	2.0
ditches (NL: sloten)	946	2	3	0.5
tertiary ditches (NL: greppels)	946	2	2	0.2
sea (NL: zee)	18 000	208	Wetted surface = area grid-cell	Based on bathymetry

[11] Digital topographic database developed by the Dutch national land register.

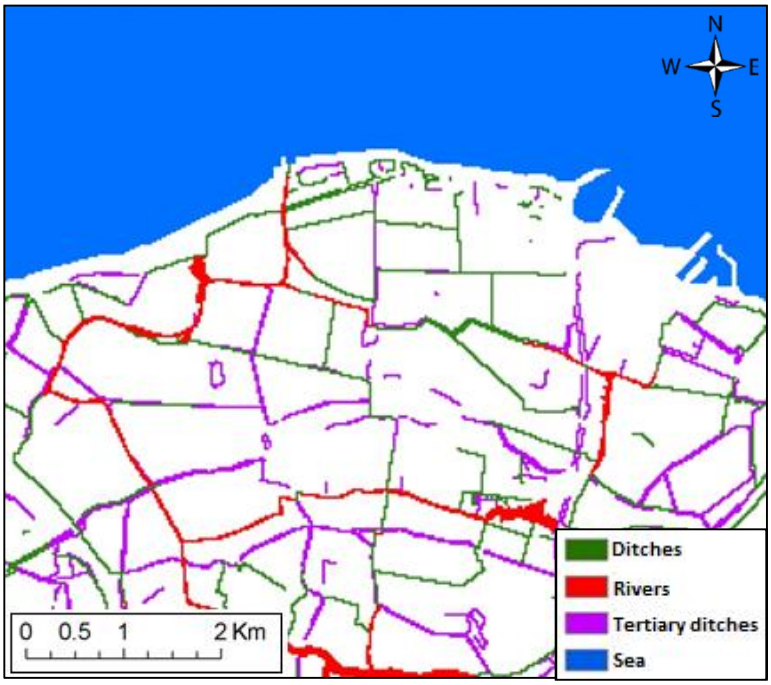

Figure 21. Classification of surface water bodies present in the Waterdunen modelling domain that have been implemented by means of the RIV-package.

3.6 Synthesis

The main characteristics of the Waterdunen model are summarized in Table 4. The parameter values as they are presented in this table define the reference simulation.

Table 4. The Waterdunen model: properties and parameters (reference situation).

Parameter	Value
model area	8 km*7 km=56 km^2
horizontal discretization	25 m
vertical discretization	0.5 – 10 m, thickness increases with depth
bottom	hydrological base, -137 m+NAP
total number of cells	3 584 000
number of active cells	2 944 049
groundwater recharge	186 mm/year (constant)
stress period length	1 year
total number of stress periods	100 (=100 years)
flow time step (fts) length	~10 days (36 fts/year)
solute time step (sts) length	2.5 – 10.0 days (automatized)
number of solute particles per cell	4
porosity	0.3
anisotropy kh/kv	1.0
longitudinal dispersion factor	0.05
transversal dispersion factor	0.005
diffusion factor	$8.64*10^{-4}$ m^2/d

CHAPTER 4: METHODOLOGY

The core of this research consisted of a sensitivity analysis applied to the Waterdunen model. To come to that analysis, first a reference simulation was prepared and the parameters to be included in the analysis were identified. This chapter follows the chronologic development of the research. First, the preparation of the reference simulation is described (4.1) and the parameters to be analysed are presented (4.2). The third subchapter is then dedicated to the sensitivity analysis itself. At the end of the chapter, in 4.4, a short note is included on the software used.

4.1 Reference simulation

In order to answer the research question, a series of sensitivity simulations was performed. To analyse the output of these sensitivity simulations a reference simulation had to be defined and described. To that end, the Waterdunen model, as it was used in November 2012, was checked and adjusted.

First of all, some small inconsistencies and errors were taken out of the model. Thereafter, decisions were taken concerning the number of flow time steps and advection particles to be used. The highest possible precision was pursued provided that the runtime for 100 stress period of one year was kept acceptable for the sensitivity analysis. In total 34 preliminary runs were needed to come to the reference simulation used in the research. The characterization of that reference simulation is given Chapter 3 – The Waterdunen Model.

The output of the reference simulation was then extensively analysed and described in Subchapter 5.1. The following output was included in this analysis:

- the freshwater lens thickness (threshold value 1 000 $mgCl^-/l$);
- the equivalent freshwater heads;
- the chloride concentration distribution;
- the effective groundwater flow velocities in the direction of the x, y and z coordinate axes;
- the general streamline pattern;
- the thickness of the mixing zone (by means of the thickness of the 30 $mgCl^-/l$, 1 000 $mgCl^-/l$ and 1 500 $mgCl^-/l$ freshwater lenses, and the location of BMix and Dmix);
- the characterization of solute-transport (constraining criterion, number of solute time steps per flow time step and the location of cell limiting the time discretization);
- the runtime of the model; and,
- the cumulative volume (water) and mass (chloride) balances.

Besides, to have an idea about the accuracy of the model, the modelled freshwater lens thickness was compared with observations derived from measurements performed by Buma (2010). These measurements consisted of 14 electrical cone penetration tests (ECPTs) collected on February 23, 2010. The measured electrical conductivities were translated to concentrations using the formulas proposed by Louw, Eeman, et al. (2011) for the Dutch south-western delta (Equation (30)), and Equation (31), which is provided with the ECPT measurement device (CMA N.D.) (see also Figure 22).

$$[Cl^-] = (EC_w * 0.36 - 0.45) * 1000 \quad (30)$$

$$[Cl^-] = EC_w * 500 \quad (31)$$

$[Cl^-] = chloride\ concentration\ (mgCl^-/l)$
$EC_w = electrical\ conductivity\ water\ (mS/cm)$.

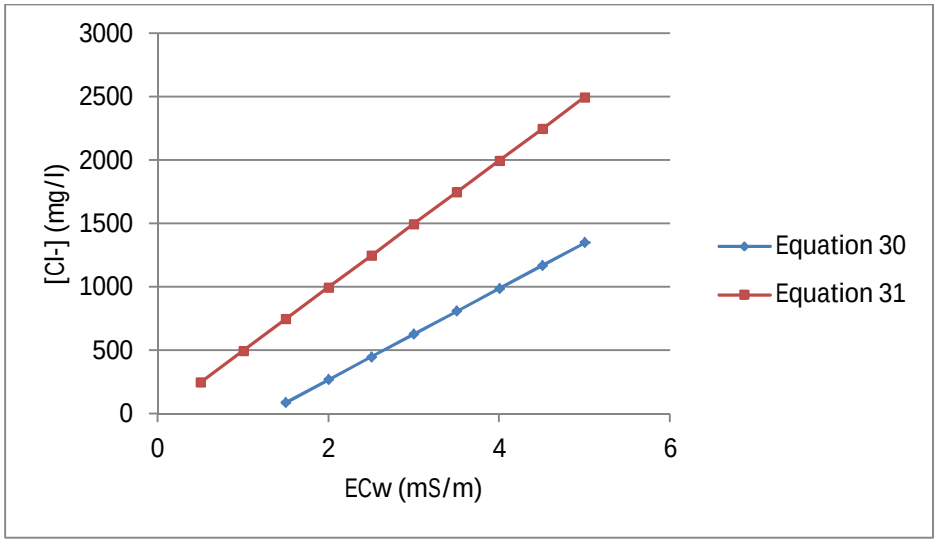

Figure 22. Graph depicting the relation between the two conversion formulas used to calculate chloride concentrations based on electrical conductivities. Equation 30 was developed by Louw, Eeman, et al. (2011); Equation 31 is provided with the ECPT measurement device (CMA N.D.).

4.2 Choice of parameters

The choice of the parameters to include in the study was based on peer reviewed articles, variable density modelling reports, an exploratory sensitivity analysis and expert judgment. Priority was given to those physical parameters that are rather uncertain and numerical parameters that are questioned most. The parameters chosen are listed in Table 5; the main reasons to look at these parameters are given in the subsequent paragraphs.

Physical parameters	Numerical parameters
Groundwater recharge (L/T)	Transmissivity GHBs (L^2/T)
Concentration rivers (M/L^3)	Discretization drainage system
River bed resistance (1/T)	Number of flow time steps
Sea floor resistance (1/T)	Number of advection particles
Effective Porosity (-)	CFL-factor
Dispersion factor (L)	

Table 5. Physical and numerical parameters looked at in the sensitivity analysis.

Groundwater recharge. Groundwater recharge was looked at because it was unclear how the value use in the Waterdunen model was exactly obtained. It was, amongst others, unclear whether direct run-off, the type of crops grown in the area and the agricultural practices were taken into account. Eeman, Leijnse, et al. (2011) found that precipitation had a large influence on the transition zone of shallow freshwater lenses and Cobaner, Yurtal, et al. (2012) showed that variable density groundwater flow models are very sensitive to groundwater extraction. The question remained to which extent the dynamics of a system of large freshwater lenses are susceptible to changes in groundwater recharge.

River concentrations. Sommeijer (2013) showed that the variability in chloride concentration in the ditches in Zeeland is high in space and time. However, no information could be found on how these river concentrations influenced the underlying groundwater system.

River bed resistance. In day-to-day modelling (consultancy companies) usually use river bed resistances somewhere between 0 and 10 d for individually modelled surface water systems. In his hydrogeological overview, Bot (2011) presents values between 0 and 5 days for well-maintained ditches in clayey soils. In the Waterdunen model a c=2 d was used. Little is known about river bed resistances (Jousma and Massop (1996) and Massop and Gaast (2006)), but even less is known about the impact of the parameter in variable density groundwater flow modelling. The variability in the values, in combination with an alleged sensitivity, provided reason enough to have a look at how the Waterdunen model reacts to variations in this parameter.

Sea floor resistance. In the Waterdunen model an arbitrarily chosen value of 208 days was attributed to the sea floor resistance. Modellers claim that this value has little influence, at least as long as the time scales are in the order of decennia to centuries, on the development of the groundwater system. Since I considered the value extremely high and I could not find any literature on the topic, I decided to include this parameter in the sensitivity analysis.

Effective porosity. It is normal amongst groundwater modellers to use just an average value for effective porosity in groundwater modelling. In 'normal' freshwater groundwater modelling this procedure seems to be fine; however, it is unclear what the influence of effective porosity is on the output of variable density groundwater flow models.

Dispersion factor. Contrary to the previously presented parameters, quite some research has already been done on the dispersion factor. Diersch, Prochnow et al. (1984), Holzbecher (1998) and Vandenbohede (2004) have shown that (both longitudinal and transversal) dispersion plays an important role in various salinization processes. Unfortunately, as Konikow (2011) explains, the estimation of the dispersion factor is problematic; the costs are high and, although the values might be indicative for the scale and duration of tracer tests, the estimates often have little value in modelling over longer times and distances. An extra difficulty results from the fact that the dispersion factor is a kind of rest term to correct for averaging out processes that occur at scales smaller than the one used in the numerical model.

Transmissivity GHBs. It is just a fact that setting adequate boundaries in groundwater modelling is very important and very difficult (Jakovovic, Werner et al. 2011); no one modeller will ever contradict that. Obviously, modellers try to set model boundaries at such a distance from the interest area that their influence is minimalized; however, they do not always manage. In the case of GHB-conditions[12], it are not only the boundary states itself that have to be set, but also the magnitude of the influence that these conditions have on the modelling domain. This is done by means of a GHB transmissivity. Since the Waterdunen model is a childmodel of the much large Zeeland model, the equivalent freshwater heads and chloride concentrations at the model boundaries are reasonably well-known. However, the order of magnitude that should be attributed to the GHB transmissivity is difficult to determine

Discretization of the drainage system. In deltaic areas most (tertiary) ditches drain the subsoil. For that reason, the top system has often a large impact on the outcome of groundwater models. Unfortunately, however, the data availability on these top systems is usually rather limited. Even when the location of the surface water bodies and tile drains is known, the characterization of these features remains difficult. Often, data is rather coarse. For the mentioned reasons, it turned out during discussions with experts that there is a genuine interest in the effect of the topsystem's resolution on the output of the model.

Number of flow time steps. As described in the theoretical background, there has to be a regularly feedback between the chloride concentration and the Darcian velocity fields. However, 'regular feedback' is not further defined. In MOCDENS3D the time discretization for solute-transport is automatized based on the Neumann, Mixing and CFL Criteria (see Section 2.3.4). Yet, modeller has to decide how often the Darcian velocity field has to be recalculated. The MOCDENS3D Users' Manual states that the duration of the flow times steps (stress period divided by the amount of flow time steps) should be chosen based on expert judgment and trial and error. An exploratory sensitivity analysis showed that the number of flow time steps can have a very large influence on freshwater lens thickness. A final reason to have a look at the number of flow time steps is in the runtime. Increasing the number of flow time steps leads to an extreme increase in runtime.

Advection particles[13]. Theory states that a high number of advection particles is very important to ensure accuracy of the mass balances when modelling solute-transport. However, as with the number of flow time steps, a higher number of advection particles leads to extreme increases in model runtimes.

The CFL-factor was looked at just for my own interest. In the reference simulation the CFL-factor was set to 4, which means that the maximum distance that advection particles are allowed to travel during each solute time step is four cells. I thought this was a rather large distance and, therefore, decided to include the parameter in the sensitivity analysis.

[12] As described in the theoretical background the boundary conditions in MOCDENS3D have to be set by means of the GHB-package.

[13] Refer to the theory on solute-transport for an explanation advection particles and the CFL-factor.

4.4 Analysis sensitivity runs

To answer the so-called "what if"-questions (Oreskes 1994), 28 sensitivity simulations were performed. As with the reference simulation, the sensitivity cases were run for a total of 100 stress periods of one year. The ranges of the parameter values that were studied are listed in Table 6.

Parameters	Reference value	Range
Groundwater recharge	186mm	139.5mm (-25%) – 232.5mm (+25%)
Concentration rivers	946 $mgCl^-/l$	662 $mgCl^-/l$ (-30%) – 1261 $mgCl^-/l$ (+30%)
River bed resistance	2 d	0.5 d – 4 d
Sea floor resistance	208 d	1.25 d – 208 d
Effective Porosity	0.3	0.2 – 0.5
Dispersion factor (long/trans)	0.05/0.005	0.005/0.0005 – 0.5/0.05
Transmissivity GHBs	500 m^2/d	0 m^2/d – 2 000 m^2/d
Discretization drainage system	25*25 m^2	25*25 m^2 – 100*100 m^2
Number of flow time steps per stress period (one year)	36	1 – 73
Number of advection particles	4	1 – 27
CFL-factor	4	0.8 – 4

Table 6. Reference values and ranges used in the sensitivity analysis. For the exact characterization of all simulations refer to Appendix H.

The output of the sensitivity simulations was analysed in comparison with the reference simulation:

- the difference in freshwater lens thickness was mapped;
- the difference between the states of the sensitivity simulations and the reference simulation were analysed over cross sections z=-0.50 m, z=-75 m, x=25 000 m and y=376 100 m. When based on this output or based on the map with the differences in freshwater lens thickness it was thought useful to look at other locations, extra cross-sections were made;
- the streamlines of the sensitivity simulations were compared with the streamlines of the reference simulation by eye;
- the difference in the characterization of the mixing zone was looked at by plotting freshwater lens thicknesses as a function of the threshold value used for freshwater lens thickness, and the location of BMix and DMix in one graph;
- the change in model runtime was looked at by means of relative differences; and,
- the cumulative volume and salt balances were compared by means of relative differences expressed in percentages.

4.2 Software

As described in the theoretical background, the MOCDENS3D-code was used to model the variable density groundwater flow in Waterdunen. The MOCDENS3D output was translated into freshwater lens thickness and prepared to be visualized in other programs with a variety of processing tools written in Pascal. Amongst others, these processing tools enabled the calculation of freshwater lens thickness, the alteration of the coordinate system and the production of movies. The analysis of the data was done in TECPLOT (Tecplot Inc.), iMOD (Deltares), ArcMAP (esri) and MS Excel 2010 (Microsoft).

CHAPTER 5: RESULTS & ANALYSIS

In this chapter the research results are presented and analysed. For reading ease the chapter is subdivided in two subchapters. The first, Subchapter 5.1 addresses the output of the reference simulation (refer to Chapter 3 for the set-up and parameterization) and is therefore crucial: the sensitivity analysis only makes sense in light of this reference output. In Subchapter 5.2 the results of the sensitivity analysis are discussed.

5.1 Reference simulation

As mentioned above, in this subchapter the output of the reference simulation is presented. However, it starts out with a small intermezzo on the time it takes for the model to reach a dynamic equilibrium state. Only thereafter the following output of the reference simulation is presented:

- the chloride concentrations;
- the freshwater lens thickness, including a comparison with observed values;
- the equivalent freshwater heads;
- the effective pore groundwater flow velocities along the X, Y and Z coordinate axes;
- the transport characterization and the runtime; and, finally,
- the cumulative mass and solute balances.

Note that for clarity purposes many horizontal and vertical cross-sections and profiles are included. Although extra maps and cross-references have been included it might be handy to refer to Figure 15 on page 28 for orientation purposes.

Dynamic equilibrium. The reference simulation refers to the run with 100 stress periods of one year. However, to check how long it takes for the model to reach a dynamic equilibrium the model was run once for 250 years. The chloride distributions of that calculation are given in Appendix C. The cross-sections presented there show that the present system does not reach a dynamic equilibrium neither after 100 years (reference simulation) nor after 250 years. The curve presented in Figure 23 confirms that finding. The total amount of fresh water present in the model is still increasing after 250 years. However, the curve also shows that it probably will not take much longer for such a dynamic equilibrium to be installed. It is plausible that a stable situation will be in place after 500 years.

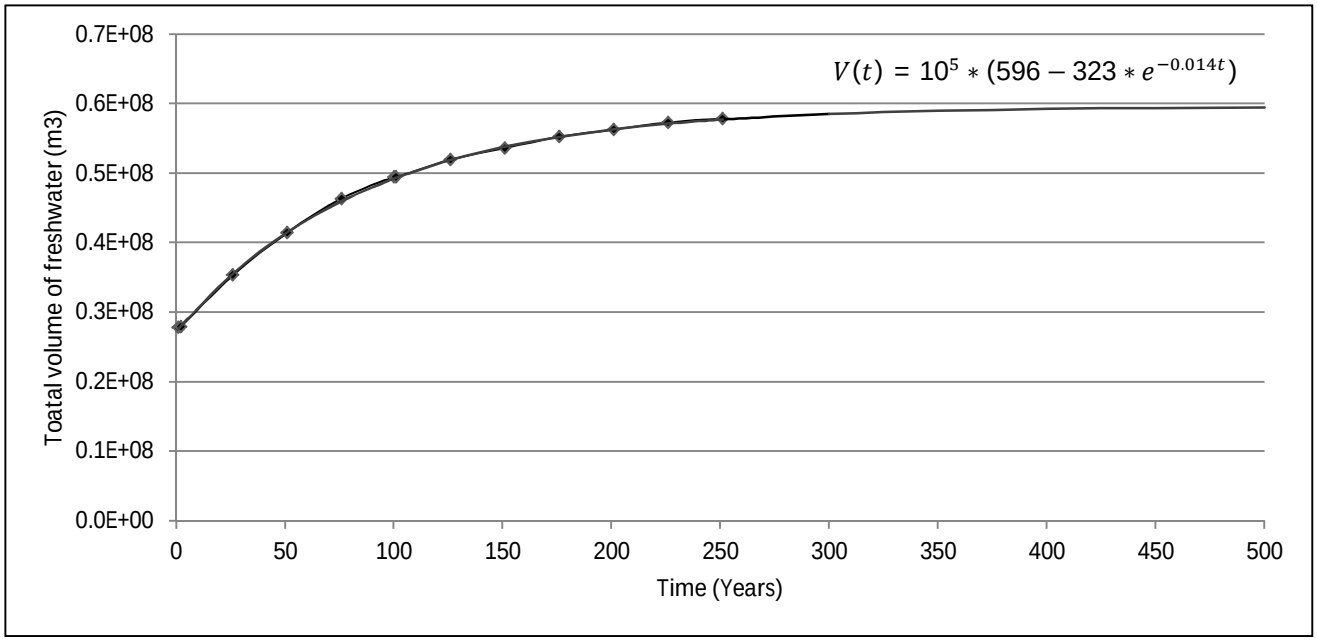

Figure 23. Time plot showing the development of the total volume of fresh water stored in lenses, including a trendline to determine how long it will take to reach an equilibrium.

Please note that from this point onwards, the output of the reference simulation –so after 100 stress periods of one year- is dealt with.

Chloride concentrations. Figure 24 gives an overview of the output chloride concentrations of the reference simulation. In plots A and B one can see freshwater lenses, with concentrations as low as that of rainwater (<30 mgCl$^-$/l), floating on top of highly saline groundwater. In the same two plots, the light-blue and light-green vertical cones in between the lenses identify upward seepage. Due to the artificially maintained low drainage levels in the surface water bodies, groundwater is discharged toward the rivers and (tertiary) ditches (see also Figure 28 on page 32). A pattern arises as if one were looking at a duvet with stitched compartments: drainage ditches subdivide a large freshwater body into freshwater lenses. Meanwhile, the larger the distance between the ditches, the thicker the freshwater lenses are.

Two important deviations from the previous pattern can be identified. At the coast locally high salinity also occurs in the top layers, e.g. see the red-spots pointed to by the arrows in plot C of Figure 24. Furthermore, it turns out that the thickness of the freshwater layer near the lateral boundaries is much thinner than in the core of the model (e.g. inland southern boundary in plot B of Figure 24).

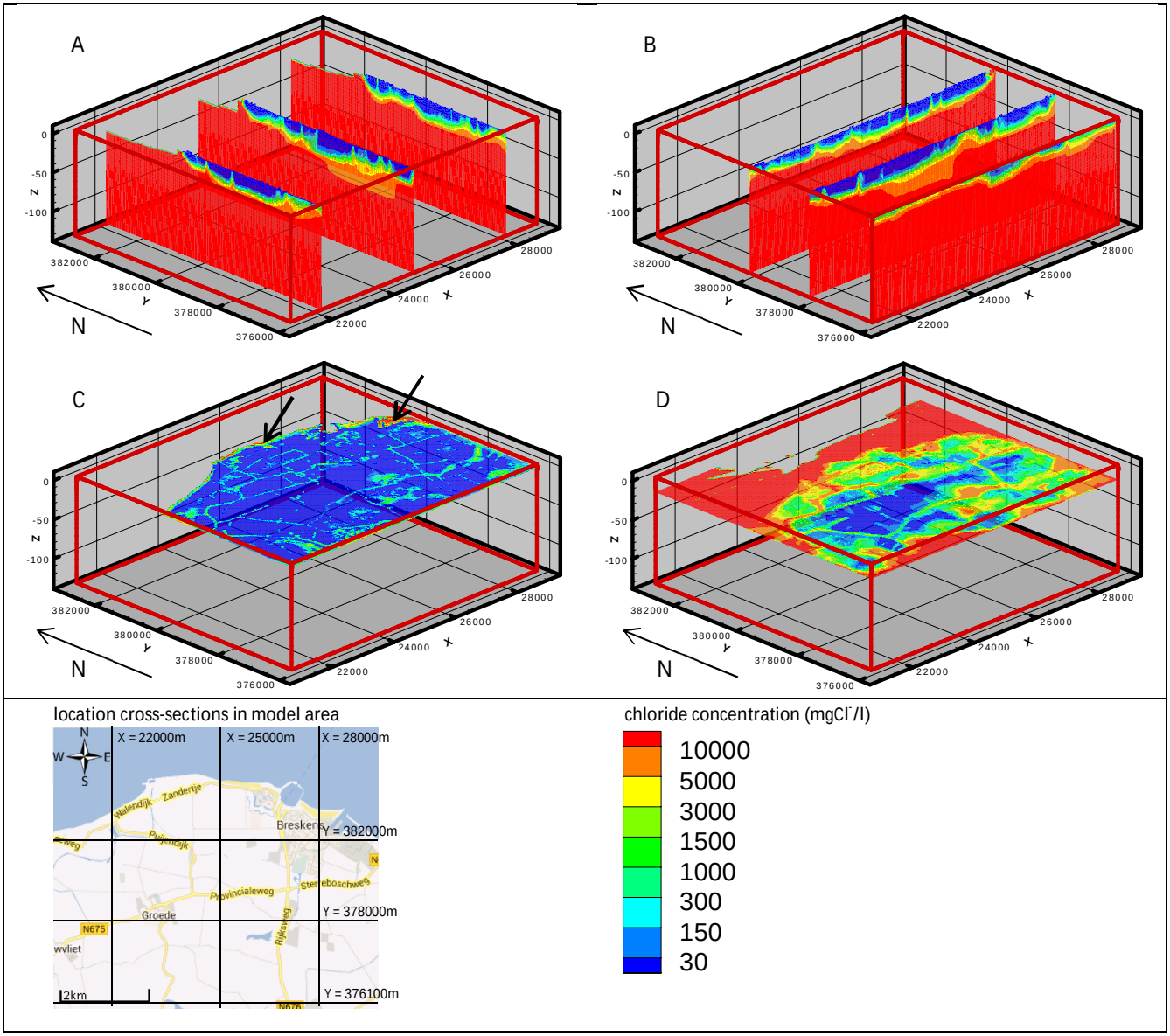

Figure 24. Distribution of the chloride concentration: A) the north-south cross-sections over x=22 000 m, x=25 000 m and x=28 000 m give an indication of the chloride concentrations in the core of the model, B) the east-west cross-sections over y=376 100 m, y=378 000 m and y=380 000 m shows that freshwater lenses (<30 mgCl$^-$/l) become thinner near the lateral model boundaries, C) the horizontal cross-section over z=-0.50 m+NAP shows marine intrusion (black arrows) and the presence of freshwater in the top layers, and D) the horizontal cross-section over z=-15.00 m+NAP clearly shows the location of the deepest freshwater lens.

Freshwater lens thickness. In this research, as mentioned in the theoretical framework, the threshold value to calculate freshwater lens thickness is 1 000mgCl$^-$/l. The obtained spatial distribution of lens thicknesses is depicted in Figure 25 on page 40. In the middle of the map it is easy to identify the (from now on referred to as) 'Large Central Freshwater Lens': a large freshwater lens with a thickness of ~30 m in the centre of the modelling domain. The thickness of most other deep lenses varies between 15 and 30 meters.

To analyse the impact of the 1 000 mgCl$^-$/l threshold value, freshwater lens thickness was also plotted as a function of the 1 500mgCl$^-$/l (Figure 26 on page 41) used by the Province of Zeeland (see also Table 1, Page 14). A comparison between the red and green line in Figure 26 turns out that the difference between the calculated freshwater lens thicknesses for the two threshold values is negligible.

Figure 26 also provides some handles to characterize the transition zone[14]. Mixing at the bottom of the deep lenses seems to be linearly correlated with the thickness of the lens (cf. the 30 mgCl$^-$/l-line is always more or less at 2/3 of the 1 000-1 500 mgCl$^-$/l-line). The distance between the 30 and 1 000-1 500 mgCl$^-$/l-lines ranges between 7 and 12 meters. Thinner lenses show relatively more mixing. When looking at BMix, DMix (dotted lines) and WMix it is noticeable that the concentrations up to a 500 m model inwards from the southern model boundary (profile distance 6 500 to 7 000 m) seem to hang strongly to the sharp transition zone defined in the GHB-package; though not presented here, the same applies for the eastern and western boundaries.

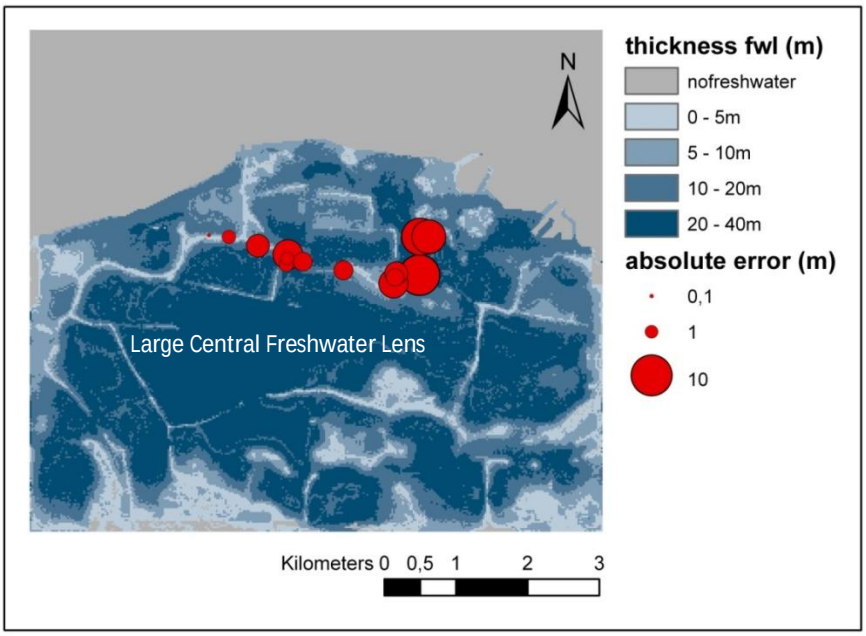

Figure 25. Map showing freshwater lens thicknesses in different shades of blue. The red dots indicate the location of measurements; their size is linearly correlated to the absolute error between the modelled and observed thickness of freshwater lenses.

Observed. In Figure 25 and Figure 27 (page 41) the modelled freshwater lens thickness is compared with observations. The two figures clearly show that the observed and modelled values are statistically independent, and that the misfit is rather large. Note, however, that differences of up already 20 m were obtained in the observed freshwater lens thickness depending on the formulas used to process the field data (Table 7 on page 41). There is a large uncertainty associated with the conversion from electrical conductance (the measured variable) to chloride concentrations. The absolute difference between the modelled and observed (using Equation (31)) freshwater lens thickness varies between 0.1 m and 9.9 m for a threshold value of 1 000 mgCl$^-$/l. The absolute mean error (MAE) equals 3.7 m and the root mean square error (RMSE) 4.7 m. Furthermore, note that the observations are concentrated in a very small part of the model domain, close to a large drainage ditch.

[14] Refer to Section 2.1.2 for the theoretical background on the characterization of the transition zone.

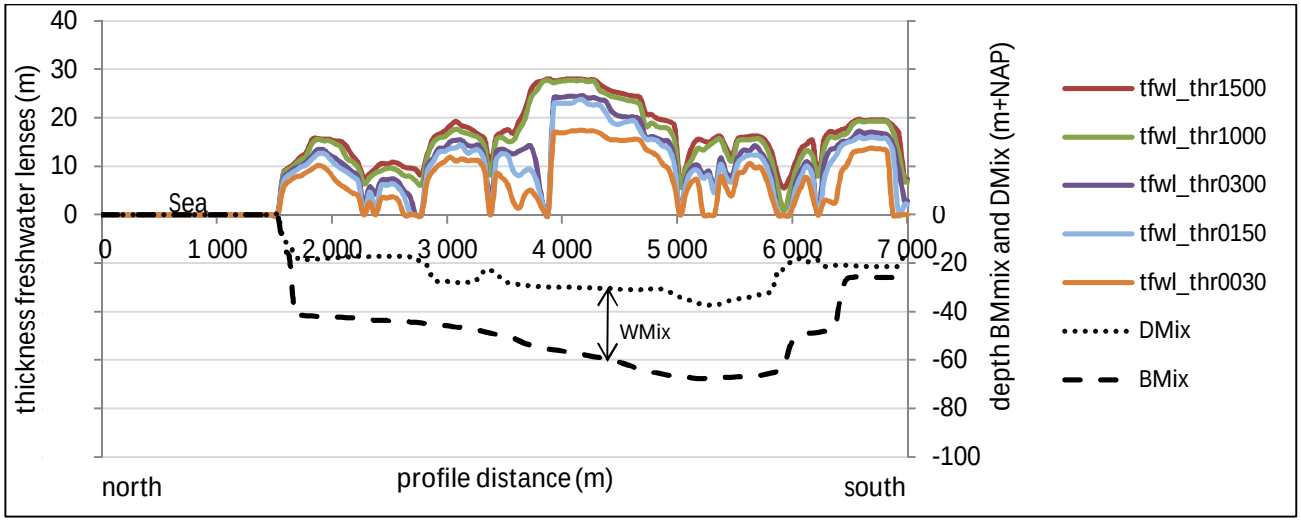

Figure 26. Freshwater lens thickness as a function of the chloride concentration threshold value (coloured lines), and an indication for the extent of the transition zone (dashed lines) over cross-section x=25 000 m (middle cross-section of plot A presented in Figure 24 on page 39). Following the characterization proposed by Eeman et al. (2011), BMix indicates the bottom of the mixing zone and DMix the centre of the mixing zone; WMix stand for the distance between BMix and DMix (see also section 2.1.1).

Table 7. Observed freshwater lens thickness (m) obtained using Equations (30) and (31) described on page 34; the difference (m) in freshwater lens thickness obtained with the two conversion equations; the modelled freshwater lens thickness (m); and the difference (m) between the modelled and observed (using Equation (31)) freshwater lens thickness.

Obs. nr.	x	y	Observed (m)		Difference (m)	Modelled (m)	MOD-OBS (m)
			Eq. (30)	Eq. (31)	Eq. (30)-Eq. (31)		Using Eq.(31)
1	24585	379724	16.4	14.6	1.8	15.8	1.2
2	24597	379812	20.4	12.5	7.9	11.5	-1.0
3	24603	379866	15.6	11.8	3.8	6.5	-5.3
4	24817	379769	28.0	8.0	20.0	5.9	-2.1
5	23782	380115	9.0	6.6	2.4	7.7	1.1
6	23504	380141	9.6	8.1	1.5	8.0	-0.1
7	26080	379463	21.0	12.2	8.8	7.2	-5.1
8	26104	379549	21.0	10.4	10.6	8.6	-1.8
9	26453	380115	6.6	5.6	1.0	13.9	8.3
10	26573	380115	5.4	4.6	0.8	11.4	6.8
11	26119	379605	10.0	7.4	2.6	10.5	3.1
12	26444	379579	9.4	7.6	1.8	17.5	9.9
13	24188	379991	24.0	7.4	16.6	10.5	3.1
14	25380	379647	8.6	8.2	0.4	6.0	-2.2

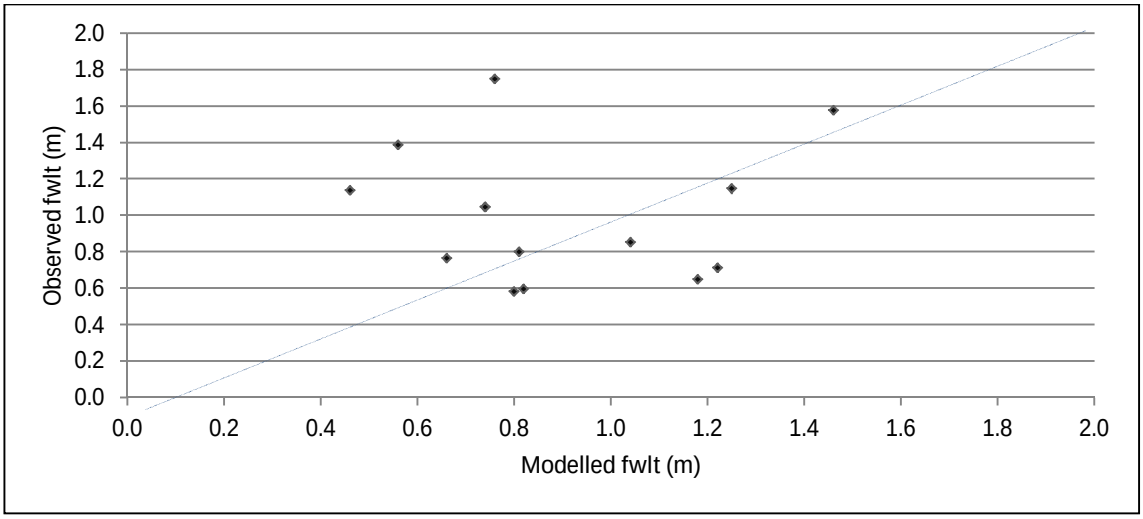

Figure 27. Comparison of the modelled freshwater lens thickness with the observed values. In blue the identity line. The plot clearly shows that there is no statistical dependency between the observed and the modelled values.

Head distribution. Figure 28 shows that in the deep aquifer isohypses for the equivalent freshwater heads run almost horizontal and parallel to each other. There, equivalent freshwater heads are mainly determined by altitude and by the chloride concentrations induced by the proximity of the sea (see also Figure 24 on page 39). The very small inclination of the isohypses is related with the gradual decrease of the buoyancy factor land inwards. The bends in the isohypses-pattern at y≈382750 m coincide with the 'fault' in Figure 17 on page 29. There is nothing known about a geologic fault at that place, so probably this is a numerical error in REGIS.

In the upper aquifer, the previous pattern is overruled by other (external) stresses. More precisely, groundwater recharge together with the drainage system seems to have a large influence. At and up to~30m below these ditches, heads are~0.50 m below the average head at surface level. As a consequence, below the ditches an elliptical pattern of isohypses arises and streamlines converge at these outlets.

In the clayey layers, the flow direction is mainly vertical, being upward or downward depending on whether either the head gradient or the buoyancy factor is dominant (cf. Equation (9) on page 17, and Appendix A). Since the magnitude of these terms is very close to each other but with opposed signs, the result is highly location specific. At location A, for example, the buoyancy factor ($1.96E^{-2}$) exceeds the head gradient ($-1.70E^{-2}$) leading to a downward flux. In B, it is the other way around; the magnitude of the head gradient ($-1.98E^{-2}$) exceeds buoyancy ($1.91E^{-2}$) and, therefore, the flux is upward (refer to Appendix D for the calculations).

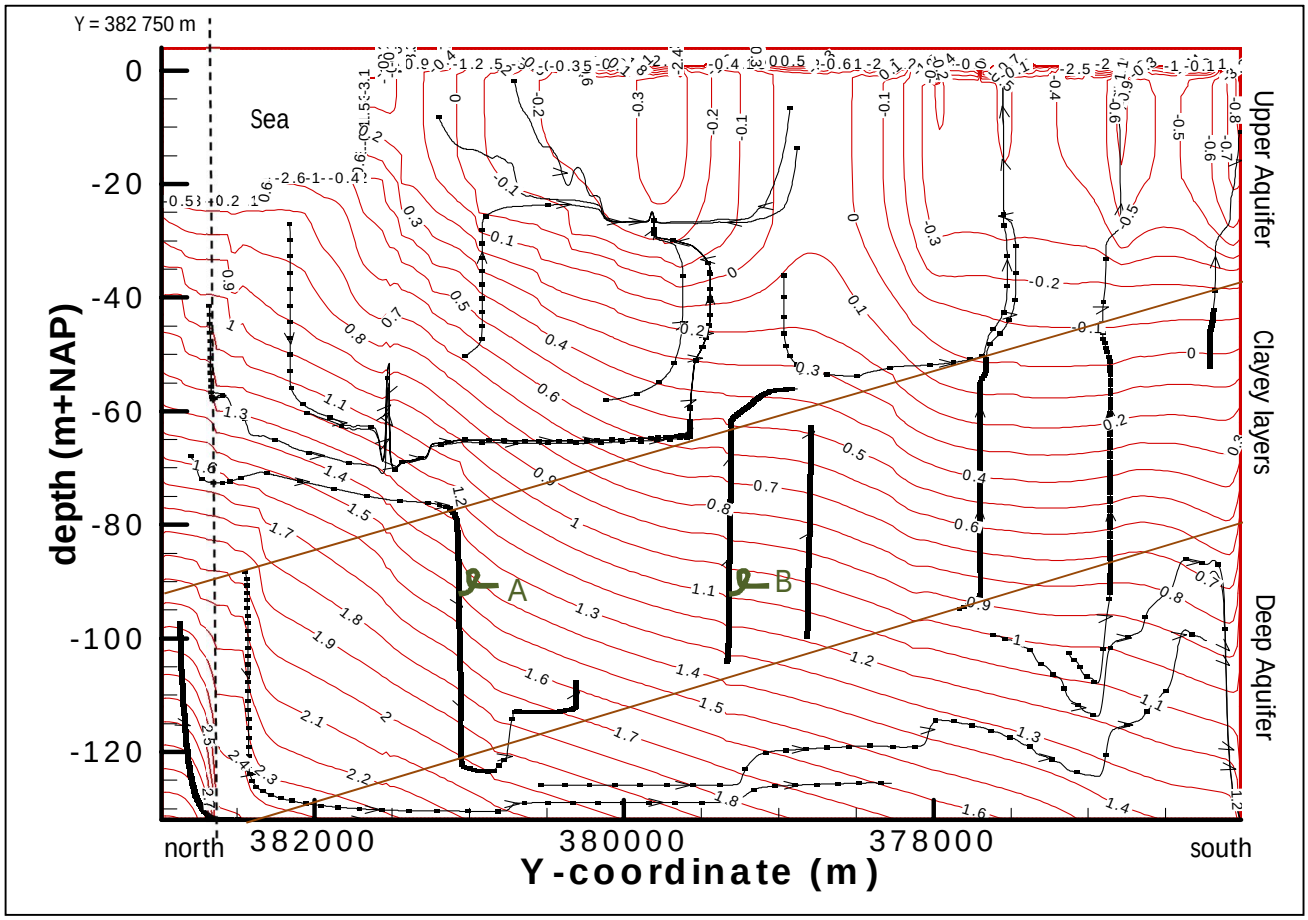

Figure 28. Isohypses and a set of streamlines over cross-section x=25 000 m (middle cross-section of plot A presented in Figure 24 on page 39). The distance between two subsequent dots stands for 1000 years of flow. In the upper aquifer velocities are up to several meters per year and therefore, at some locations, almost no dots area visible; in the clayey layers, velocities are in the order of 0.001 mm/year and, thus, the dots form one thick line (compare also with the geology in Figure 16 on page 29) . The arrowheads indicate the flow direction. Streamlines are not perpendicular to isohypses because a) depth is exaggerated and b) density differences affect vertical velocities by means of the buoyancy factor.

Velocity field. The dark blue and red patchwork of horizontal Vx- and Vy-velocities (surrounded by yellowish-bluish colours) in Figure 29 on page 43 can be explained by the interaction between soil conductivity and drainage. The areas with high velocities (red and blue) in cross-sections Vx z=-0.50 m and Vy z=-0.50 m correspond with higher altitude areas build-up by highly conductive sands, i.e. dunes and creek ridges (see Figure 19). The sharply defined edges of these patches indicate, depending on the location, either drainage ditches or east-west/north-south 'water divides' (as, for example, at the locations pointed to by the white arrows).

The lower two maps, depicting the vertical velocities, neatly show the differentiation between infiltration and seepage areas. As with the horizontal velocities the sandy areas are easy to identify because of the high infiltration rates. Note too, once again, how the red drainage ditches cut through the infiltration areas as if it were the stitches of the duvet.

Though not shown in the figures, it is important to comment on the magnitude of the velocities. In the clayey layers, average velocities are in the order of 0.001 millimetres per year. In the upper aquifer in the order of meters per year (refer also to distance between the dots in Figure 28 on page 42).

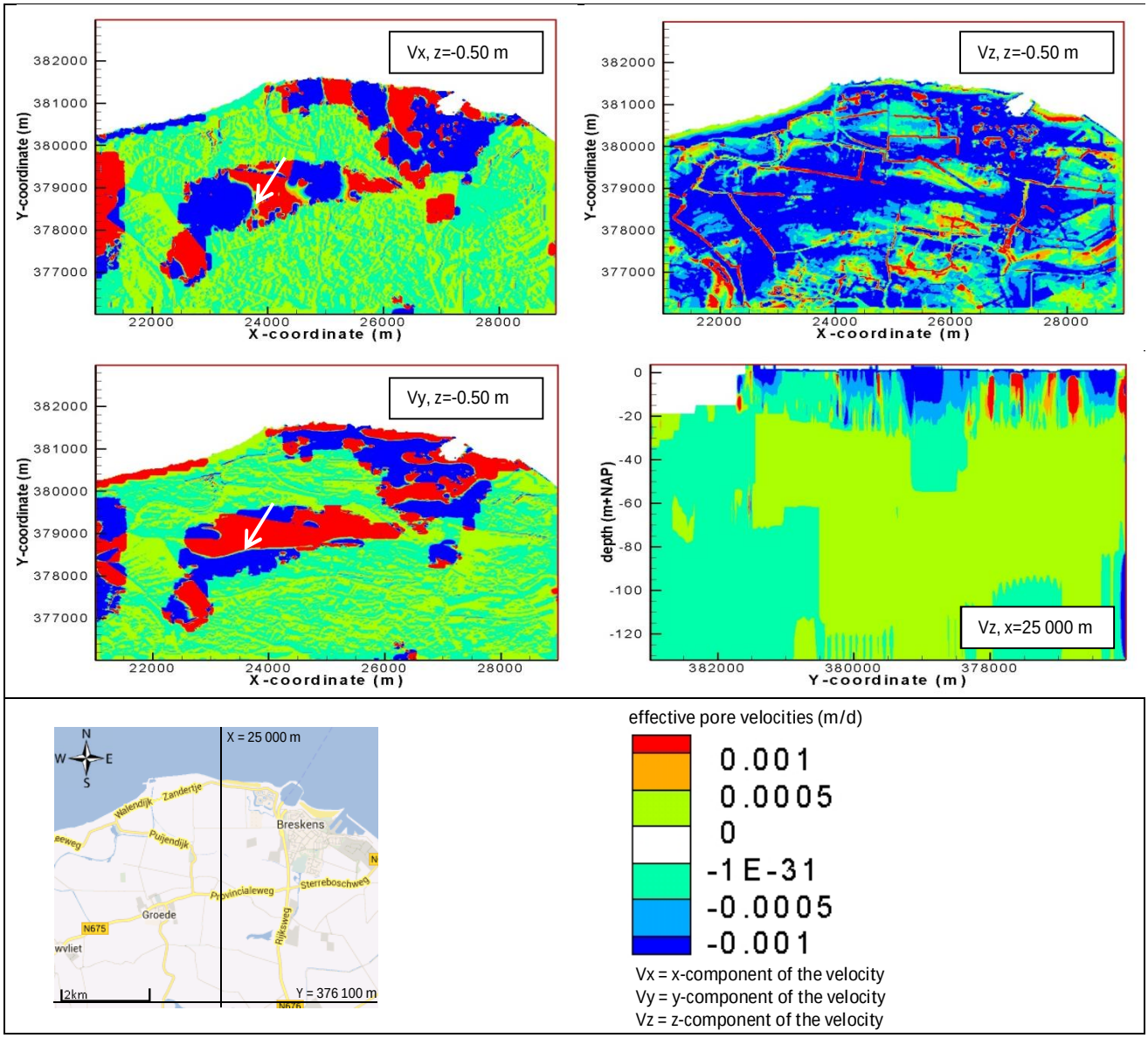

Figure 29. Output velocity distribution of the reference simulation. In the text boxes, Vx, Vy and Vz identify the velocity components along the x, y and z axes (velocities are positive when the flow goes along with the axes); the second value indicates the location of the cross-section. The white arrows indicate the north-south and east-west 'water divides' over the creek ridge. In the two maps on the right hand side (Vz) seepage locations are really well visible, as red indicates the upward flux. The light blue vertical lines at the bottom of the lower right figure are a consequence of the contouring technique.

Transport characterization and runtime. The Mixing Criterion is the limiting condition to the temporal discretization of solute-transport. In combination with the calculated velocities, it imposes a subdivision of each flow time step into three solute time steps, leading to a total of 36*3=108 solute time steps per stress period. The runtime of the model, strongly associated with these numbers, is 26h19min.

Cumulative balances. In Table 8 the cumulative mass (chloride) and water volume balances are shown. Note the extremely high contribution of the GHBs to the mass balance. Apparently, there is a lot of solute-transport across the GHBs. Yet, the exact origin of these numbers is unknown; it is possible, for example, that water highly saline water enter the model via one cell and immediately leaves the model by a neighbouring cell. These fluxes would have a large influence on the cumulative mass balance, but almost do not have any influence on the groundwater system as a whole. The relative difference between the in- and outflow of mass is 1%.

Concerning the volume balances, almost 60% of the water flows into the model via the GHBs, while the approximately 40% comes from groundwater recharge. Concerning the outflow, more than 25% of the water volume leaves the model via RIV-cells, while almost 20% is discharged through tile drainage (DRN-package). The quotient between DRN-salt mass and -volume shows that the average salinity of that water is 317mgl^{-}/l (compare with the values in Table 1 on page 14). The explanation for this low concentration is in the fact that tile drains generally do not intercept deep upward seepage; the latter fluxes are usually oriented toward the drainage (tertiary) ditches (RIV-package).

Table 8. Cumulative salt mass and volume balances after 100 stress periods (years). NB: the bottom of the sea is modelled with the RIV-package and, thus, the amounts indicated in the RIV-cells row are a sum of fluxes over the sea bottom and those over the bottom of inland surface waters (e.g. ditches, rivers).

CUM. BALANCES	Mass		Volume	
	ABS (g)	REL (%)	ABS (m3)	REL (%)
IN				
Groundwater recharge	1.3376E+10	0	6.6900E+08	40
RIV-cells	6.0927E+11	5	5.0994E+07	3
GHBs	1.1476E+13	95	9.3536E+08	57
TOTAL IN	1.2099E+13	100	1.6554E+09	100
OUT				
RIV-cells	-1.1320E+12	9	-4.3439E+08	26
Tile drains	-9.9496E+10	1	-3.1386E+08	19
GHBs	-1.0758E+13	90	-9.0713E+08	55
TOTAL OUT	-1.1989E+13	100	-1.6554E+09	100
IN-OUT (ABS)	1.0915E+11		-3.1904E+04	
IN-OUT (% of IN)		1		0

Synthesis. The reference situation shows 15 to 30 meters thick lenses floating on top of highly saline water. These lenses are bounded by brackish to saline seepage fluxes towards the drainage ditches. The discrepancy between the modelled thickness of these lenses and the observed value is high. In the vertical direction, concentrations change gradually from fresh to saline, except for the boundary regions where salinity hangs strongly to the sharp transition set in the GHB-package. In the clayey layers velocities are in the order of 0.001 mm/year, being up- or downward oriented depending on the dominance or not of the buoyancy factor over the head gradient. In the upper aquifer, there is infiltration in the sandy areas and seepage at rivers and (tertiary) ditches. Regarding the cumulative mass and volume balances, it is most important to keep that more than 25% of the water volume leaves the model via RIV-cells, while almost 20% is discharged by the tile drains.

5.2 Sensitivity analysis

In this subchapter, the results of the sensitivity simulations are discussed. Although an attempt is done to refer as much as possible to the different simulations by means of the changed parameter, for clarity reasons it sometimes is inevitable to use the code of the simulation. An overview of all simulations is included in Table 9 (for more details on the model input refer to Chapter 3 and Appendix H).

Each parameter is discussed in a separate section. The output of the simulations is presented with respect to the output of the reference simulation described in Subchapter 5.1, i.e. the states (e.g. freshwater lens thickness, equivalent freshwater heads, etc.) of the reference simulation are subtracted from the states of the sensitivity simulations. To illustrate: in order to analyse the influence of 25% more groundwater recharge on the equivalent freshwater heads distribution, the difference equivalent freshwater head field ϕ_f(WD049)- ϕ_f(WD035) is looked at. As mentioned already in the methodology, all sensitivity simulations and the reference simulation were run for 100 stress periods of one year.

At the end of each section, a short synthesis on the effects of the parameter on the model output is provided. At the end of the subchapter, the major findings of the sensitivity analysis are summarized in a Table 16 on page 69.

Table 9. Overview of the codes used to identify the simulations, including the sections in which the sensitivity to each parameter is discussed (for more details refer to Appendix H).

Parameter looked at	Section (page)	Reference value	Value used for sensitivity analysis	Code simulation
Groundwater recharge	5.2.1 (46)	186 mm	139.5 mm (-25%)	WD048
			232.5 mm (+25%)	WD049
			167.4 mm (-10%)	WD050
			204.6 mm (+10%)	WD051
Concentration rivers	5.2.2 (48)	946 $mgCl^-/l$	662 $mgCl^-/l$ (-30%)	WD056
			1261 $mgCl^-/l$ (+30%)	WD057
River bed resistance	5.2.3 (49)	2 d	0.5 d	WD054
			4 d	WD055
Sea floor resistance	5.2.4 (51)	208 d	1.25 d	WD052
			12.5 d	WD053
Effective porosity	5.2.5 (53)	0.3	0.2	WD060
			0.4	WD061
			0.5	WD062
Mechanical dispersion (long/trans)	5.2.6 (55)	0.05/0.005	0.005/0.0005	WD058
			0.5/0.05	WD059
Transmissivity GHBs	5.2.7 (57)	500 m^2/d	0 m^2/d	WD045
			100 m^2/d	WD046
			2 000 m^2/d	WD047
Discretization drainage system	5.2.8 (61)	25*25 m^2	100*100 m^2	WD035b
Nr. of flow time steps per year	5.2.9 (63)	36 (duration 10 d)	1 (duration 1 year)	WD038
			12 (duration 1 month)	WD039
			73 (duration 5 d)	WD040
Number of advection particles	5.2.10 (65)	4	1	WD041
			8	WD042
			27	WD043
CFL-factor	5.2.11 (68)	4	0.8	WD036
			2	WD037
Reference simulation	Subchapter 5.1	-	-	WD035

5.2.1 Groundwater recharge

In the reference simulation 186 mm of groundwater recharge is supplied to the model per year. To test the sensitivity of the Waterdunen model to this quantity, in simulation WD048 25% more and in simulation WD049 25% less water is applied. As with the reference simulation, the distribution of the supply is kept constant over the year.

Freshwater lens thickness. The changes in freshwater lens thickness are shown in Figure 30. The map on the left shows the impact of a 25% reduction in groundwater recharge on freshwater lens thickness. Especially close to the coast and in the vicinity of some ditches and rivers (black arrows), freshwater lens thickness decreases with several meters. Nonetheless, contrary to our expectations, there are some areas in which freshwater lens thickness slightly grows when less groundwater recharge is applied (blue-greyish spots). An increase of groundwater recharge with 25% leads to changes in freshwater lens thickness at the same places, but in the opposite direction.

Effective pore groundwater velocities. Figure 31 on page 47 depicts the difference in effective vertical pore groundwater velocities between the 25% less groundwater recharge simulation and the reference simulation. In the coloured green, yellow and red the difference in effective pore groundwater velocity is positive. In the green and yellow areas, where the top layers consist mostly of peat and clay (refer to Figure 19 on page 30) this means that the intensity of seepage increases with up to 0.6 mm/day. At the red lines and spots, which in most cases coincide with drainage ditches (see also the black arrows), the seepage flux increases with >1 mm/d. The blue areas indicate a negative difference in effective vertical pore velocity. Since these blue areas coincide with infiltration locations (same figure, lower plot) the intensity of the downward fluxes decreases with up to 0.6 mm/d.

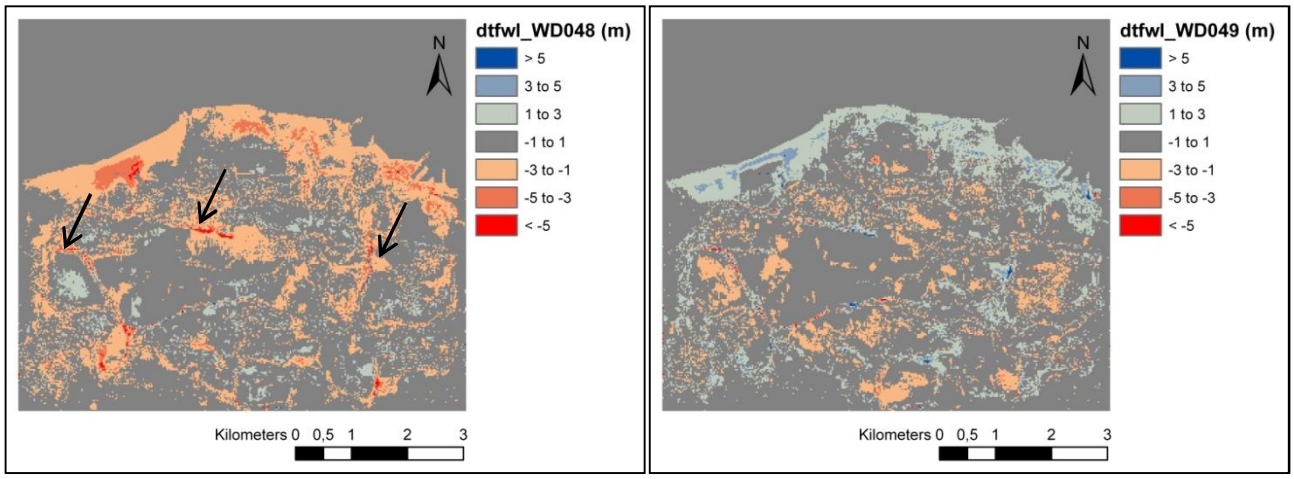

Figure 30. Difference in freshwater lens thickness (dtfwl) for model runs with 25% less (left, run WD048) and 25% more (right, run WD049) groundwater recharge when compared to the reference run (186 mm/year).

Concentrations and heads. For the concentration field, it holds that, in general, if less groundwater recharge is applied to the model, more marine intrusion occurs, the chloride concentrations become higher at the bottom of the lenses (increases of some hundreds of mg of chloride per litre) and the distance between the 30 $mgCl^-/l$ and 1 500 $mgCl^-/l$ isohalines becomes larger, i.e. the transition zone becomes thicker. The latter feature is at times a consequence of a downward movement of the 1 500 $mgCl^-/l$ isohaline and at others the result of a upward movement of the 30 $mgCl^-/l$ isohaline. In the end, these changes in chloride concentration lead to de- and increases of the horizontal velocities with several mm/d in the upper aquifer.

Balances. The balances in Table 10 show that the total water volume inflow to the model is not linearly correlated with groundwater recharge (e.g. 25% less groundwater inflow does result only in a 10% decrease of the total water volume inflow). Less inflow via groundwater recharge is (partly) compensated by changes of the in- and outflow via RIV- and DRN-cells: when less recharge is applied, more water enters the groundwater reservoir via RIV-cells and less flows out via RIV- and DRN-cells, and vice versa.

Other. The solute-transport stability numbers and runtime of the model do not change under influence of groundwater recharge.

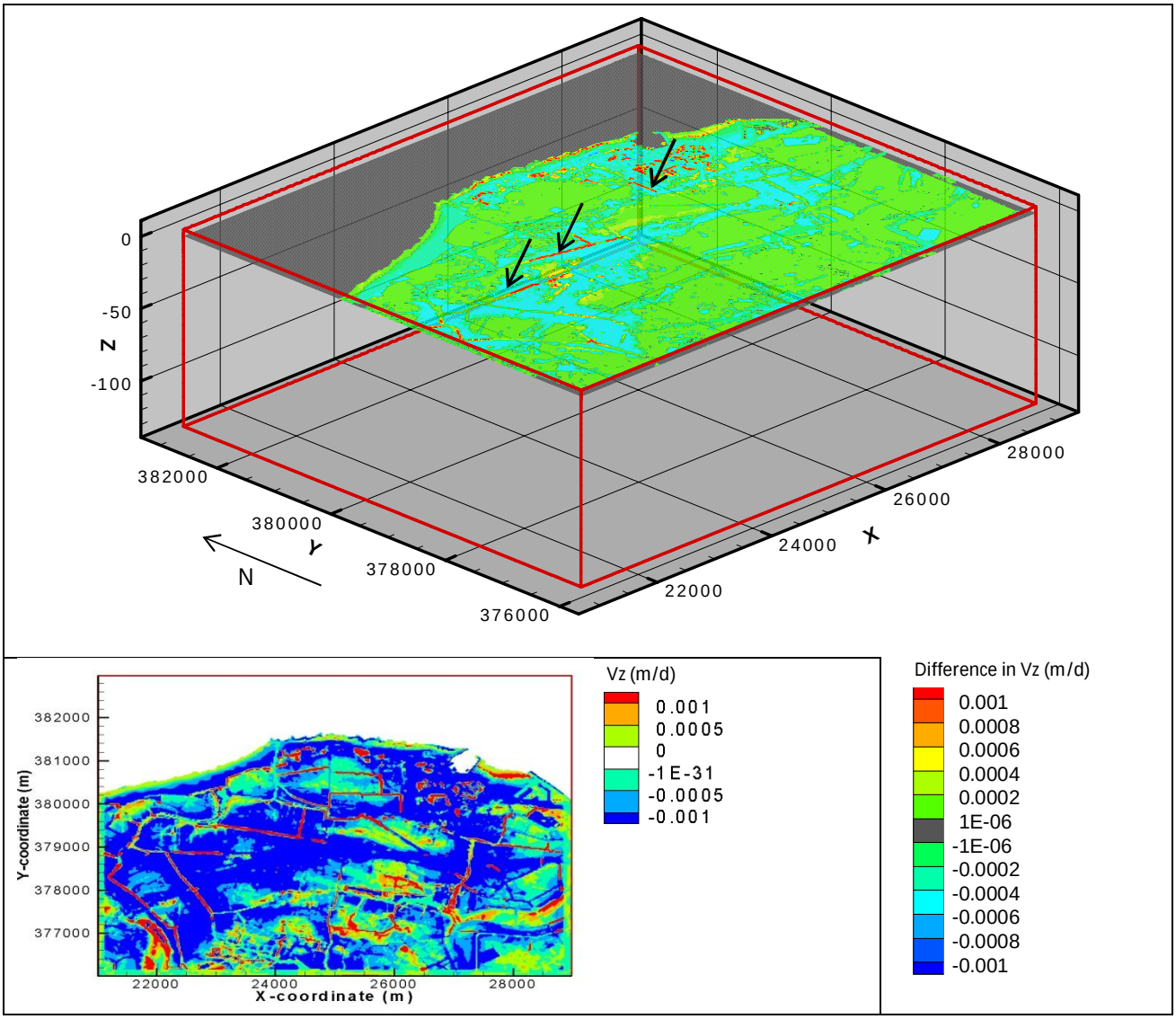

Figure 31. Upper plot: difference in effective pore vertical groundwater velocities between the simulation with 25% less recharge (WD048) and the reference simulation at z= -0.50 m. Lower plot: reference effective pore velocity along the z-coordinate axis (run WD035) at z= -0.50 m.

Table 10. Absolute and relative cumulative mass and volume budgets of simulations WD035 (reference simulation), and relative (compared to the absolute values of the reference simulation) budgets for simulations WD048 and WD049 with, respectively, 25% less and 25% more groundwater recharge.

	WD035 (reference)		WD048 (RCH-25%)		WD049 (RCH+25%)	
	Mass	Vol.	Mass	Vol.	Mass	Vol.
	ABS (g)	ABS (m3)	(%ref.run)	(%ref.run)	(%ref.run)	(%ref.run)
IN						
Groundwater recharge	1.34E+10	6.69E+08	75	75	125	125
RIV-cells	6.09E+11	5.10E+07	109	110	93	92
GHBs	1.15E+13	9.35E+08	100	100	100	100
TOTAL IN	1.21E+13	1.66E+09	101	90	100	110
OUT						
RIV-cells	-1.13E+12	-4.34E+08	98	89	103	109
Tile drains	-9.95E+10	-3.14E+08	102	64	99	139
GHBs	-1.08E+13	-9.07E+08	100	100	100	100
TOTAL OUT	-1.20E+13	-1.66E+09	100	90	100	110

Synthesis. A decrease in groundwater recharge results in more marine intrusion and, thus, thinner freshwater lenses at the coast. The transition zone between fresh and saline water at many points becomes thicker. The difference in effective vertical pore velocities and the cumulative water volume balance show that the RIV- and DRN-cells (partly) compensate for changes in groundwater recharge.

5.2.2 Concentration rivers

In the reference simulation the concentration of the RIV-cells –excluding the ones simulating the sea – is 946 mgCl$^-$/l. In order to test the sensitivity of the Waterdunen model to this parameter, the model is run once with a concentration 30% lower (662 mgCl$^-$/l) and once with a concentration 30% higher (1 261 mgCl$^-$/l) than the reference 946 mgCl$^-$/l.

Freshwater lens thickness. The output of the sensitivity runs shows that the effect of the concentration of rivers and ditches on the model output is negligible. The explanation for this is probably in the fact that most ditches and rivers drain the area; so, the new concentrations do not infiltrate. An analysis of the equivalent freshwater heads, chloride concentrations, effective pore groundwater velocities, streamlines, transition zone and cumulative balances does not reveal any significant changes. In line with this finding, Figure 32 shows that the influence of the river concentration on freshwater lens thickness is minimal.

Notwithstanding the previous conclusions, effectively there are some 20 cells in the right map that do show more than five meters decrease in lens thickness. To explain what is happening at these locations, a cross-section was made over x= 27 156 m (Figure 33 on page 49). The complementing zoom in Figure 34 (same page) confirms that freshwater lens thickness (remind that the threshold value used throughout this research is 1000mgCl$^-$/l, the green line) decreases with more than five meters at some sites when the concentration in the rivers is augmented with 30%. A more in depth analysis of the data shows that at these points a) the RIV-package is active and b) between approximately -2 m+NAP and -11 m+NAP the concentrations in the reference simulation come close to but do not surpass the 1000 mgCl$^-$/l-threshold, while in the simulation with 30% higher concentrations this threshold is reached (see also Appendix F). Though the change in concentrations is small (~300 mgCl$^-$/l), it locally leads to more than five meters decrease in freshwater lens thickness. As for the rest, this anomaly only occurs at approximately 20 cells because it requires the specific combination of an infiltrating river and a series of consecutive cells with concentrations that are already very close to the threshold value.

Other. The location of BMix and DMix, the solute-transport stability numbers and runtime of the model do not change under influence of the river concentration.

Synthesis. The impact of the river concentration on the output of the Waterdunen model is negligible. None of the output elements looked into, changes significantly.

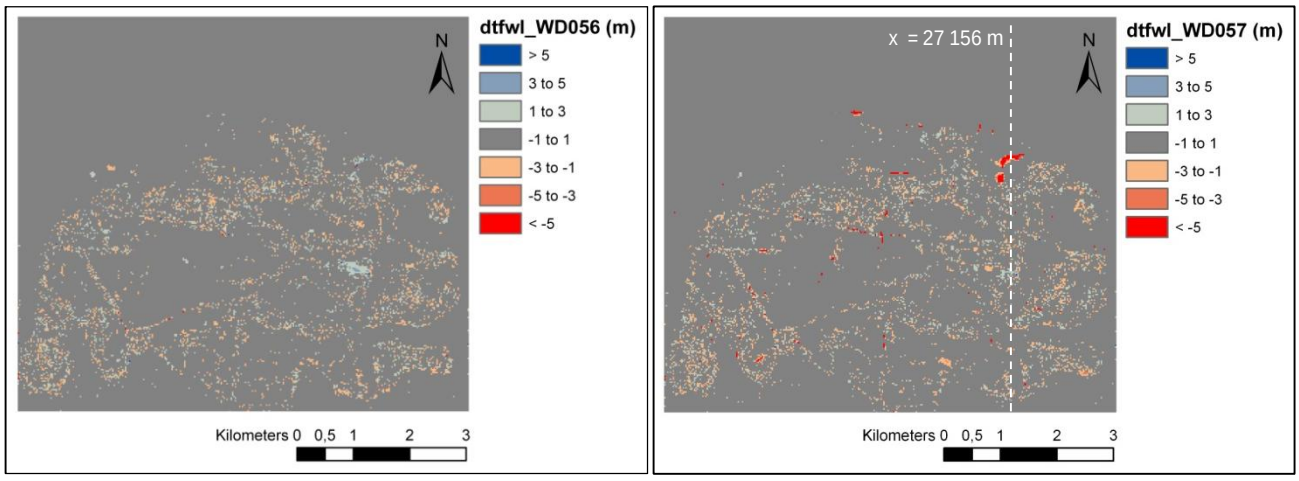

Figure 32. Difference in calculated freshwater lens thickness for model simulations with a river concentration 30% lower (left, WD056) and 30% higher (right, WD057) in comparison with the reference simulation. The changes are negligible, although in the +30%-case there are some 20 cells in which freshwater lens thickness decreases with more than 5 meters.

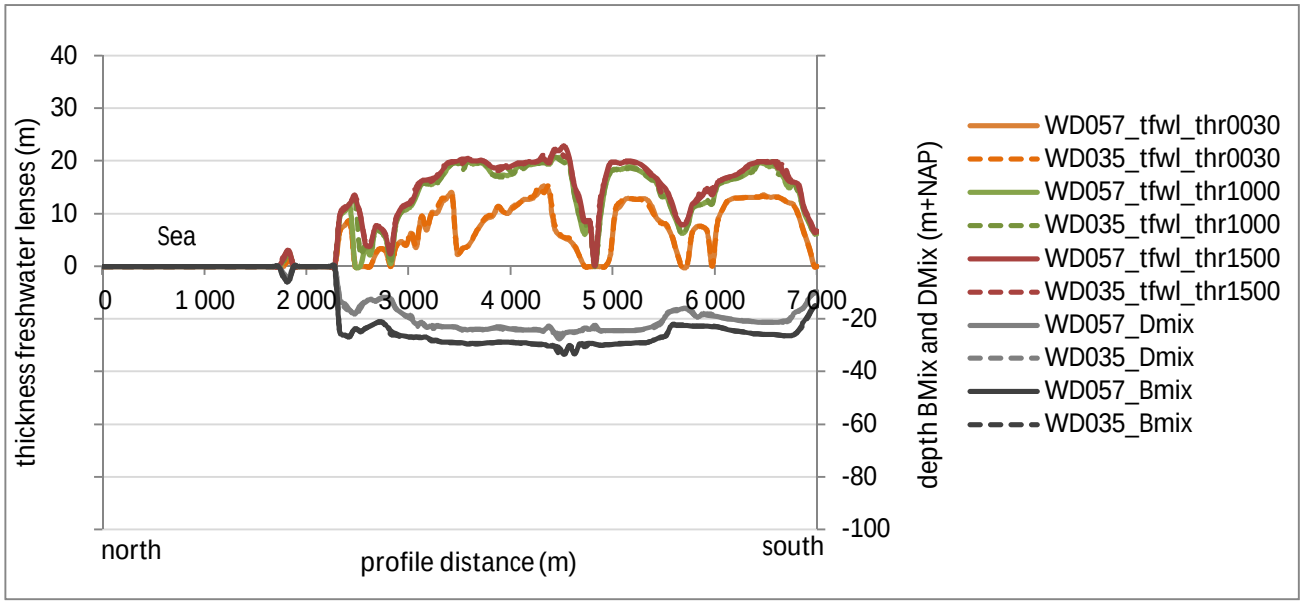

Figure 33. Thickness of freshwater lenses (as a function of the threshold value) for the reference simulation (WD035, dashed lines) and the simulation wherein river concentrations were set 30% higher (WD057, solid lines). For the location of the profile refer to Figure 32 on page 48.

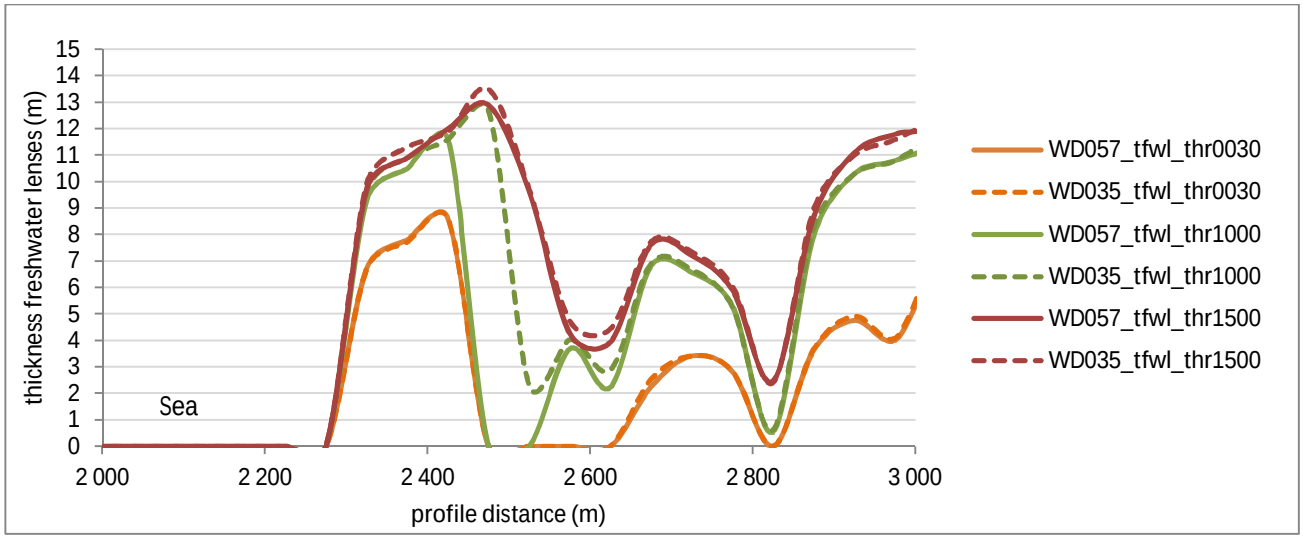

Figure 34. Freshwater lens thickness as a function of the threshold value for both the reference simulation (WD035, dashed lines) and the simulation wherein the river concentrations are 30% higher (WD057, solid lines), zoomed-in to a location where freshwater lens thickness decreases with more than 5 m.

5.2.3 River bed resistance

In the reference simulation, the resistance of rivers and (tertiary) ditches was set to two days (c=2 d). In order to analyse the sensitivity of the model to this parameter, the model was run once with a resistance four times as small (c=0.5 d) and once with a resistance twice as large (c=4.0 d). The results show a monotone relation between river bed resistance and the model output. E.g.: if freshwater lens thickness in a certain area increases when river bed resistances are lowered then it decreases if resistances are set higher (Figure 35 on page 50); if concentrations become lower when the resistance is decreased then they increase in the case of a higher resistance; and so forth. Therefore, only the output of an increase in river bed resistance is discussed here.

Freshwater lens thickness. An increase of the river bed resistance to four days leads to a severe decrease in freshwater lens thickness, especially between the Large Central Freshwater Lens and the coast (see right map Figure 35). In most cases, difference is one to five meters, but at some sites the decrease is almost 10 m.

Heads. To a great extent, the changes in the equivalent freshwater head distribution explain the reduction in freshwater lens thickness. A higher resistance of the river beds leads to an overall increase (up to 10cm) in equivalent freshwater heads in the 'core' of the model domain (see upper plot Figure 36). This effect seems plausible; the pressure in the model increases because groundwater drainage is constrained. These higher equivalent freshwater heads in the 'core' of the model constrain lens formation in the upper aquifer. Associated with this increase in equivalent freshwater heads, come large changes in effective horizontal pore velocities in the creek ridges and dunes (see, for example, the effective pore groundwater velocities in the direction of the y coordinate in the lower plot of Figure 36), which also lead to more dispersion. The largest changes in effective vertical pore groundwater velocities occur below surface water bodies (not shown here).

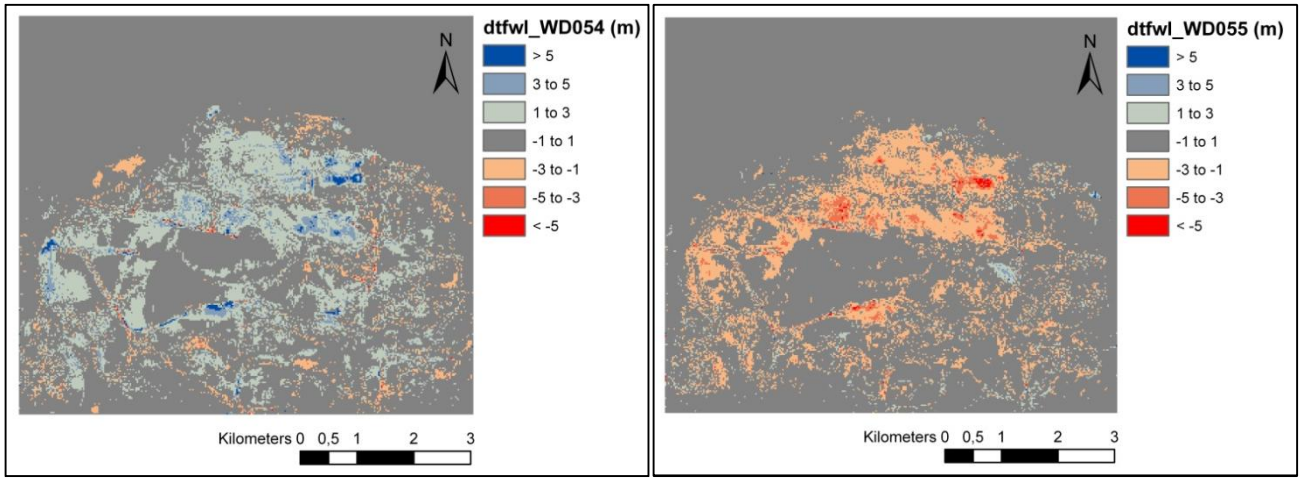

Figure 35. Difference in calculated freshwater lens thickness for model simulations with river bed resistance c=0.5 d (left, WD054) and c=4.0 d (right, WD055) when compared to the reference simulation.

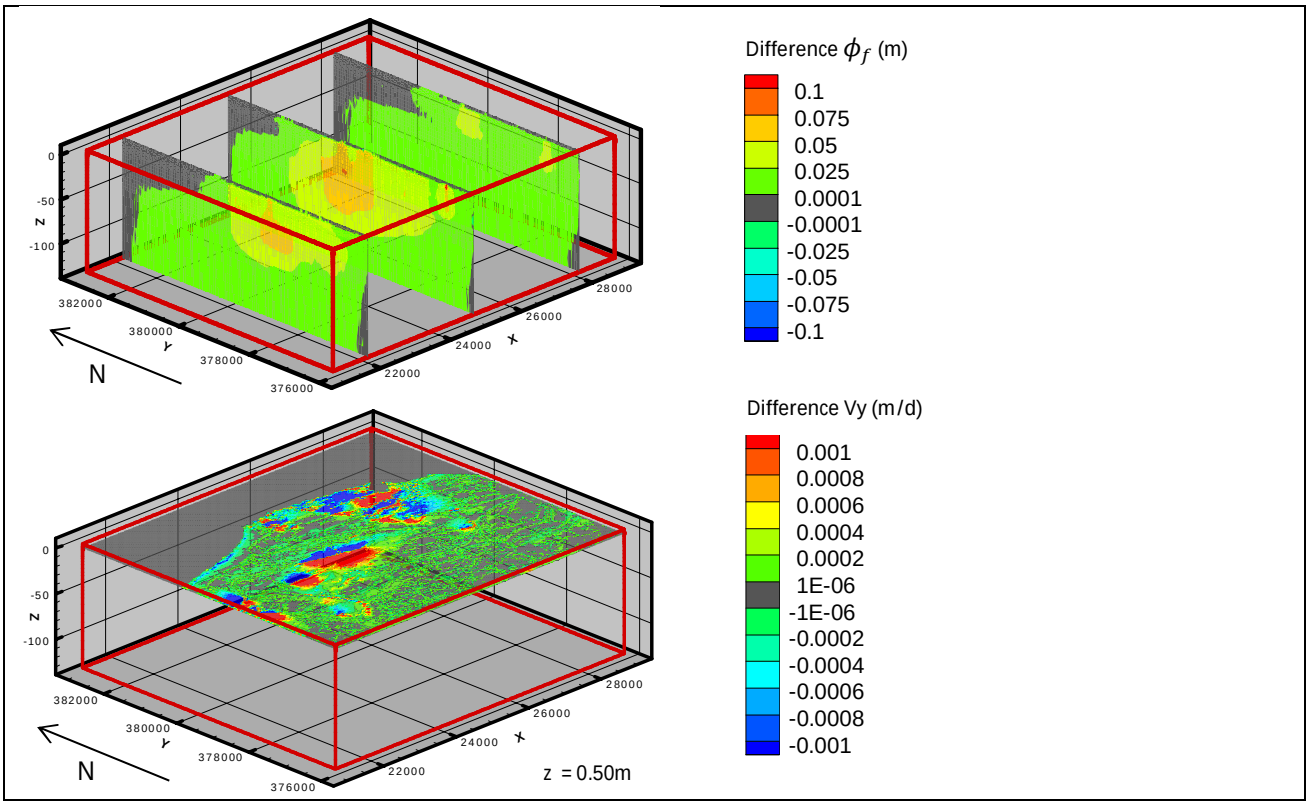

Figure 36. Upper plot: difference between the output equivalent freshwater heads of simulation WD055, in which c=4 d, and the output heads of the reference simulation. For the locations of the cross-sections consult Figure 15 on page 28. Lower plot: difference between the effective pore groundwater velocity in the direction of the y-coordinate of simulation WD055 (c=4 d) and the reference simulation (c=2 d).

Balances. A river bed resistance of four days severely reduces the interaction between the rivers and the groundwater body. The total volume of in- and outflow through RIV-cells decreases, respectively, with 17% and 10%. On the contrary, the volume of water leaving the model domain via tile drains (DRN-package) increases with 9%. This shift in outflow preference probably contributes to the decrease in lens thickness; tile drains mainly cross freshwater zones, while rivers and ditches usually drain deep saline seepage. Consequently, more freshwater and less saline water leaves the model.

Other. The location of BMix does not change; at some sites DMix moves up or down with two meters.

Synthesis. The Waterdunen model is very sensitive to changes in river bed resistance. A doubling of the resistance, from two to four days, (locally) leads to a decrease of freshwater lens thickness of more than five meters (mainly between the Large Central Freshwater Lens and the coast). Behind this reduction is a generalized increase in heads at the 'core' of the model, accompanied with an intensified freshwater outflow through tile drains (DRN-cells). In addition, horizontal velocities are severely altered in the sandy areas. A decrease in river bed resistance results in the contrary: lower heads, less outflow via tile drains and thicker freshwater lenses.

5.2.4 Sea floor resistance

As described in Chapter 3, in the Waterdunen model the sea is modelled with RIV-cells. In the reference simulation the resistance of sea floor cells is 208 days. Since this resistance is deemed rather high for the sea floor, during the sensitivity analysis resistances of c=1.25 d and c=12.5 d are used.

Freshwater lens thickness. The output of the two sensitivity runs is very similar. A decrease to 12.5 or 1.25 days of the sea floor resistance leads to thinner freshwater lenses at two sites, namely at the harbour and at the outflow of the major river present in the modelling domain (Figure 37). At these locations, freshwater lens thickness decreases with one to three meters. An analysis of the cross sections shows that the changes are restricted to the first row of lenses from the shore. The difference in concentration field depicted in Figure 38 on page 52 provides an explanation to why the thickness of the freshwater lenses decreases. The lower sea floor resistance leads to an increase in marine intrusion, which restricts the growth of freshwater lenses at the coast. Note that the increase in marine intrusion was already expected, however it was assumed that the magnitude of the changes would much and much larger, especially along the coast.

Balances. Besides the reduction of freshwater lens thickness, upward saline fluxes also lead to extra salt outflow via RIV- and DRN-cells (Table 11 on page 32). It seems that the increase in marine intrusion leads to an intensification of saline seepage toward rivers, (tertiary) ditches and tile drains immediately behind the coastal dike. The almost 12-fold increase in mass (chloride) inflow through RIV-cells is for sure caused by an increase in infiltration of marine water over the sea bottom.

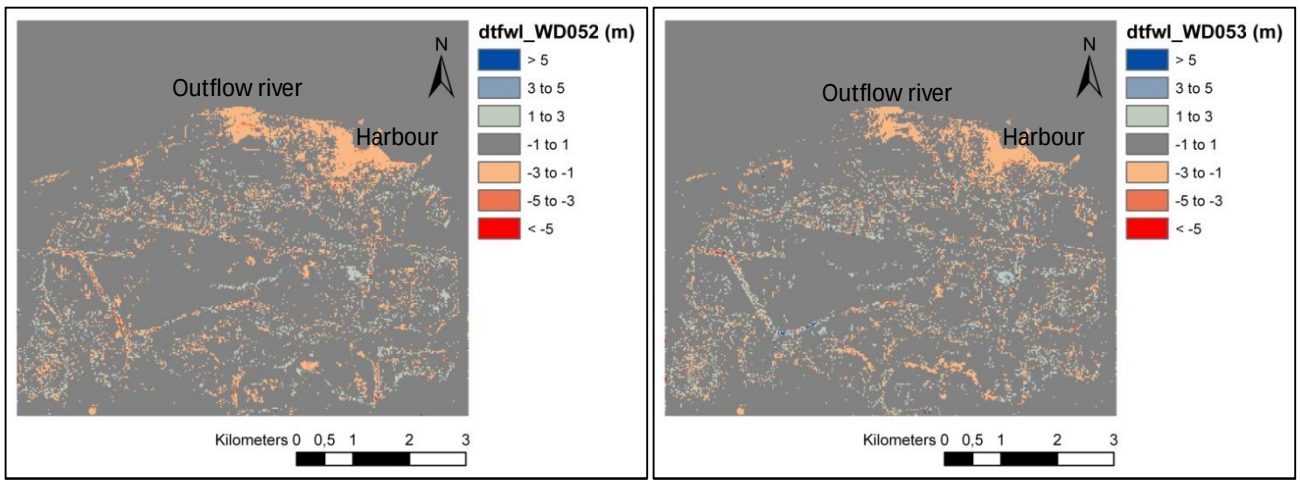

Figure 37. Difference in calculated freshwater lens thickness for model runs with a sea floor resistance of 1.25 d (left, WD052) and 12.5 d (right, WD053) when compared to the reference situation.

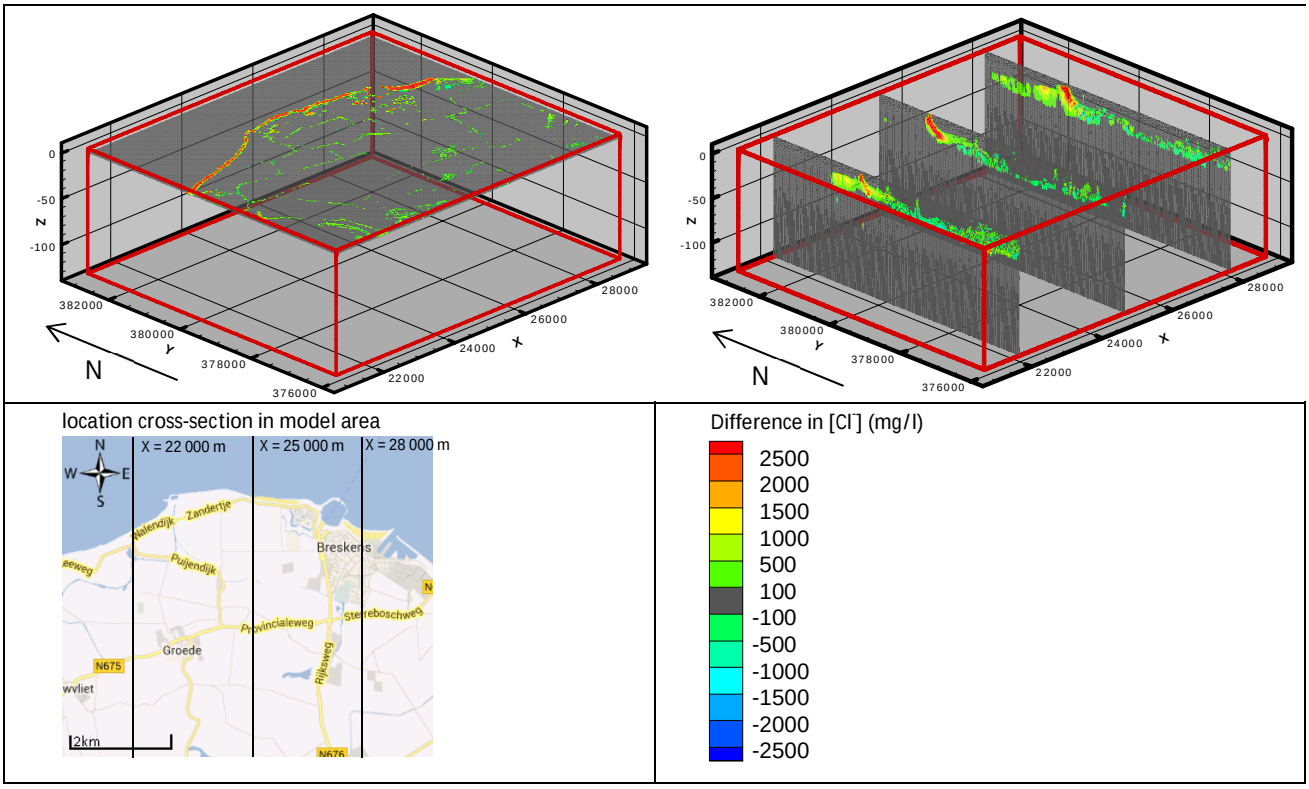

Figure 38. Difference between the output chloride concentrations of simulation WD053 -in which the resistance of the sea bottom is 1.25 d- and the output chloride concentrations of the reference simulation (resistance sea floor = 208 d). The upper left plot shows a horizontal cross-section over z=-0.50 m+NAP; the upper right plot shows vertical cross-sections over x=22 000 m, x=25 000 m and x=28 000 m.

Table 11. Cumulative mass and volume balances for the reference simulation (absolute numbers) and the simulations with sea floor resistances equal to 1.25 d and 12.5 d.

	WD035 (Reference)		WD052 (c=1.25 d)		WD053 (c=12.5 d)	
	Mass	Vol.	Mass	Vol.	Mass	Vol.
	ABS (g)	ABS (m3)	(% ref.run)	(% ref.run)	(%ref.run)	(%ref.run)
IN						
Recharge	1,34E+10	6,69E+08	100	100	100	100
RIV-cells	6,09E+11	5,10E+07	1181	816	471	345
GHBs	1,15E+13	9,35E+08	100	100	100	100
TOTAL IN	1,21E+13	1,66E+09	155	122	119	108
OUT						
RIV-cells	-1,13E+12	-4,34E+08	675	184	294	129
Tile drains	-9,95E+10	-3,14E+08	123	101	117	100
GHBs	-1,08E+13	-9,07E+08	100	100	100	100
TOTAL OUT	-1,20E+13	-1,66E+09	154	122	118	108

Other. In both sensitivity runs, the CFL-factor limits the time discretization; the runtimes increase to 38h24min and 27h17min, respectively, for the run with c=1.25 d and the run with c=12.5 d. The location of BMix and Dmix does not change.

Synthesis. Decreasing the sea floor resistance leads to thinner (one to three meters) freshwater lenses at the harbour and outflow of the major river. At the same time, an increase in marine intrusion results in higher concentrations and thus heads at depth along the coast, which in turn lead to more chloride mass outflow via rivers, (tertiary) ditches and tile drains immediately behind the coastal dike.

5.2.5 Effective porosity

In the reference simulation an effective porosity equal to 0.3 is used. To test the sensitivity of the Waterdunen model to this parameter, effective porosity values of 0.2 and 0.5 are used.

Freshwater lens thickness. Figure 39 shows the difference in calculated freshwater lens thickness of the sensitivity simulations compared to the reference simulation. The simulation wherein an effective porosity of 0.2 is used shows a clear increase in freshwater lens thickness). In most places an increase of one to three meters thickness is reached, while along the edges of the Large Central Freshwater Lens the increases mount up to more than five meters (left map. On the contrary, the map on the right shows that a higher porosity (0.5) leads to a decrease in freshwater lens thickness. Without waving aside the large changes in the rest of the domain, the effect are highest along the edges of the Large Central Freshwater Lens (freshwater lens thickness decreases with more than five meters).

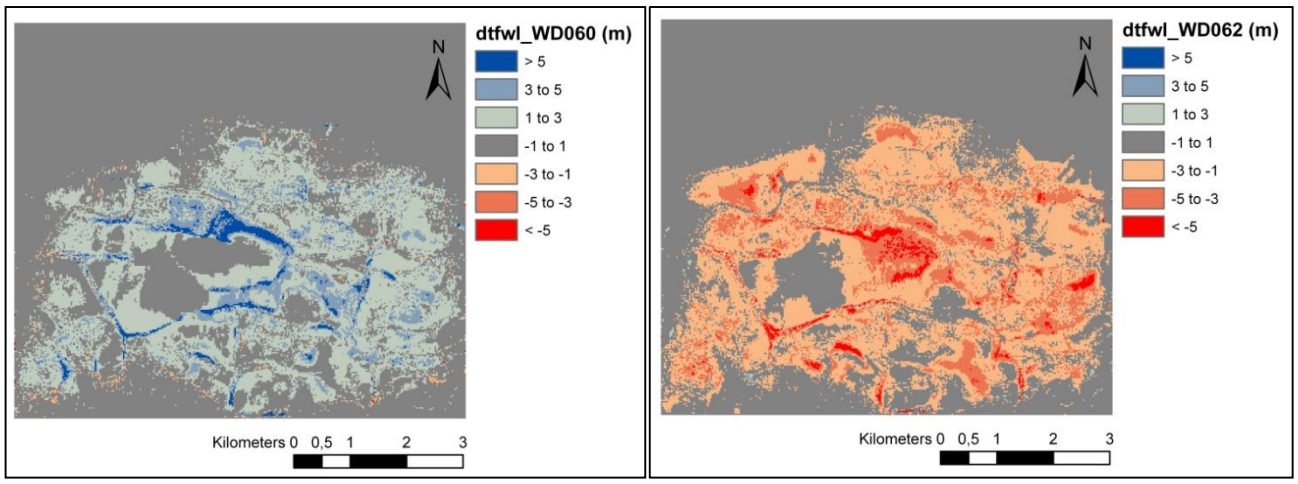

Figure 39. Difference in calculated freshwater lens thickness for model simulations with porosity 0.2 (left, WD060) and 0.5 (right, WD062) when compared to the reference simulation (porosity 0.3). The sensitivity of the freshwater lens thickness to porosity is extreme.

Concentrations. In line with the above described alterations, the difference in concentration field confirms that the higher the porosity the more the isohalines move upward. Since this movement is in the same direction and at the same pace for all isohalines the thickness of the transition zone remains the same. Apart from the effect on the inland freshwater lenses, a higher porosity also results in an increase in marine intrusion over the whole length of the coast.

Velocities. The effect of the porosity on the output effective pore groundwater velocity is large. This is logic because the effective pore groundwater velocity is equal to the specific discharge divided by the effective porosity. Depending on the location, velocities are up to three orders of magnitude higher or lower than in the reference simulation. In this, it is important to mention that the change in intensity is not linearly correlated with porosity. Both in the 0.2 as well as in the 0.5 porosity cases, the horizontal velocities at some points become much higher, and at others much lower. Apparently, the flow pattern (also) changes. Regarding the effective vertical groundwater velocities presented in Figure 40 on page 54, it turns out that the higher the porosity, the slower the infiltration in the sandy areas (see orange in the WD062-map) and the lower the seepage rate at the rivers and ditches (see dark blue in the WD062-map).

Balances. The cumulative *volume* balance does not show any changes. The cumulative *mass* balance, on the contrary, shows that the higher the porosity the more salt leaves the model via rivers, (tertiary) ditches and tile drains. Quantitatively, the 0.2-run shows a 9% decrease of salt mass leaving the model through RIV- and DRN-cells, while the 0.5-run shows an increase in mass outflow through rivers, (tertiary) ditches and tile drains of, respectively, 8 and 11%.

Other. Neither the solute-transport stability numbers nor the runtime of the model are affected by porosity. The location of BMix does not change; DMix is displaced up- or downward depending on the location and with a maximum of two meters.

Synthesis. In general, a higher porosity leads to a decrease in freshwater lens thickness, especially along the edges of large freshwater lenses, and an increase in seepage via rivers and (tertiary) ditches that adjoin large freshwater lenses, and tile drainage. Note, however, in this simulation time scales might have a very large impact on tnjhe findings (e.g. due to the changed relation between total mass and volume and the applied stresses). The cumulative volume balance is not affected; the cumulative mass balance confirms the increase in chloride outflow via ditches and tile drains.

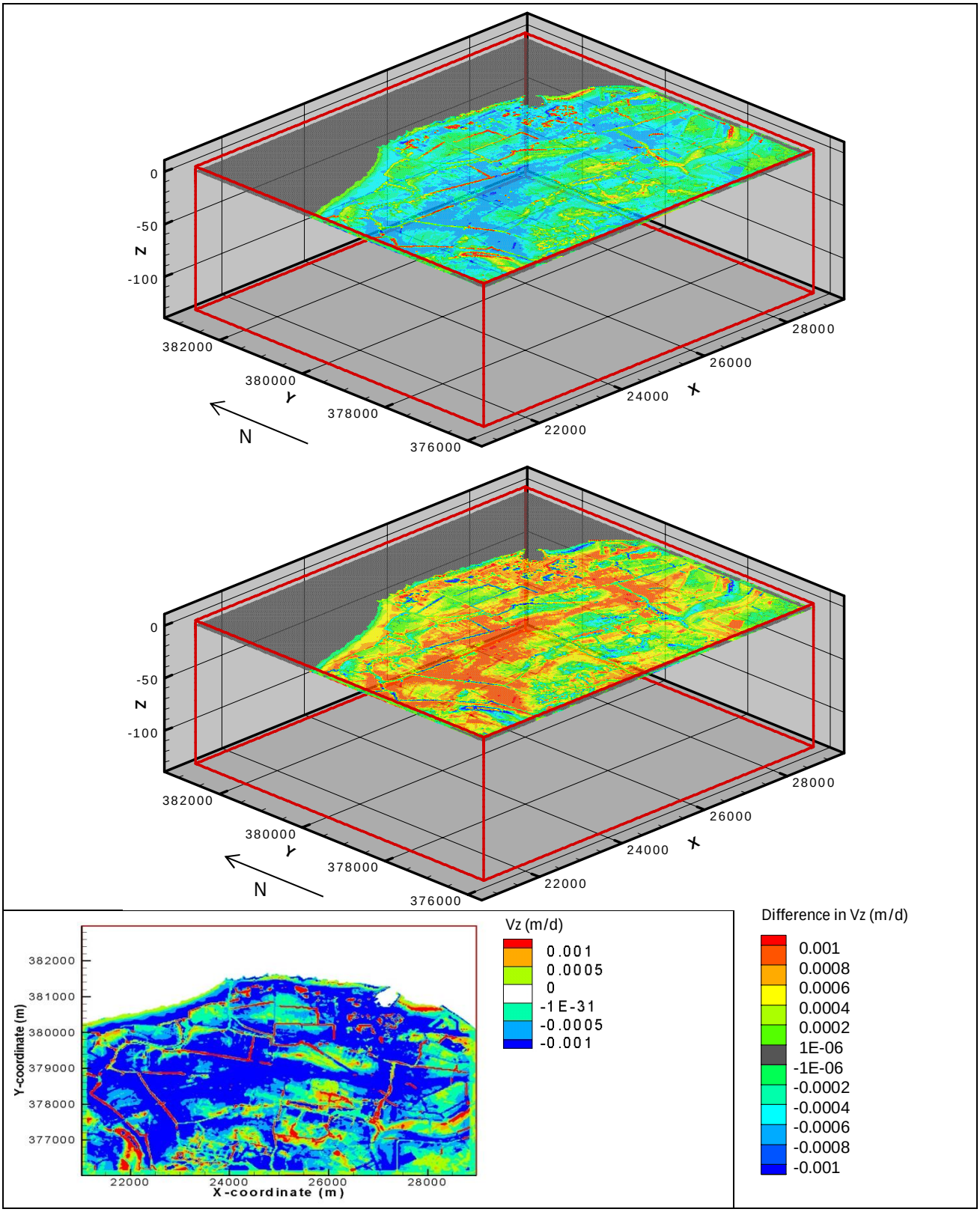

Figure 40. Upper two plots: difference in effective vertical groundwater velocities between the simulations with porosity 0.2 (WD060) and 0.5 (WD062), and the reference simulation with porosity 0.3. Lower plot: reference z-velocity (run WD035); cross-sections are over z=-0.50 m+NAP.

5.2.6 Dispersion factor[15]

In the reference simulation the longitudinal and transversal dispersion factors are, respectively, 0.05 and 0.005. To check the sensitivity of the model to mechanical dispersion, the model is run once with (both longitudinal and transversal) dispersion ten times as high (WD058) and once with a dispersion factor ten times smaller (WD059) than in the reference simulation.

The difference between the output of the reference simulation and the simulation with mechanical dispersion ten times smaller is negligible. Neither the chloride concentrations, nor the equivalent freshwater heads or cumulative mas and volume balances show significant differences. Consequently, the freshwater lens thickness remains the same (see right map Figure 41). This non-sensitivity to a lowering of the dispersion factors indicates that in the reference simulation solute-transport is dominated by advection processes.

Freshwater lens thickness. On the contrary, a dispersion factor ten times as high does have a considerable impact on the model output and leads to quite some changes in freshwater lens thickness (Figure 41, left hand side). Along the coast and at the edges of large freshwater lenses –see also the reference freshwater lens thickness in Figure 46 on page 58- freshwater lens thickness decreases with a couple of meters. In the rest of the domain there are local increases and decreases visible.

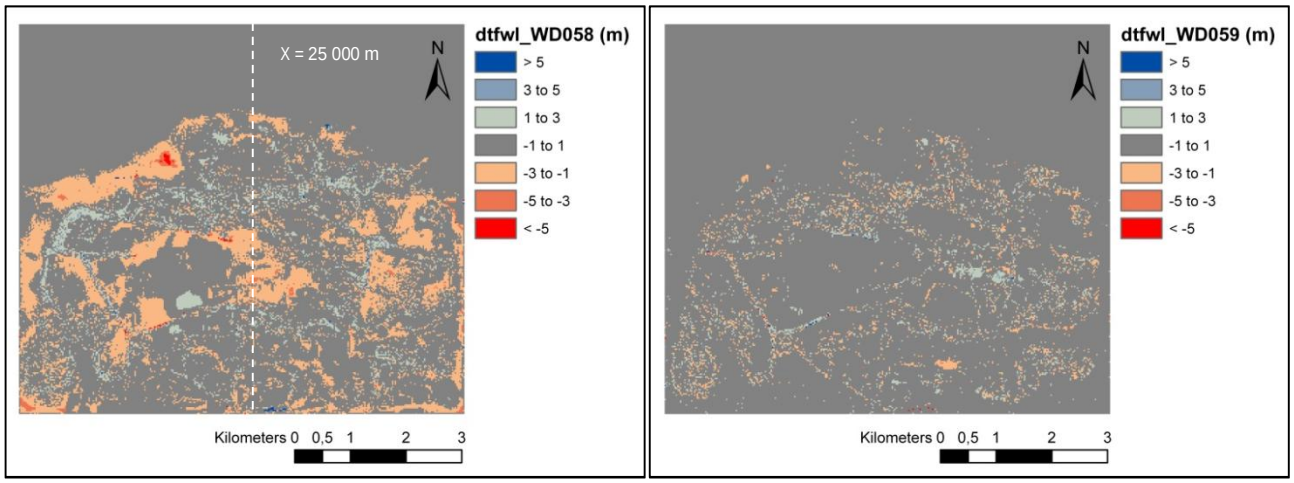

Figure 41. Difference in calculated freshwater lens thickness for simulations with a dispersion factor ten times as high (left, WD058) and ten times as low (right, WD059) compared to the reference simulation. The dashed line indicates the location of the profile presented in Figure 42.

Transition zone. Figure 42 and Figure 43 (page 56) show that the decrease in freshwater lens thickness is caused by an increase in mixing; the transition zone becomes thicker. The thickness of the 30 $mgCl^-/l$-lenses and 1 000 $mgCl^-/l$-lenses decreases, which means that the 30 $mgCl^-/l$- and 1 000 $mgCl^-/l$-isohalines move upwards. Meanwhile, the maximum thickness of the 1 500 $mgCl^-/l$-lenses does not change. At profile distance PD=4 200 m, for example, the thickness of the 30 $mgCl^-/l$-lenses decreases with two meters, while the location of the 1500$mgCl^-/l$-line does not change; this implies a more gradual transition from 30 to 1 500 $mgCl^-/l$. A side-effect of this expansion is the (at many points) smaller inclination of the lateral lens boundaries (cf. Figure 43). The angular displacement α to β is not extreme, but it does have a considerable effect on freshwater lens thickness at the edges of the large freshwater lenses (e.g.: $D \approx 1.5*d$). The location of BMix does not change; DMix moves down –depending on the location- with up to two meters.

The increase in mixing leads to higher chloride concentrations in the tile drain outflow. Unlike all other fluxes in the that remain unchanged, the mass of chloride that leaves the model via the DRN-package increases with almost 15% (see Table 12 on page 52).

Runtime. In the reference simulation the Mixing Criterion is the limiting factor to time discretization. A decrease in dispersion does not change anything to this and, thus, the model runtime does not change. On the contrary, it takes over 40 hours to run the model with a dispersion factor ten times as high, which is over one and a half time as long as the reference simulation. In the latter case, as could be expected, the Neumann criterion (dispersion) becomes highly limiting for time discretization (refer to Section 2.3.4 for an explanation on the solute-transport stability criteria).

[15] Refer to the theoretical background on solute-transport (page 7 and onwards) for the definition of hydrodynamic, mechanical, transversal and longitudinal dispersion.

Other. The changes is horizontal and vertical effective pore groundwater velocities and in the equivalent freshwater head distribution are negligible.

Synthesis. The mechanical dispersion factor used in the reference simulation is so small that flow is dominated by advection processes. A dispersion factor which is ten times as high results in more mixing and, therefore, leads to a more gradual transition from fresh to salt. The effect of these changes on freshwater lens thickness varies in space; along the edges of large freshwater lenses and along the coast freshwater lens thickness decreases. The increase in mixing also leads to higher chloride concentrations in the top layers, which is reflected in an increase in mass outflow via tile drains (DRN-package). Finally, from the moment on that the Neumann criterion becomes limiting to time discretization, a further increase of the dispersion factor leads to a longer runtime.

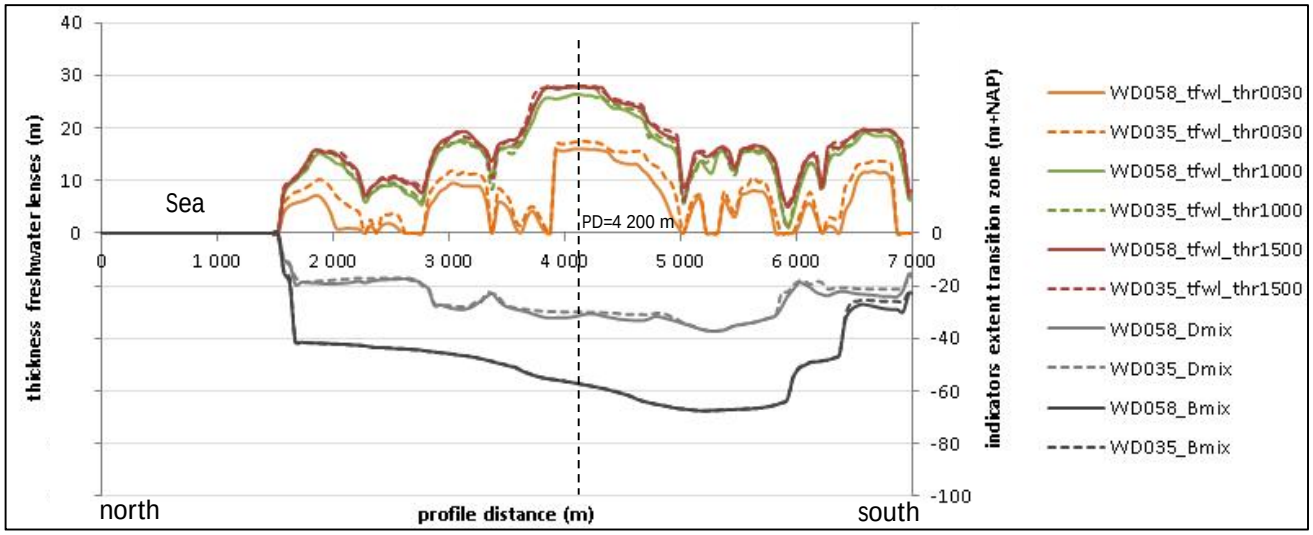

Figure 42. Freshwater lens thickness (as a function of the threshold value used) for both the reference simulation (WD035, dashed lines) and the run wherein mechanical dispersion is ten times as high (WD058, solid lines). The freshwater lens thickness calculated for a threshold value of 30 mgCl$^-$/l decreases with one to five meters. For the location of the profile refer to Figure 15 on page 28.

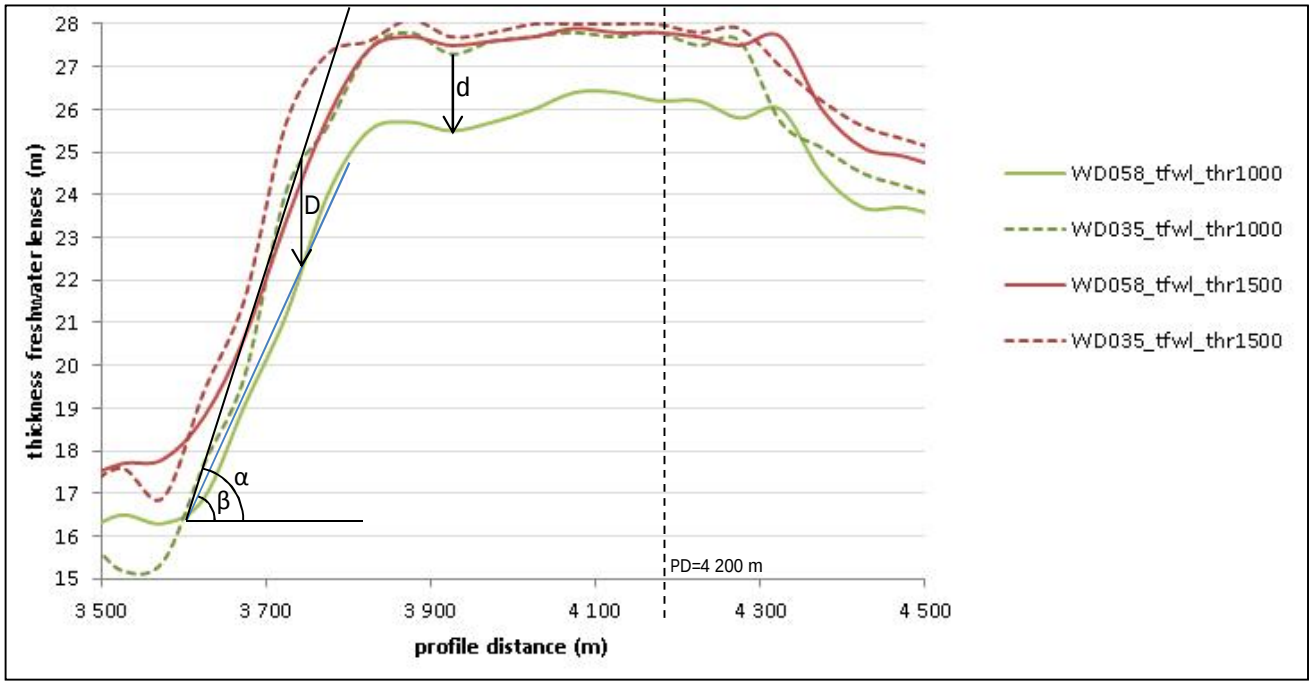

Figure 43. Freshwater lens thickness as a function of the threshold value for the reference simulation (WD035, dashed lines) and the simulation with dispersion factor ten times as high (WD058, solid lines), zoomed-in to the lateral boundary of the Large Central Freshwater Lens. The angles 'α' and 'β' denote the inclination of the lens boundaries and 'd' and 'D' the decrease in freshwater lens thickness; PD=4 200 m is an example location referred to in the text.

Table 12. Absolute cumulative mass and volume balances for the reference run and the run with dispersion ten times as high. The concentration of the tile drainage outflow increases with 14% when a dispersion factor ten times as high as in the reference siulation is used.

	WD035 (Reference)		WD058 (disp x 10)	
	Mass	Volume	Mass	Volume
	ABS (g)	ABS (m3)	(% ref.run)	(% ref.run)
IN				
Recharge	1.34E+10	6.69E+08	100	100
RIV-cells	6.09E+11	5.10E+07	101	101
GHBs	1.15E+13	9.35E+08	99	100
TOTAL IN	1.21E+13	1.66E+09	100	99
OUT				
RIV-cells	-1.13E+12	-4.34E+08	97	101
Tile drains	-9.95E+10	-3.14E+08	114	99
GHBs	-1.08E+13	-9.07E+08	99	98
TOTAL OUT	-1.20E+13	-1.66E+09	99	99

5.2.7 Transmissivity GHBs

As described in Chapter 3, in the reference simulation the GHB-transmissivity is set to 0 m^2/d (no-flow) at the aquitards and 500 m^2/d at the aquifers. In order to analyse the sensitivity of the model to this parameter, the GHB-transmissivity of all lateral model boundaries is subsequently set to 2 000 m^2/d, 100 m^2/d and 0 m^2/ d at the aquifers (the GHB-transmissivity at the aquitards is kept to 0 m^2/d in all simulations).

Freshwater lens thickness. Figure 45 shows that, where it concerns freshwater lens thickness, it makes no significant difference whether the transmissivity of the GHBs is 100, 500 or 2 000 m^2/d at the aquifers. The freshwater lens thickness almost does not change, as does not do the characterization of the transition zone, i.e. the thickness of the 30, 1000 and 1500 mgCl^-/l-lenses and the depth of BMix and DMix remains unchanged (Figure 45 on page 58). An analysis of the equivalent freshwater heads and the streamlines shows no significant changes either.

Restricting the interaction with the outside world to nil changes freshwater lens thickness, especially within the first kilometre from the boundaries (cf. Figure 46 and Figure 47 on page 58). The changes (up to 10 meters) are location specific. The concentrations imposed by the mother model at the lateral boundaries are more saline than the concentration distribution obtained in the reference simulation. Consequently, lenses become thicker at locations where previously there was an inflow of water over the lateral boundaries, and thinner at the locations where there was an outflow of water over the lateral boundaries. The displacement of BMix and DMix is extreme –five to ten meters- with reference to the other sensitivity analyses performed in this research.

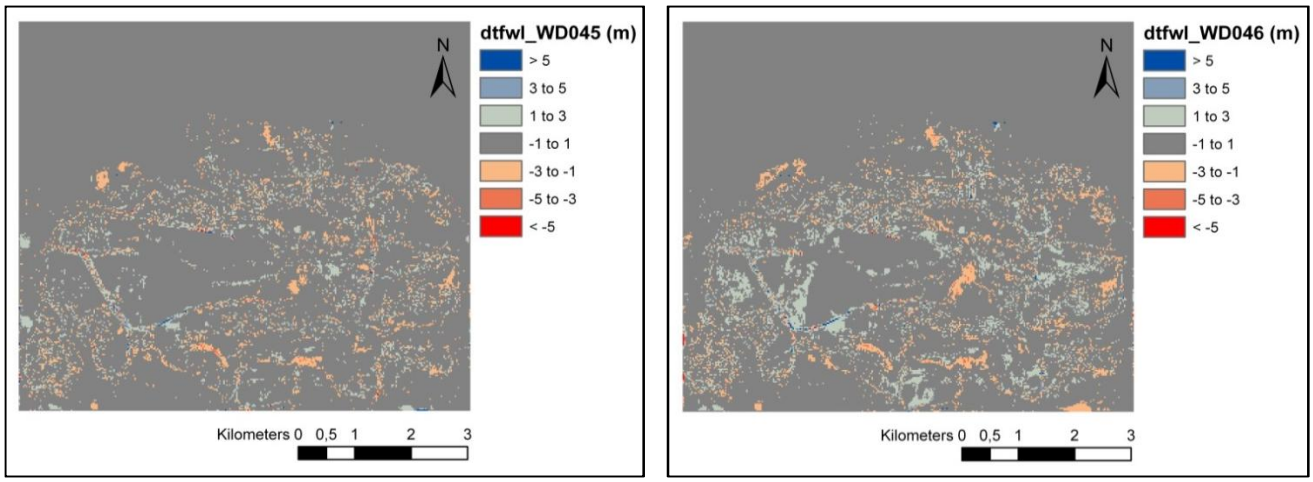

Figure 44. Difference in calculated freshwater lens thickness for model simulations with GHB-transmissivities 2 000 m^2/d (left, WD045) and 100m^2/d (right, WD046) when compared to the reference run (500 m^2/d).

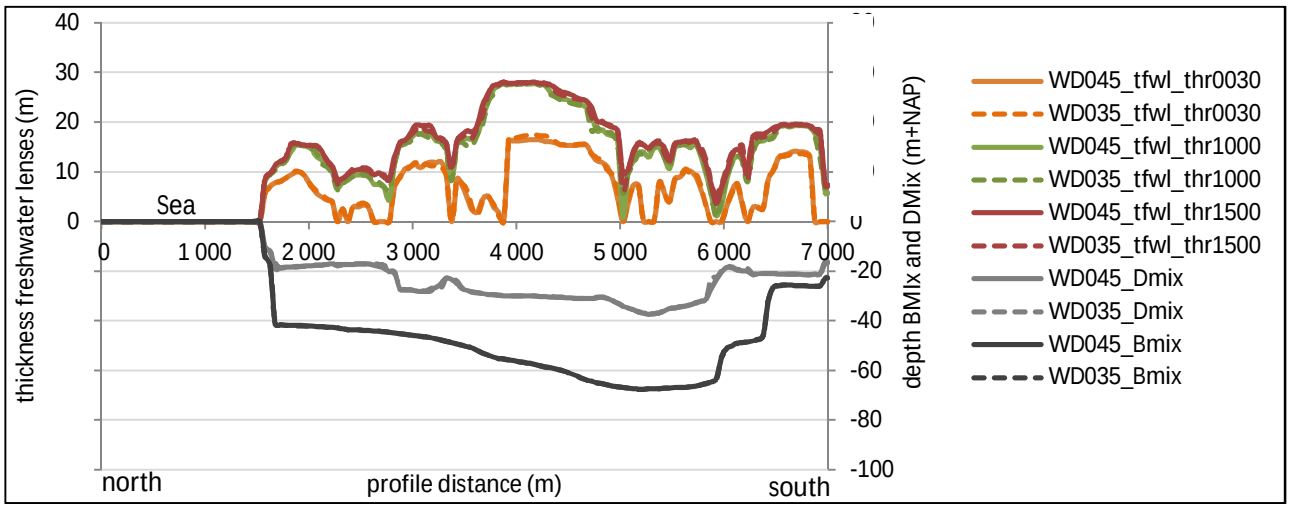

Figure 45. Freshwater lens thickness (as a function of the threshold), BMix and DMix for the reference simulation (WD035, dashed lines) and the 2 000 m^2/d-simulation (WD045, solid lines); profile over x=25 000 m (see Figure 15 on page 28 for an orientation map). The graph for the simulation with a GHB-transmissivity equal to 100 m^2/d at the aquifers looks similar.

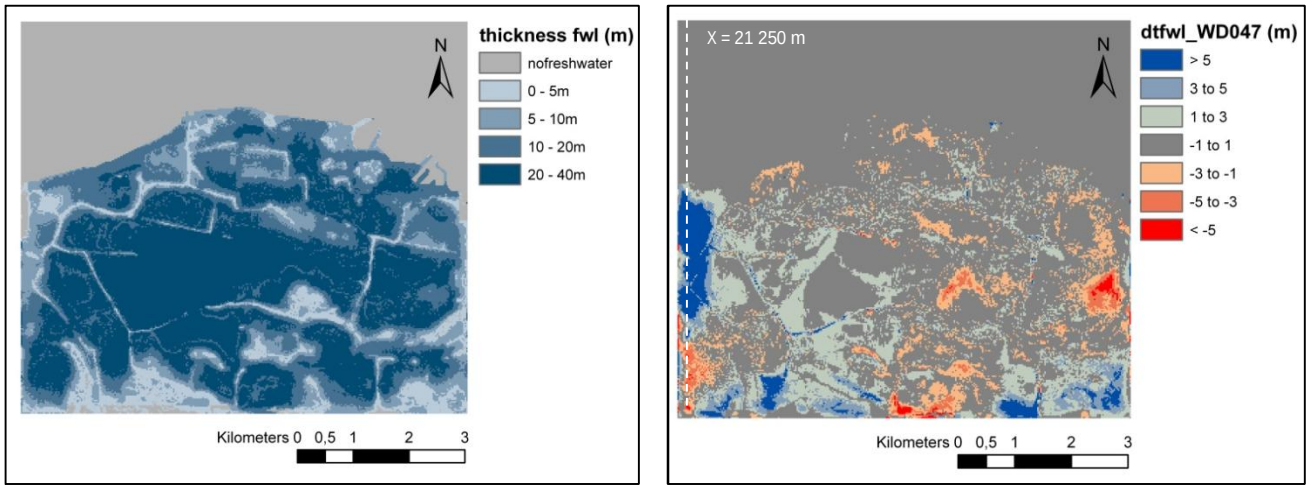

Figure 46. On the left hand side, the reference freshwater lens thickness is shown. On the right hand side, the difference in freshwater lens thickness between the reference simulation and the simulation with GHB-transmissivity 0 m^2/d (no-flux) is mapped. The dashed white line indicates the location of the profile presented in Figure 47 on page 58.

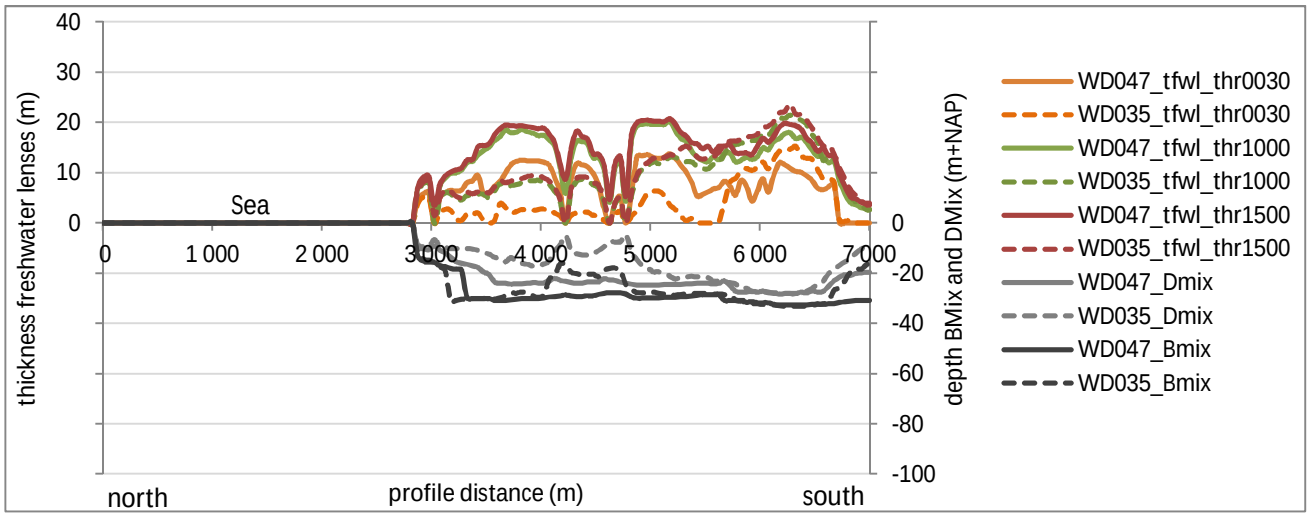

Figure 47. Freshwater lens thickness (as a function of the threshold value),BMix and DMix for the reference simulation (WD035, dashed lines) and for the 0 m^2/d-simulation (WD047, solid lines); profile over x=21 250 m (250 m from the western boundary, see Figure 46 on page 58).

Head distribution. In the 0 m^2/d-simulation, the equivalent freshwater heads (Figure 48) and the streamlines deep in the model change considerably. At seaside and in the upper aquifer, equivalent freshwater heads decrease. On the contrary, land inward and at the bottom of the model heads become higher. Together these changes lead to more upward oriented streamlines. How to reconcile the limited change in freshwater lens thickness in the centre of the model with the increase in upward oriented saline fluxes? The explanation is in the effective vertical pore groundwater velocity-field. In the clayey layers effective vertical pore groundwater velocities are below 0.001 mm/day (Figure 17 on page 29, Figure 28 on page 42 and Figure 29 on page 43), which means it would take many thousands to millions of years for the reorientation of the fluxes to affect freshwater lens thickness. In this research, the model is run for 100 years and, thus, there are no visible changes.

Balances. Table 13 (page 60) shows that, as expected, the amount of in- and outflow over the lateral model boundaries is directly (though not linearly) related with the transmissivity of the GHBs. The amount and characterization of the water leaving the model via the DRN-package stays similar. In contrast, the water volume and salt mass influxes via the RIV-package increase with respectively 7 and 9%, and the concentration and volume of the RIV-outflow decreases (23 and 5%) in the no-flux scenario. The earlier described lowering of the equivalent freshwater heads leads to more infiltration over the sea floor and, on land, to less seepage toward the ditches.

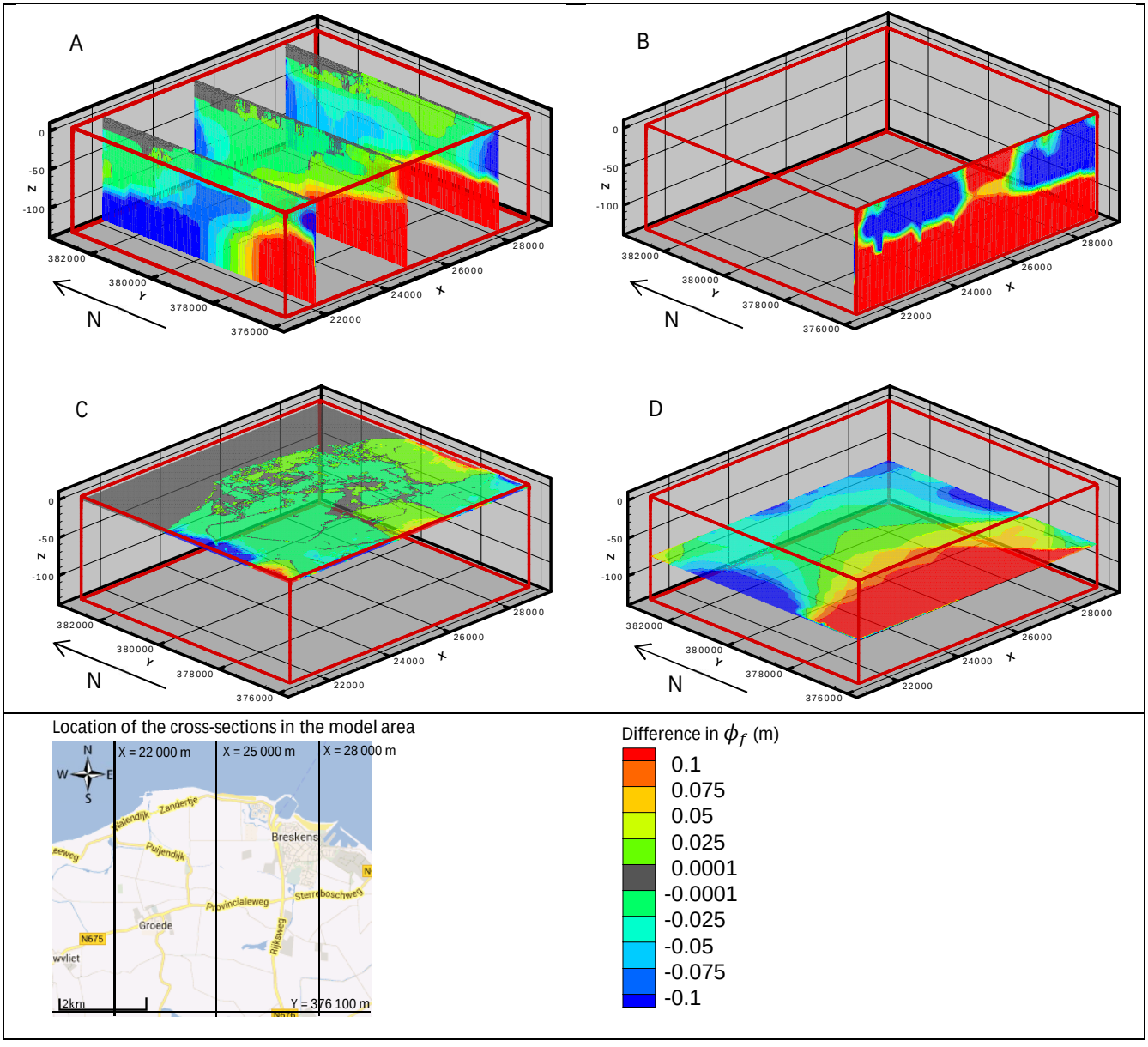

Figure 48. Fences showing the difference in equivalent freshwater heads between simulation WD047 in which the GHB-transmissivity is 0 m^2/d and the reference simulation in A) over cross-sections x=22 000 m, x=25 000 m and x=28 000 m, in B) over cross-section y=376 100 m, in C) over cross-section z=-0.50 m and in D) over cross-section -75 m.

Runtime. In the 2 000 m^2/d-simulation, the high transmissivity locally leads to much higher horizontal velocities at the southern boundary (Appendix E). As a consequence, the Mixing Criterion constrains the time discretization and each flow time step is automatically subdivided into 8 solute time steps. As a result, the runtime is augmented to 38h06min, which is over one and a half time as long as the reference simulation. On the other hand, decreasing the GHB-transmissivity to 100 m^2/d leads to a decrease in runtime from 26h19min to 22h17min. A further decrease to 0 m^2/d does not alter the runtime anymore. Apparently, boundary velocities are limiting the time discretization in the case of high transmissivities, while below a certain threshold value other velocities become restricting. This is confirmed by the solute output file. In the 2000 and 500m^2/d-situations the cells limiting the time discretization are located at the boundaries; in the 100 and 0m^2/d-situations that is not the case anymore.

Synthesis. For the freshwater lens thickness it makes no difference whether the calculations are performed with a GHB-transmissivity equal to 100-, 500- or 2 000 m^2/d-GHB[16]. However, if the cell with the highest velocity is situated at a model boundary, a higher GHB-transmissivity can have an enormous effect on the runtime of the model: the higher the transmissivity, the finer the time discretization becomes, and, thus, the longer it takes to run the model. At the same time, an though the underlying head distribution changes considerably, for a runtime of 100 years most effects of a no-flux boundary on freshwater lens thickness are restricted to a 1km-broad band along the model boundaries. Herein, the limited effect of the changed heads on freshwater lens thickness is associated with the extremely low velocities in the clayey layers. The cumulative balances, finally, show that a) the in- and outflow over the GHBs is directly but non-linearly related to the GHB-transmissivity, and that b) in case of a zero-flux boundary, the equivalent freshwater heads become lower in the upper layers, which leads to more infiltration over the sea bottom and less seepage on land.

Table 13. Absolute and relative cumulative mass and volume budgets for simulation WD035 (reference, GHB-transmissivity=500 m^2/d), and relative (compared to the absolute values of the reference simulation) cumulative mass and volume budgets for simulations with GHB-transmissivities 2000, 100 and 0 m^2/d.

	WD035 (Reference)				WD045 (2000m2/d)		WD046 (100m2/d		WD047 (0m2/d)	
	Mass		Volume		Mass	Volume	Mass	Volume	Mass	Volume
	ABS (g)	(%)	ABS (m3)	(%)	(% ref.run)	(% ref.run)	(% ref.run)	(% ref.run)	(% ref.run)	(% ref.run)
IN										
Recharge	1.34E+10	0	6.69E+08	40	100	100	100	100	100	100
RIV-cells	6.10E+11	5	5.10E+07	3	100	100	100	100	109	107
GHBs	1.15E+13	95	9.35E+08	57	160	165	50	48	0	0
TOTAL IN	1.21E+13	100	1.66E+09	100	157	137	53	71	6	44
OUT										
RIV-cells	-1.13E+12	9	-4.34E+08	26	99	100	98	100	77	95
Tile drains	-9.95E+10	1	-3.14E+08	19	98	100	99	106	94	99
GHBs	-1.08E+13	90	-9.07E+08	55	164	167	49	47	0	0
TOTAL OUT	-1.20E+13	100	-1.66E+09	100	157	137	54	72	8	44

[16] NB: an exploratory analysis has shown that this conclusion does not hold when the flow time step duration is augmented from ~10days to ~1year.

5.2.8 Discretization drainage system[17]

In the reference simulation, the diffuse top system is discretized on a 25*25 m^2 resolution. To analyse the sensitivity of the model to this characterization, the input data is scaled up to a 100*100m^2 resolution. The upscaling mainly changes the characterization of the sea RIV-cells and the DRN-cells[18]. Downscaling is not possible because the necessary data is not available. Note that the computation grid does not change

Freshwater lens thickness. The major differences in freshwater lens thickness due to the upscaling occur near surface water bodies, at the harbour and around the outflow of the largest river present in the modelling domain. At these locations, the differences in freshwater lens thickness mount up 11.5 m (Figure 49 on page 61). Note that, as a result, the maximum depth of the large freshwater lenses rarely changes. It is often the seepage areas in between that become more fresh of saline (cf. Figure 50 on page 62, black arrows).

Concentrations. In general, the major changes in chloride concentration are located below ditches and rivers and along the coast. The intensity of marine intrusion increases, implying (in this case) both an increase in concentrations as well as in the extent of the subsurface saline tongue. Associated with these chloride concentration changes come changes in equivalent freshwater heads: equivalent freshwater heads (very locally) increase or decrease with more than 10cm.

Velocities. On their turn, and following the local changes in equivalent freshwater heads, effective pore horizontal groundwater velocities change in direction and magnitude along the coast and below ditches and rivers. Effective pore vertical groundwater velocities below and close to rivers and ditches augment or decrease, depending on the location, with a factor of more than 2 (Figure 51 on page 62, black arrows). Altogether these changes lead to a 10% decrease in inflow via the RIV-package.

Other. The transport stability numbers are not affected by the discretization of the RIV- and DRN-parameterization. The runtime decreased with 1 hour.

Synthesis. Contrary to the expectations, the upscaling of the characterization of RIV- and DRN-cells from 25*25 m^2 to 100*100 m^2 leads only to minimal changes in freshwater lens thickness. However, the concentration distribution underneath surface water bodies and along the coast does change. These changes are in the order of several thousands of $mgCl^-/l$ and result in very local but large changes in equivalent freshwater heads (>10cm), which, on their turn, lead to large in- and decreases in effective vertical pore groundwater velocities and freshwater lens thickness. The effects are limited to the coast, ditches and rivers.

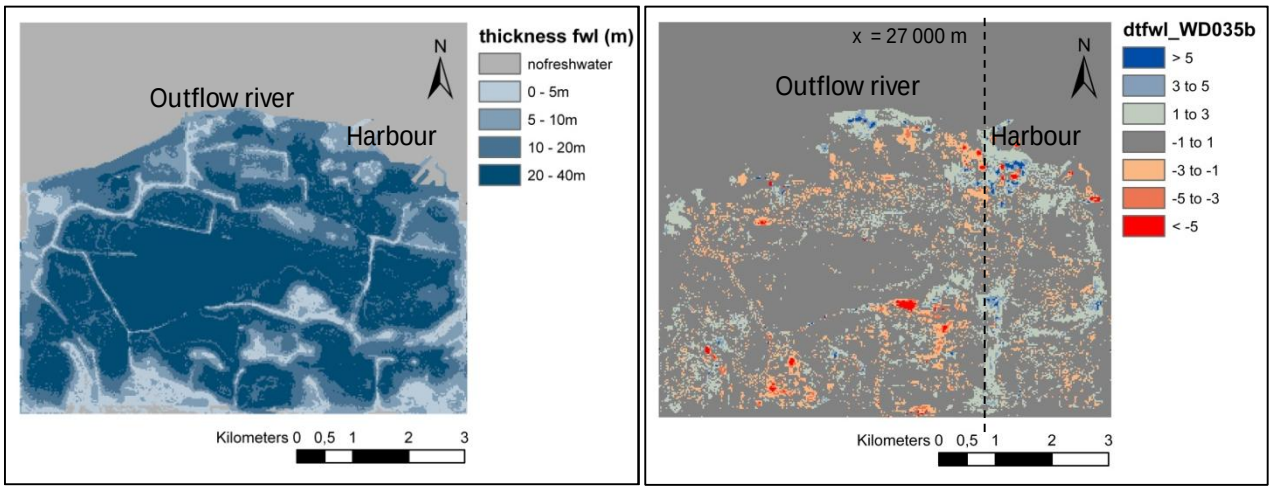

Figure 49. Left: freshwater lens thickness in the reference simulation. Right: absolute difference between freshwater lens thickness when the characterization of surface water bodies and tile drainage is at a 100*100 m^2 resolution and the reference simulation (resolution=25*25 m^2).

[17] See Section 2.3.6 and Subchapter 3.5 for more information on the implementation of the top system and the role of resolution on this characterization.

[18] The characterization of inland rivers and ditches hardly changes due to upscaling because the 25*25m^2 parameterization of these features was already based on rather coarse data.

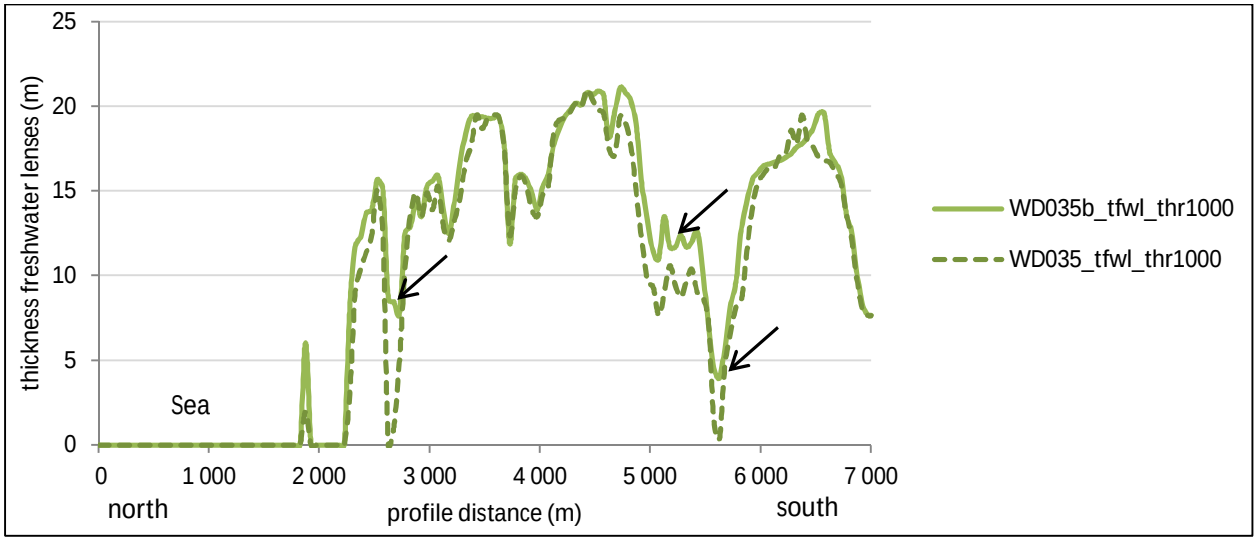

Figure 50. Freshwater lens thickness (threshold value 1 000 mgCl$^-$/l) for the reference simulation (WD035, dashed lines) and the simulation wherein the RIV- and DRN-packages were up scaled (WD057, solid lines); profile over x=25 000 m (for an orientation map see Figure 15 on page 28).

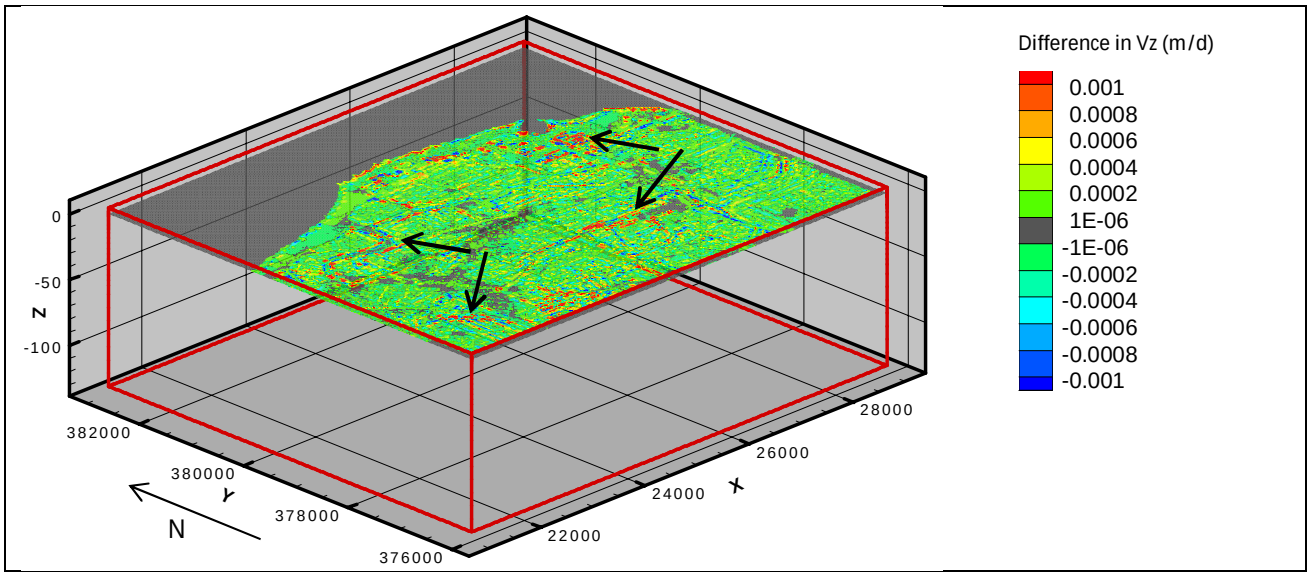

Figure 51. Difference between the effective pore vertical groundwater velocities of simulation WD035b -in which the RIV- and DRN-packages are parameterized on a 100*100 m^2 grid- and the effective pore vertical groundwater velocities of the reference simulation (resolution 25*25 m^2). The black arrows indicate some of the surface water bodies.

5.2.9 Flow time steps

In the reference simulation 36 flow time steps per stress period of one year are used, which means that the duration of each flow time step is ~10days. To test the sensitivity of the model to this parameter, it is subsequently run with one, 12 and 73 flow time steps (i.e. flow time steps with duration of 1 year, 1 month and 5 days).

Freshwater lens thickness. In the plots below the difference in freshwater lens thickness of the three sensitivity runs compared to the reference run is shown. Standing out is the decrease, at some places with almost 10 m, in freshwater lens thickness when only one flow time step is used per stress period of one year (plot B). When 12 flow time steps are used, these differences are almost everywhere reduced to less than 3 m (plot C). In the last case (73 flow time steps with a duration of 5 days), the differences with the reference are minimized to some (seemingly) arbitrarily distributed spots (plot D).

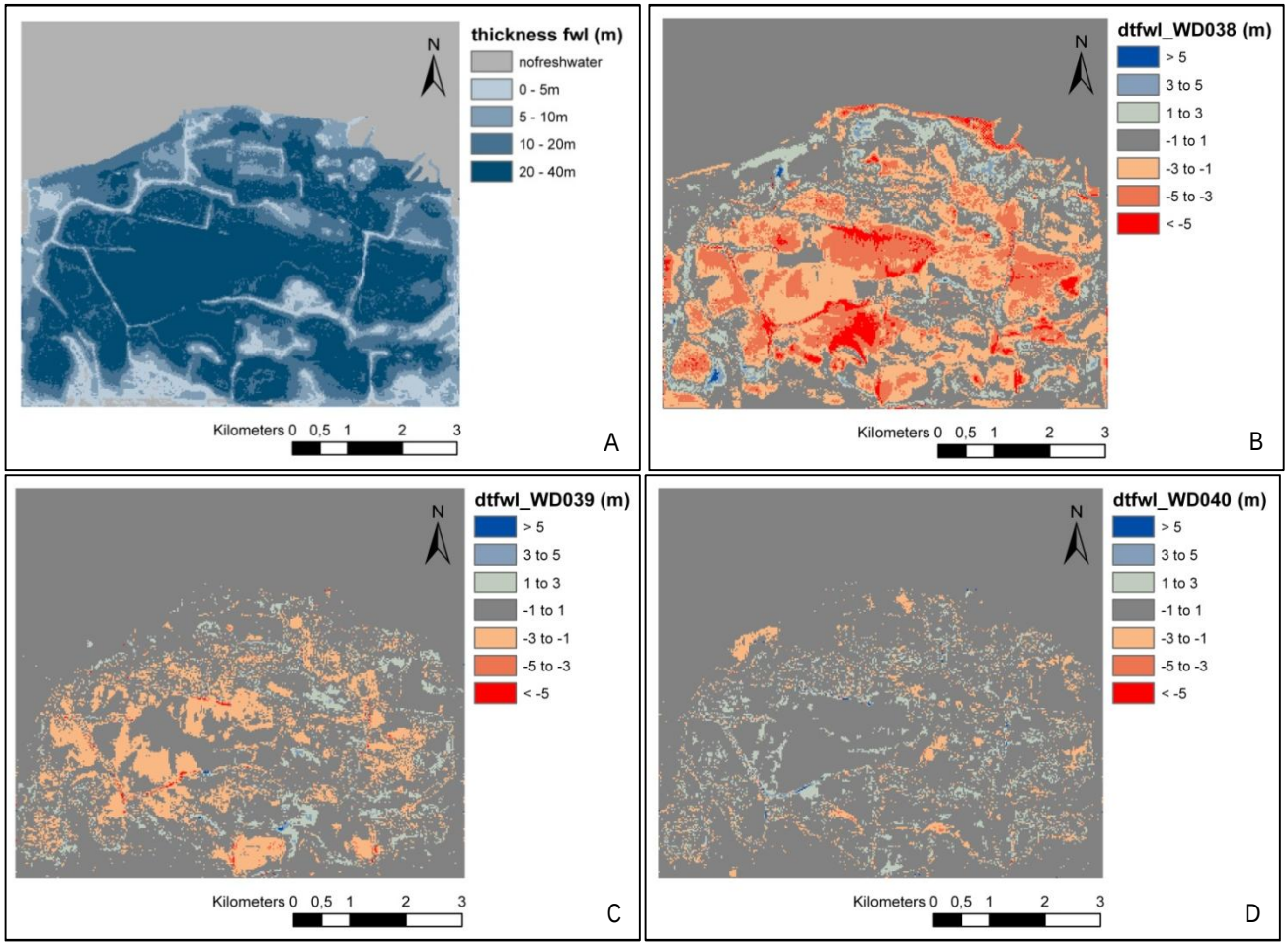

Figure 52. A: reference freshwater lens thickness. B, C and D: respectively, the difference in freshwater lens thickness when compared to the reference simulation of the simulations with one (WD038), 12 (WD039) and 73 (WD040) flow time steps per stress period of one year.

Concentrations. An exploratory analysis of the concentration field, complemented with concentration probes per layer at locations where freshwater lens thickness changes most, shows that the explanation for many changes is in the amount of mixing (see also Appendix G). At general holds that the smaller the number of flow time steps (i.e. the longer the duration of each flow time step) used, the more mixing occurs in the upper aquifer. As a result the isohalines move upward and, thus, freshwater lens thickness decreases. This upward movement as a consequence of more mixing is interesting. It was expected that the thickness of the transition zone would increase, but that this would lead to an upward movement of the isohalines was not thought of.

Balances. The increase in mixing in the case of only one flow time step leads to a, respectively, 9% and 14% higher mass outflow via RIV- and DRN-cells. In the other two cases these differences are reduced to less than 3% of the original values (cf. Table 14 on page 32).

Stability numbers. For all simulations applies that the Mixing Criterion is the constraining stability factor. Furthermore, the smaller the number of flow time steps (i.e. the longer their duration) the larger the number of solute time steps per flow time step required. In the case of one, 12, 36 and 73 flow time steps, this means a subdivision in, respectively, 76, seven, three and one solute time steps. Note that the multiplication of the two does not give a constant number of solute time steps per stress period. Meanwhile, the runtime of the model increases with the amount of flow time steps: 13h49min, 16h02min, 26h19min and 37h55min for, respectively, the runs with one, 12, 36 and 73 flow time steps per stress period.

Other. In the one flow time step-situation, BMix and Dmix are displaced with up to three meters in the vertical direction (at some places up at others down) near the lateral model boundaries and the coast.

Synthesis. The smaller the number of flow time steps per stress period (i.e. the longer their duration), the more mixing occurs in the upper aquifer. At most locations this leads to an upward movement of the isohalines and, thus, to a decrease in freshwater lens thickness. Note, however, that the difference in freshwater lens thickness between the runs with 73 and 36 flow time steps is minimal, while the runtime of the latter is 30% shorter.

Table 14. Absolute cumulative mass and volume balances of the reference simulation (36 advection particles) and balances of simulations WD038, WD039 and WD040 with, respectively, 1, 12 and 73 flow time steps as percentages of the reference simulations.

	WD035 (Reference)		WD038 (1fts/sp)		WD039 (12fts/sp)		WD040 (73fts/sp)	
	Mass	Vol.	Mass	Vol.	Mass	Vol.	Mass	Vol.
	ABS (g)	ABS (m3)	(%ref.run)	(%ref.run)	(%ref.run)	(%ref.run)	(%ref.run)	(%ref.run)
IN								
Recharge	1.34E+10	6.69E+08	100	100	100	100	100	100
RIV-cells	6.09E+11	5.10E+07	103	102	100	100	100	100
GHBs	1.15E+13	9.35E+08	102	107	100	100	100	100
TOTAL IN	1.21E+13	1.66E+09	102	104	100	100	100	100
OUT								
RIV-cells	-1.13E+12	-4.34E+08	109	100	103	100	98	100
Tile drains	-9.95E+10	-3.14E+08	114	100	102	100	98	100
GHBs	-1.08E+13	-9.07E+08	101	107	100	100	100	100
TOTAL OUT	-1.20E+13	-1.66E+09	102	104	100	100	100	100

5.2.10 Advection particles

The reference simulation is run with four advection particles per cell. During the sensitivity analysis the model was run with one, eight and 27 particles.

Freshwater lens thickness. For the effects on the freshwater lens thickness refer to Figure 53 on page 66. The first point to make is that there is a generalized decrease in freshwater lens thickness with more than 5 meters when the amount of advection particles is reduced to one per cell (plot B). When the model is run with eight or 27 advection particles, at some sites freshwater lens thickness increases and at others it decreases (differences <3 m). In the latter cases, the increases are concentrated along the edges of the Large Central Freshwater Lens (plots C and D). The difference between simulations with eight and 27 particles is negligible.

The profile in Figure 54 on page 66 shows that, for the run with one particle, not only the 1000 mg^{-}/l-freshwater lens thickness (threshold value for the freshwater lens thickness), but also the 30 $mgCl^{-}$/l- and the 1500 mg^{-}/l-freshwater lesn thickness decrease with more than 10 m. The depth of DMix decreases with a maximum of five meters. The cumulative mass and volume balances (see Table 15 on page 65) confirm the salinization of the top layers: i.e. the volumes of water leaving the model via the DRN- and RIV-packages remain the same, but the outflow of solute mass via these pathways increases exponentially. On the contrary, augmenting the number of advection particles leads to a less saline outflow by means of these packages.

Streamlines. Though the general flow pattern for all four runs looks similar, some of the streamlines in the upper aquifer become less erratic when more advection particles are used, and vice versa (Figure 55 on page 67). It seems that, on the one hand, the direction of the effective pore groundwater velocities determining the behaviour of these streamlines mainly depends on the homogeneity of the chloride concentration field, and that, on the other hand, the precision of the latter is directly related with the amount of advection particles used.

Runtime. A final remark concerning the sensitivity to the amount of advection particles concern the runtime of the model. The reference (four particles), eight and 27 particles simulations show an extreme increase in runtime, namely 26h19min, 32h16min and 85h43min hours. Yet, this trend does not continue when decreasing the amount of particles; the one particle simulation also shows a slight (2 hours) increase in runtime when compared to the reference simulation

Synthesis. Increasing the amount of advection particles leads to a more precise calculation of the concentration field. In the case of the Waterdunen model, this increase in precision leads to less mixing, thicker freshwater lenses, less erratic streamlines and a significantly less saline outflow via the RIV- and DRN-packages. However, increasing the amount of particles also leads to an extreme increase in runtime.

Table 15. Cumulative mass and volume balances of the model simulations with one, eight and 27 advection particles in percentages of the reference simulation.

	WD035 (Reference)				WD041 (1 adv part)		WD042 (8 adv part)		WD043 (27 adv part)	
	Mass		Vol.		Mass	Vol.	Mass	Vol.	Mass	Vol.
	ABS (g)	(%)	ABS (m3)	(%)	(%ref.run)	(%ref.run)	(%ref.run)	(%ref.run)	(%ref.run)	(%ref.run)
IN										
WEL-cells	1.34E+10	0	6.69E+08	40	100	100	100	100	100	100
RIV-cells	6.09E+11	5	5.10E+07	3	98	98	100	100	100	100
GHBs	1.15E+13	95	9.35E+08	57	102	102	100	100	100	100
TOTAL IN	1.21E+13	100	1.66E+09	100	102	101	100	100	100	100
OUT										
RIV-cells	-1.13E+12	9	-4.34E+08	26	278	96	91	100	76	101
Drains	-9.95E+10	1	-3.14E+08	19	344	104	94	100	90	100
GHBs	-1.08E+13	90	-9.07E+08	55	101	103	100	100	100	100
TOTAL OUT	-1.20E+13	100	-1.66E+09	100	120	101	99	100	98	100

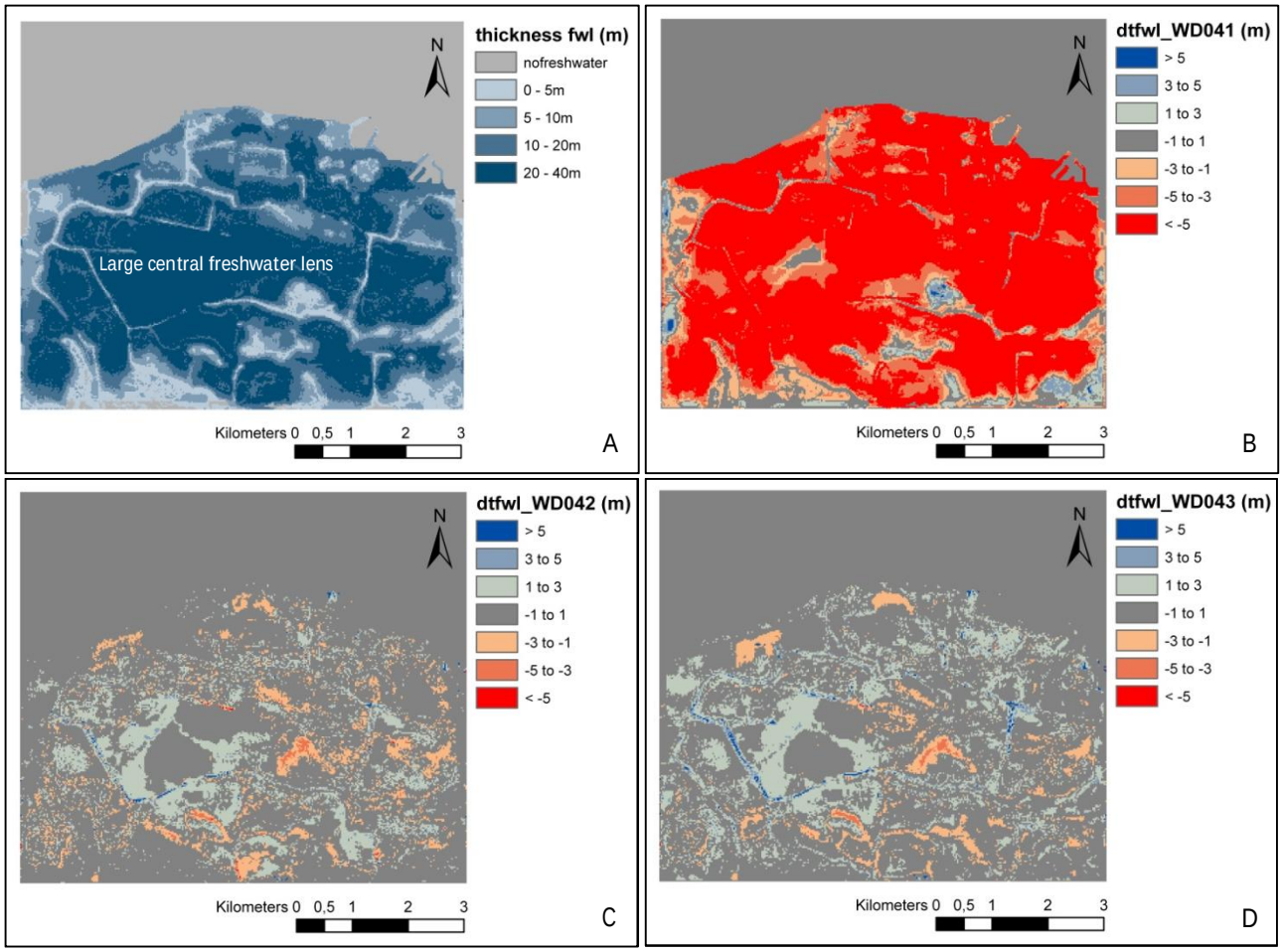

Figure 53. The effect of the number of advection particles on freshwater lens thickness. A: Freshwater lens thickness in the reference simulation. B, C, and D: difference in calculated freshwater lens thickness for, respectively, model runs with one, eight and 27 advection particles when compared to the reference simulation.

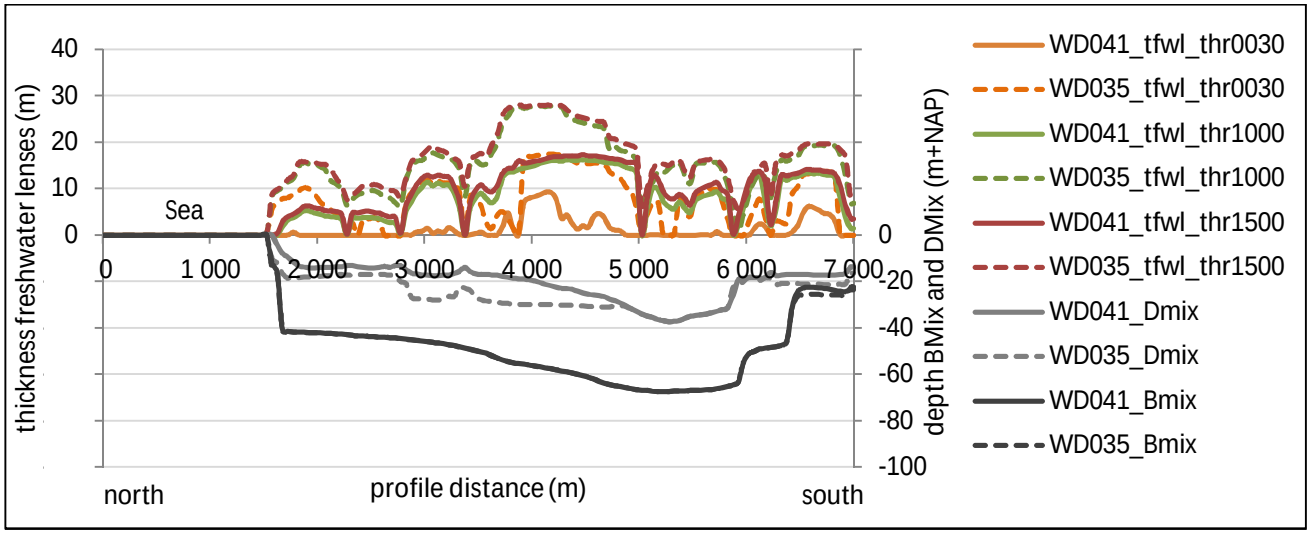

Figure 54. Freshwater lens thickness (as a function of the threshold value), BMix and Dmix over cross-section x=25 000 m for model simulation WD041 with one advection particle (solid lines) compared to the reference simulation WD035 (dashed lines). Refer to Figure 15 on page 28 for an orientation map.

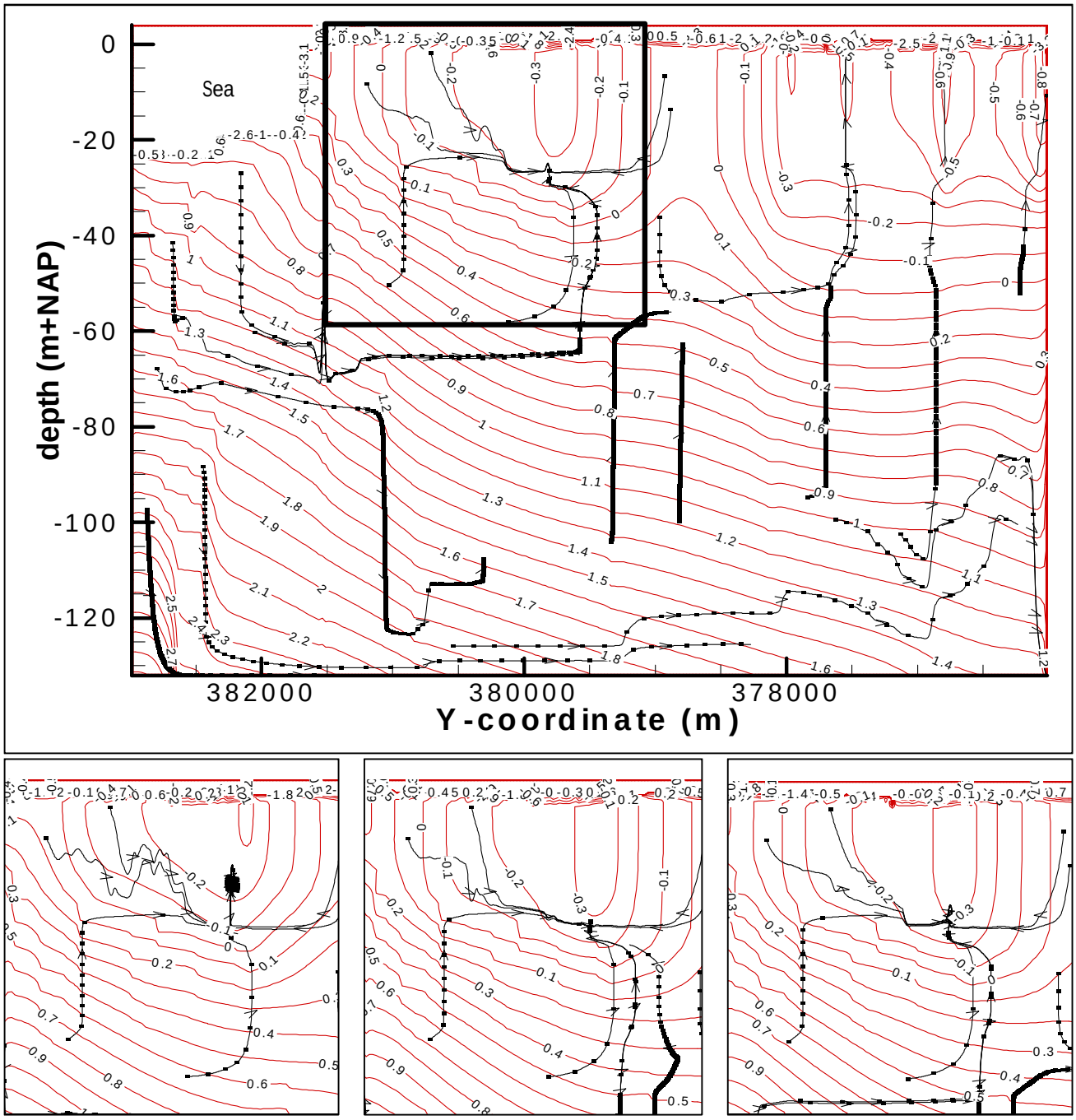

Figure 55. More advection particles lead to less erratic streamlines. Top cross section: streamlines over X=25 000 m(orientation map in Figure 15 on page 28) for the reference simulation (four advection particles). Bottom from left to right: changing streamlines in the area identified with the square for the cases with one, eight and 27 advection particles.

5.2.11 CFL-factor

The Courant-Friedrich-Lewy (CFL) factor stands for the maximum relative distance advection particles are allowed to travel within one solute time step; the factor is needed to determine the CFL numerical stability criterion (for a more detailed description refer to page 23). Yet, as time discretization in the reference simulation is fully constrained by the Mixing Criterion, and thus not by the CFL-criterion, there is no use in analysing the effect of a larger CFL-factor; the output of the model would be exactly the same. However, on the contrary, it is probable that with a decrease of the CFL-factor, the CFL-Criterion at a certain point takes over the restricting function of the Mixing Criterion. In the reference run the CFL-factor is four; to analyse the sensitivity of the model to this factor it was first reduced to two, and thereafter to 0.8.

Time discretization. The hypothesis stated above is confirmed by the model output of the two sensitivity runs. Both for the CFL=2 and the CFL=0.8 case, the CFL-criterion becomes constraining to time discretization. As a consequence, the flow time steps are automatically subdivided into, respectively, three and nine smaller solute time steps. This finer time discretization leads to longer runtimes. The runtime of, respectively, the reference simulation, the CFL=2 and the CFL=0.8 simulations is 26h19min, 29h09min and 42h16min.

Output. The impact of this restriction on the output states is very limited. Changes in equivalent freshwater heads, effective pore groundwater velocities, streamlines and cumulative volume and mass balances are negligible. Consequently, as shown Figure 56, freshwater lens thickness also almost does not change. It is striking, however, that the changes in freshwater lens thickness that do take place, seem to be larger in the CFL=2-case than in the CFL=0.8-case. This seems to indicate there is no trend in the changes.

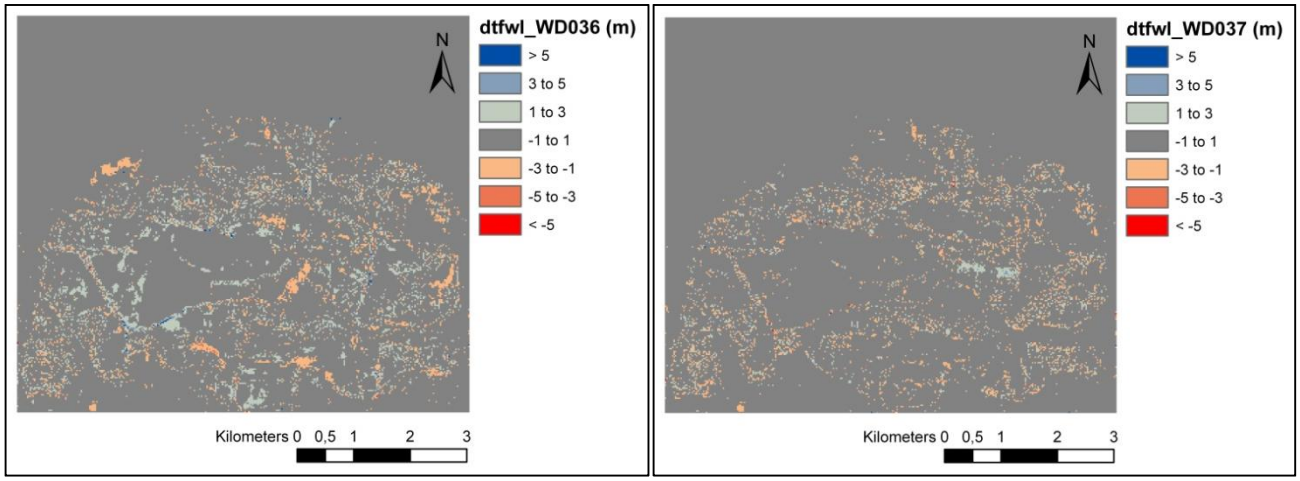

Figure 56. Difference in modelled freshwater lens thickness for model simulations with CFL=2 (left, WD036) and with CFL=0.8 (right, WD037) compared to the reference simulation.

Other. The location of Bmix and Dmix remains unchanged for all situations.

Synthesis. When the CFL-factor is the constraining time discretization criterion, decreasing the CFL-factor leads to more solute time steps and, therefore, to longer runtimes. The effect of the CFL-factor on the output states is minimal, when not absent.

5.2.12 Summary

Table 16. Tabular summary of the sensitivity analysis. Be careful, this table jumps to general conclusions, while there is a lot more to be said. Please refer to the previous subchapters for a more elaborate description.

Parameter	Short description impact	Sensitivity
Recharge	A decrease in groundwater recharge leads to thinner freshwater lenses, especially close to the coast; the transition zone becomes thicker. The effective vertical pore groundwater velocities and the cumulative volume balance show that differences in applied groundwater recharge are partly corrected by changes in the in- and outflow via RIV- and DRN-cells.	High
Concentration rivers	Negligible.	None
River bed resistance	An increase from two to four days of the river bed resistance leads to higher (up to 10cm) heads in the core of the model, changes in the horizontal velocities in the sandy areas, more outflow via tile drains and a severe (one to five meters) decrease in freshwater lens thickness between the Large Central Freshwater Lens and the coast. A decrease in resistance leads to opposite effects.	High
Sea floor resistance	A decrease of the sea floor resistance leads to an increase in marine intrusion and, consequently, to more saline drainage via RIV- and DRN-cells immediately behind the coastal dike. Freshwater lens thickness decreases slightly close the harbour and the outflow of the major river of the modeling domain.	Moderate
Porosity	A higher porosity results in much thinner freshwater lenses, higher horizontal velocities and an increase in the salt mass outflow via ditches, rivers and tile drainage. The effects are highest along the edges of large freshwater lenses.	High
Mechanical dispersion	A higher mechanical dispersion leads to more mixing, which results in a decrease in freshwater lens thickness. The effects are highest near the coast and at the edges of large freshwater lenses. In addition, from the moment on that the Neumann criterion becomes limiting to time discretization, a higher dispersion leads to a longer runtime.	Moderate
Transmissivity GHBs	There is little difference in using a GHB-transmissivity at the aquifers of 100, 500 or 2 000 m^2/d. Yet, when the highest effective pore groundwater velocity occurs in a lateral model boundary cell, higher transmissivities can result in an extreme increase in runtime. Closing-off the model by using a GHB transmissivity equal to nil, alters the equivalent freshwater head distribution in the whole model, and leads to large (>10m) changes in freshwater lens thickness in a 1km-broad band along the lateral model boundaries.	Moderate
Discretization drainage system	Although one sensitivity run is too little to legitimize general statements, chloride concentrations, equivalent freshwater heads and effective pore groundwater velocities change most at the coast, near ditches and rivers. The thickness of the large freshwater lenses does not change.	Low
Flow time steps	The smaller the amount of flow time steps (i.e. the longer their duration), the more mixing occurs and the thinner (decreases of several meters) freshwater lenses become. More flow time steps stand for (much) longer runtimes. Therefore, depending on the objectives, it is questionable up to where precision still outweighs time input.	High
Advection particles	Increasing the amount of advection particles results in a more precise calculation of the concentration field, less erratic streamlines in the upper aquifer and a significantly less saline outflow via the RIV- and DRN-packages. In the Waterdunen case this leads to thicker freshwater lenses.	Moderate
CFL-factor	The effect on the output states is negligible. When the CFL-criterion is constraining, a decrease in the CFL-factor leads to an extreme increase in runtimes.	Negligible

CHAPTER 6: DISCUSSION

The main goal of this research was to list the input parameters that deserved more attention in variable density groundwater flow modelling. In this regard, a sensitivity analysis was performed on the Waterdunen model. Although the results of that analysis are by no means universal, they shine a light on the processes influenced by each parameter, the locations where most change is triggered and the type of reactions that can be expected. In the previous chapter, the sensitivity of the model output to each parameter was discussed one by one. But, is it also possible to draw up the intended list of priority parameters? And, if yes, what is then the validity and legitimacy of that list?

This chapter starts out with some remarks on the discretization requirements of MOCDENS3D, the definition of 'freshwater lenses' and the comparison of the modelled with the observed freshwater lens thicknesses. Thereafter, the overarching outcomes of the sensitivity analysis are discussed. The last part of the chapter is dedicated to a short methodological discussion.

Verification of the model

In theory, the particle tracking algorithm applied by MOCDENS3D requires a constant volume of water in all cells (Konikow, Goode et al. 1996; Oude Essink 1996c). In the Waterdunen model, column width (25m), row width (25m) and effective porosity (0.3) are constant, but layers become thinner toward the surface; the water volume per cell is, therefore, variable. Yet, unlike what theory tells us, the quality of the model seems not to be put in jeopardy at all by this choice; the discrepancy in the cumulative mass balance is just 1%. It seems that the fine discretization of the top layers –in combination with the gradual transition from saline to fresh water- is sufficient to avoid the introduction of a bias.

Validation of the model

Freshwater lenses are usually referred to as if there is a well-established definition of the phenomena. Fairly at the beginning of this report, this principle of pure freshwater lenses floating on top of saline water is discussed (see Figure 3 on page 15). This simplification is very useful for rapid assessments and explanatory purposes, but it is not representative for the Dutch coastal system where the interface between fresh and salt is rarely sharp (Oude Essink 2001a). The output of the reference simulation described from page 38 onwards confirms that also in the Waterdunen case the transition from fresh to salt water is gradual. For that reason, a (chloride) concentration threshold value is needed to define the dimensions and characterization of a freshwater lens. As a consequence, obtained freshwater lens thickness can vary even though the mass distribution in the model remains unchanged. Therefore, one should proceed with caution when making use of and communicating on 'freshwater lenses'.

In this research, to determine freshwater lens thickness, a threshold value of 1 000 $mgCl^-/l$ is used. However, in the Province of Zeeland the 1 500 $mgCl^-/l$ threshold is also common (see also the modified classification by Stuyfzand on page 14). With the existence of such a considerable transition zone, knowledge on the impact of the threshold value becomes relevant. For that reason, the distance between the 1 000 $mgCl^-/l$ or 1 500 $mgCl^-/l$ lines was analyzed in all freshwater lens thickness profiles obtained during this research. This exercise turns out that it does not matter whether a threshold value of 1 000 $mgCl^-/l$ or 1 500 $mgCl^-/l$ is used; the differences in calculated freshwater lens thickness are negligible. The maximum difference occurs in the extreme situation of a no-flux boundary (GHB transmissivity=0 m^2/d) and is ~2 m.

On the contrary, the same profiles –complemented with probes of concentrations- show that the use of a threshold in itself does behold the danger of overemphasizing minor concentration differences. This might happen in two ways.

1. First, there is the situation in which consecutive cells are characterized by very similar concentrations that are close to the threshold value applied. In those cases, small changes in concentrations can lead to large changes in freshwater lens thickness; a situation that happened, for example, with the sensitivity runs on the river concentrations (Appendix F).
2. The second issue concerns the algorithm used to calculate freshwater lens thickness and was already touched upon by Morway, Niswonger et al. (2012). To calculate freshwater lens thickness, concentrations are only probed in the vertical direction; freshwater lens thickness is determined by the first cell wherein the established threshold value is exceeded. Consequently, a small lateral displacement of the freshwater lens boundary can have a large effect on freshwater lens thickness. This happens, for example, in simulations WD054 and WD055 (sensitivity analysis river bed resistance, page 49).

In both situations, the analysis is numerically correct, but exaggerates the intuitive importance that is attached to the changes.

Because of its ease of comparison and its importance for stakeholders, freshwater lens thickness was used to evaluate the quality of the Waterdunen model. Within the Waterdunen project, 14 soundings were available to this end. However, there are at least four important aspects of that analysis that are worth to be thoroughly discussed here.

1. First, there is the number of soundings. For a total area of 56km^2, 14 samples seem to be very few. Obviously this is a consequence of the high costs, but that does not alter the fact that it might be too little to assess the quality of the model.
2. The second aspect concerns the location of the soundings. As presented in Figure 25 on page 40, all observations are concentrated in a very small part of the model domain. Though this is a logical outcome of the aim to monitor the changes in the fresh-salt distribution in the vicinity of the project area, it is a major limitation for assessing the overall quality of the modelled freshwater lens thickness.
3. Also related with the spatial distribution is the third issue. The soundings are all in the vicinity of the river, albeit the sensitivity runs have shown that the spatial variability in concentrations in these areas is very is high. Consequently, small horizontal displacements, as mentioned earlier, might lead to a misleading large error (see also the previous paragraph).
4. Fourth, and lastly, there is a large variability in the calculation of observed freshwater lens thickness. Actually, it looks straightforward: one should translate the electrical conductivity obtained with the ECPTs into concentrations and then, using the chosen threshold value, calculate freshwater lens thickness. However, there is a major difficulty in the first step. To transform electrical conductivity, which at times had to be extrapolated, into concentration different formulas can be used (see also the equations on page (30)). The differences in the formulas are a result of the dependency on the local chemical composition of the pore water and the bulk resistivity of the geologic formation (cf. Louw, Eeman et al. (2011), Van Meir and Lebbe (2003), Insituto Geológico de España (2004) and Connors and Kester (1974)). In this research, the concentrations were calculated using the formulas proposed in Louw et al. (2011) and CMA (N.D.). The differences between the two calculation methods mount up to 20 m (cf, Table 7 on page 41), which indicates an extremely high derived uncertainty in freshwater lens thickness.

For the four reasons mentioned above, I think freshwater lens thickness might not be the best state to compare modeled with observed values. I would even advise not to attach too much importance to the misfit shown in Figure 25 on page 40. There is a large chance that a different comparison method would give better results. Altogether, as Grift and Griffioen (2008) also showed, there is just an intrinsic difficulty in simulating point observations with 3D-models.

The sensitivity analysis

The results of the sensitivity analysis show that there are two major lines along which the output changes as a function of the input parameters: the type of response and the location. Here, with type of response I refer to the quantitative development of the output when changing an input parameter; with location I mean the place where the largest changes occur when varying the input. The results of the sensitivity analysis are discussed along these two lines.

Concerning the type of response, it turns out that the input parameters analyzed can be categorized into three classes: input parameters that do only have a negligible effect on the model output (1), parameters to which the output shows a monotone response (2) and parameters that above or below a certain threshold value (almost) do not change the model output anymore (3) (see Table 17).

The following parameters have a negligible effect on the model output:

- river concentration: because, as in most deltaic areas, the majority of the rivers and ditches drains the area the changing RIV-concentrations infiltrate and, thus, do not affect the salinity of the subsurface; and,
- CFL-criterion: has no effect because of the low effective groundwater velocities.

On the contrary, the physical parameters

- groundwater recharge;
- river bed resistance;
- sea floor resistance;
- effective porosity; and
- the dispersion factor

show a monotone correlation with the output throughout the used parameter ranges. In this, I think the extreme sensitivity to the river bed resistance and porosity deserves some extra attention. In groundwater modeling it is usual

to use an average value for the river bed resistance. The main reason to do so is in the fact that the spatial variability (and at some places also the temporal variability) of the parameter is very high (Jousma and Massop, 1996; Massop and Gaast, 2006). In 'normal' freshwater groundwater modeling the use of such average values is more or less accepted. However, the results presented in Section 5.2.5 show that variable density groundwater flow models are very sensitive to this parameter.

The numerical parameters
- GHB trasmissivity
- Flow times step duration
- Number of advection particles

belong to the threshold category. The output of the Waterdunen model does not change anymore for GHB-transmissivities above 100 m^2/d, flow time step durations of less than 10 days and more than eight advection particles.

Only the discretization of the drainage system cannot be categorized by type of response because to find out whether a trend in the results exists at least 3 simulations are needed for comparison.

PHYSICAL PARAMETERS	NUMERICAL PARAMETERS
Groundwater recharge	Transmissivity GHBs
Concentration rivers	Discretization drainage system
River bed resistance	Number of flow time steps
Sea floor resistance	Number of advection particles
Porosity	CFL-factor
Mechanical dispersion	

Table 17. Classification of the parameters according to the type of response they induce in the output. In green the parameters that have a negligible effect on the model output, in red the parameters to which the output show a monotone response and in orange the parameters that above or below a certain threshold value do not affect the model output anymore.

The second line along which to organize the results is the location of the major changes. Depending on the physical processes influenced by a parameter, certain locations are more sensitive to changes than others. The five locations identified as most sensitive during the analysis were the 1km-band along the lateral model boundaries, the shoreline, the vicinity of rivers & ditches, the bottom & edges of large freshwater lenses and the sandy creek ridges (Figure 57 on page 73).

The 1km-band along the lateral model boundaries is very, though only, sensitive to nullification of the interaction with the outside world. When the GHB-transmissivity is reduced to 0 m^2/d, freshwater lens thickness in this area changes with up 5 to 10 meters. Henceforth, it seems that the model needs approximately 1 km to balance the settings of outside world with its own parameterization.

The shoreline, and especially the harbor and the outflow of the largest river, is also rather sensitive to changes in the parameterization. Groundwater recharge, sea floor resistance, the dispersion factor and the duration of the flow time steps, all affect the extent and the concentration of marine intrusion. Consequently, the freshwater lens thickness and the cumulative salt mass balance are also affected: more marine intrusion leads to thinner freshwater lenses and a

higher salt outflow via tile drains and ditches. The sensitivity of this area is probably induced by the combination of high conductivities (coastal sands) and the proximity of very large differences in chloride concentrations.

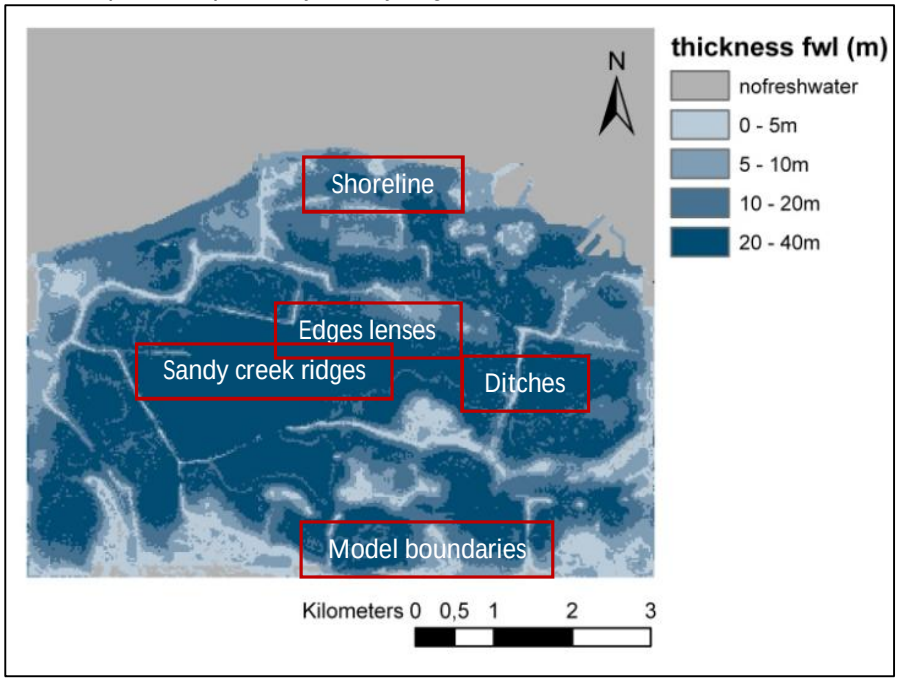

Figure 57. Map of the reference freshwater lens thickness with an indication of the most sensitive areas in the model.

A large part of the fresh-salt battle is fought over in the vicinity of rivers and ditches. Not only the evident river bed resistance, but also groundwater recharge, sea floor resistance, effective porosity, the duration of the flow time steps and the number of advection particles have a considerable impact on the processes close to rivers and ditches. The changes are reflected especially in the freshwater lens thickness and the cumulative volume and mass balances.

Under influence of the river bed resistance, porosity, mechanical dispersion, the duration of the flow time steps and the number of advection particles, large changes are identified along the edges and the bottom of the large freshwater lenses. Two main processes seem to determine these changes: a change in the form of the freshwater lenses and dispersion. River bed resistance and porosity change the form of the lenses. The first changes the total volume of freshwater stored in the model; the latter changes the soil volume occupied by the freshwater. The dispersion factor, the duration of the flow time steps and the number of advection particles determine the intensity of dispersion, and thus the amount of mixing.

In the sandy ridges, finally, both the direction and the magnitude of velocity change quite a lot when groundwater recharge, river bed resistance, porosity or the number of advection particles is changed. It seems that when the overall equilibrium of the model changes (e.g. seepage becomes infiltration or vice-versa), this has primarily consequences for the situation in the sandy creek ridges. In line with Darcy, this sounds plausible: conductances are highest in sandy areas and, thus, there changes are easily passed on.

The above five locations are the ones where the sensitivity of the model emerges first. However, on the contrary, deep in the model there is (almost) no change. The only parameter that has influence below -50 m+NAP is the transmissivity of the GHBs when the interaction with the outside world is nullified. Yet, even then, changes are only translated to the top layers of the model to a very limited extent. The explanation for this is in the existence of an almost impermeable layer halfway the model (Figure 17 on page 29). Based on these results, I would suggest (for short time-spans) to cut-off the model where the impermeable layer starts and to concentrate all computational resources on the upper part of the model.

Comments on the methodology and code

As elsewhere, also in this research, time was a major limitation. On the one hand there was the runtime of the model that in most cases was in the order of 24 to 36 hours. On the other, the post-processing, visualization and analysis of the data was also very time-consuming. Notice that the total output of each simulation consisted of 3.5GB of data. Even though large parts of the data processing were automatized, it took a lot of time to find out about the relations, the meaning and the physical processes that could explain the output of the 28 sensitivity runs. At the same time, it feels like it would have been better to do more simulations per parameter, so that the change throughout the input range could be monitored more closely. An alternative could have been the use of a much simpler synthetic model. However, as Konikow (2011) already said "we do not know what we do not know". It is well possible that certain interactions pop up because of the attempt to simulate reality as closely as possible; the regional scale, heterogeneity and, for example, the specific lay-out of the top system might lead to processes that would not have been identified when using a synthetic model. I think there is a major value in the use of a model that simulates as well as possible a specific real-life situation.

In addition, there is the issue of the modeling code. In recent years MOCDENS3D is being overtaken by the USGS alternative SEAWAT. I think this is partly the consequence of the limiting reporting on the MOCDENS3D-code and the fact that it has not been updated and improved regularly. Unfortunately, this means that the connection with the groundwater community is slowly but surely being lost, which probably implies the loss of an alternative to SEAWAT in groundwater modeling. This is a pity since I would say it is always better to have more to choose off.

Notwithstanding all what has been said before, I think it is most important to always keep in mind that a) "a model is by definition a simplification of a very complex reality, so an end point will never be reached where a model is a precise representation of reality [...]" (Clement 2011), and that b) "for science to advance, we must [remain] critical of existing knowledge" (Oreskes and Belitz 2001).

CHAPTER 7: CONCLUSION

The objective of this research on fresh-salt groundwater flow modelling in Waterdunen, The Netherlands, was to analyse to which physical and numerical parameters variable density groundwater flow models are most sensitive. The idea was that such an analysis would provide modellers valuable information to decide which parameters to give priority to increase model accuracy when resources (e.g. time and budget) are limited. However, the study shows there exist no such clear-cut list of 'priority parameters'. The importance that should be attributed to a parameter highly depends on the location and the specific output the modeller is interested in; based on these specific circumstances, parameters worth extra investments can be selected.

Despite the fact that the ultimate result is not a list, the sensitivity analysis definitely provides valuable insights on the processes controlled and the output most influenced by each parameter. Five locations, for example, could be identified as being, in general, most sensitive to changes in parameterization: a 1km-band along the lateral model boundaries, the shoreline, the vicinity of rivers & ditches, the bottom & edges of large freshwater lenses and the sandy creek ridges. Besides, the parameters included in the study could be categorized according to the type of response. Some parameters have an overall negligible effect on the model output (river concentrations and CFL-factor). On the contrary, the output shows a monotone response to most physical parameters. In most cases, numerical parameters do not change the model output anymore above or below a certain threshold value.

In addition, the research pointed out that the comparison between modelled and observed freshwater lens thickness is not straightforward:

1. there is no unanimity on the formulas to translate electrical conductivity into chloride concentrations ;
2. small differences in concentration are often overemphasized because the threshold method to determine the freshwater lens thickness reduces 1D-data concentration data to a single value;
3. freshwater lens thickness only considers the vertical dimension; therefore, knowing that the 3D choride concentration field is very heterogeneous, small lateral displacements of the threshold-isohaline can lead to large errors in freshwater lens thickness; and, finally,
4. measurement practices are not consistent with the findings of the sensitivity analysis: performing electrical cone penetration tests is the easiest in the vicinity of rivers and ditches, but this is one of the locations where the output of variable density groundwater models is most sensitive to changes in the parameterization.

Altogether, the research shows that variable density groundwater flow modelling is not trivial. The solute-transport equation adds a lot of extra complexity to groundwater flow modelling. First, this is because the concentration field – which has a large influence on groundwater flow in deltaic areas- is very heterogeneous and largely unknown. Second, there is the issue of the time scales that are very different. Solute-transport is a much slower process than groundwater flow. Third, groundwater flow is calibrated on heads and a head difference of a couple of centimetres makes no difference. However, because of changes in flux direction such relatively small changes in heads can have devastating effects on solute-transport. Finally, the physical and numerical processes of groundwater flow and solute-transport often interlock with one another, and not seldom reinforce each other.

Although this research shows that there is still a long way to go in fresh-salt groundwater modelling, a lot of progress has also been made in recent years. It is possible to numerically model coupled solute-transport with groundwater flow, and the general pattern of infiltration and seepage, the existence of freshwater lenses and the occurrence of marine intrusion seem to be modelled correctly. There are certainly also glimmers of hope.

CHAPTER 8: RECOMMENDATIONS

As in every research, the attempt to answer one question rises many new ones. Also in this case. In view of the increasing interest in the availability of freshwater, the impacts of climate change, the chloride concentrations in ditches and rivers and many more, and the current variable density groundwater flow modeling practices it is advised to do further research on:

- the sensitivity of variable density groundwater models when two or more variables are changed at the same time; it is suspected that, due to the complexity of the processes, it is not possible just to sum up the impact of the different parameters;
- the sensitivity of transient groundwater models to the analyzed physical and numerical parameters;
- the explanation for the discrepancies in calculated freshwater lens thickness when using the different methods to translate electrical conductivity into chloride concentrations; and, finally,
- alternative methods to compare modeled with observed values (e.g. making use of the vertical concentration distribution, solving the conversion problem from electrical conductivity to concentration and determining best locations for collecting observations).

APPENDICES

Appendix A: Derivation analytical formulae

Darcy's Law

$$q_x = -\frac{\kappa_x}{\mu_i}\frac{\partial P}{\partial x} \qquad q_y = -\frac{\kappa_y}{\mu_i}\frac{\partial P}{\partial y} \qquad q_z = -\frac{\kappa_z}{\mu_i}\left(\frac{\partial P}{\partial z} + \gamma\right)$$

Equivalent freshwater head

$$\phi_f = h_f + z = \frac{P}{\rho_f g} + z$$

Hydraulic conductivities

$$K_{xx} = \frac{\kappa_x \rho_f g}{\mu_f} \qquad K_{yy} = \frac{\kappa_y \rho_f g}{\mu_f} \qquad K_{zz} = \frac{\kappa_z \rho_f g}{\mu_f}$$

Density dependent groundwater fluxes

$$q_x = -\frac{\kappa_x}{\mu_i}\frac{\partial P}{\partial x} = -\frac{\kappa_x}{\mu_i}\frac{\partial\left((\phi_f - z)\rho_f g\right)}{\partial x} = -\frac{\kappa_x}{\mu_i}\frac{\partial(\phi_f \rho_f g)}{\delta x} = -\frac{\kappa_x \rho_f g}{\mu_i}\frac{\partial \phi_f}{\partial x} = -K_{xx}\frac{\partial \phi_f}{\partial x}$$

$$q_y = -\frac{\kappa_y}{\mu_i}\frac{\partial P}{\partial y} = -\frac{\kappa_y}{\mu_i}\frac{\partial\left((\phi_f - z)\rho_f g\right)}{\partial y} = -\frac{\kappa_y}{\mu_i}\frac{\partial(\phi_f \rho_f g)}{\delta y} = -\frac{\kappa_y \rho_f g}{\mu_i}\frac{\partial \phi_f}{\partial y} = -K_{yy}\frac{\partial \phi_f}{\partial y}$$

$$q_z = -\frac{\kappa_z}{\mu_i}\left(\frac{\partial P}{\partial z} + \gamma\right) = -\frac{\kappa_z}{\mu_i}\left[\frac{\partial\left((\phi_f - z)\rho_f g\right)}{\delta z} + \rho_i g\right] = -\frac{\kappa_z}{\mu_i}\rho_f g\left(\frac{\partial \phi_f}{\partial z} - \frac{\partial z}{\partial z} + \frac{\rho_i g}{\rho_f g}\right) = -K_z\left(\frac{\partial \phi_f}{\partial z} - 1 + \frac{\rho_i}{\rho_f}\right)$$
$$= -K_{zz}\left(\frac{\partial \phi_f}{\partial z} + \frac{\rho_i - \rho_f}{\rho_f}\right)$$

Where:
$q_x, q_y, q_z = Darcian\ specific\ discharges\ (LT^{-1})$
$\kappa_x, \kappa_y, \kappa_z = intrinsic\ permeability\ along\ the\ x, y\ and\ z\ coordinate\ axes\ \ (L^2)$
$\mu_i = dynamic\ viscosity\ (ML^{-1}T^{-1})$
$P = pressure\ (ML^{-1}T^{-2})$
$\gamma = \rho_i g = specific\ weight\ (ML^{-2}T^{-2})$
$\rho_i = groundwater\ density\ (ML^{-3})$
$\phi_f = equivalent\ freshwater\ head\ (L)$
$z = elevation\ with\ respect\ to\ reference\ level\ N.A.P.\ (L)$
$h_f = pressure\ head\ expressed\ in\ freshwater\ (L)$
$K_{xx}, K_{yy}, K_{zz} =\ hydraulic\ conductivity\ along\ the\ x, y\ and\ z\ coordinate\ axes\ (LT^{-1})$
$\rho_f = fresh\ groundwater\ density\ (ML^{-3})$
$g = gravity\ acceleration\ (LT^{-2})$
$\mu_f = dynamic\ viscosity\ freshwater\ (ML^{-1}T^{-1})$
$\frac{\rho_i - \rho_f}{\rho_f} = buoyancy\ factor\ (-)$

Assumptions:

- $\mu_i = \mu_f$, which means viscosity differences are not taken into account
- $density\ differences\ do\ not\ affect\ hydraulic\ conductivity.$

Appendix B: Calibration Zeeland model (Van Baaren, Oude Essink et al. 2011)

In this appendix, a summary of the calibration of the Zeeland model as it was reported by the modellers is given. For more details please refer to the report of the Zeeland model by Van Baaren, Oude Essink et al. (2011).

The Zeeland model was calibrated on equivalent freshwater heads. The calibration was performed by means of a comparison between the modelled heads and the piezometric measurements that are available at TNO-DinoLoket (2008) for the period between 1-1-1990 and 31-12-2000. In total the dataset comprised 3037 piezometric filters. However, by no means all these measurements were used in the calibration. The following selections were applied to filter the data:

1. First, all measurements were subjected to a time series analysis. Eight hundred and eighty three data series were deleted because they could not, or poorly, be explained by the groundwater recharge dynamics. This filter is applied because groundwater recharge (excluding the summer and winter stages in the rivers and ditches) is the only boundary condition that is known with sufficient accuracy to be correctly implemented in the model;
2. To increase the reliability of the average head used, all series with less than four measurements were excluded from the calibration set;
3. One series was deleted because the filter depth was unknown;
4. Eight series were deleted because the piezometers were located too close (<300 m) to large well extractions (> 30 000 m^3/year). This was done because upconing below such wells is flattened out when spatially discretising a numerical model;
5. 183 series were deleted because they were too close to large rivers and ditches. Heads in the vicinity of rivers and ditches are supposed to be highly dependent on the stages of the rivers and ditches. On the one hand the stages in the rivers are not calibrated because they are supposed to be sufficiently well-known; on the other it is not considered 'fair' to compensate eventual discrepancies with adjustments in other parameters;
6. 158 series were excluded of the calibration set because they were located in a clayey layer;
7. 13 series were excluded because they were located below the deepest model layer.

Attribution of the measurements to the model layers. The measurements were attributed to the sandy model layer with which the filter showed most overlap. When only the top or the bottom of the filter was known the height of the filter was assumed to be 1 m.

Density correction and statistics. Since a stationary calibration was performed the median and corresponding variance were input to the calibration. The medians were obtained by:

1. Deleting outliers;
2. Interpolating all measurements to obtain a series of heads for all days between 1-1-1990 and 31-12-2000;
3. The medians of the values obtained in step 2 were then calculated;
4. The obtained heads were corrected for differences by means of the equation of state (Equation (3)), assuming that the concentration of saline water is 18 600 $mgCl^-/l$ with a corresponding density of 1 025 kg/m^3, and that the density of fresh water is 1 000 kg/m^3. For the chloride concentrations, either concentration measurements were used (341 series) or the 3D concentration field developed by Pebesma in 2009 was used;
5. To quantify the uncertainty of each median, the amount of sufficient uncorrelated measurements was determined for each series; with this amount, the variance of the median was calculated. The uncertainty associated with the density correction was added to this variance;
6. After these corrections, 89 extra data series were excluded from the calibration set because there was such a big difference between the modelled and the measured values because a) a conceptual error is suspected in the dunes of Schouwen-Duiveland and b) a very large uncertainty of some fresh-salt corrections resulted in equivalent freshwater heads 1.5 m higher than the measured piezometric heads which is deemed unrealistic.

In the end the calibration set consisted of 517 measured median equivalent freshwater heads.

Calibration method. The calibration was performed with the software program PEST developed by Dougherty in 2005. In the program, the parameter set is optimized by minimizing the following function:

$$J_{meas} = \sum_{i=1}^{m} \left(w_i \left(\phi_{f\,model,i} - \phi_{f\,med,corr,i} \right) \right)^2 \quad (32)$$

$J_{meas} = error\ indicator(L)$
$w_i = weight\ assigned\ to\ measurement\ i\ (-)$
$\phi_{f\,model,i} = modelled\ equivalent\ freshwater\ head\ at\ the\ location\ of\ measurement\ i\ (L)$
$\phi_{f\,med,corr,i} = measured\ median\ equivalent\ freshwater\ head\ i\ (L)$
$m = total\ number\ of\ measurements(-)$

NB: the weights assigned to the measurements were directly correlated with the variance of the medians.

PEST uses the Levenberg-Marquart algorithm to find the minimum value for Equation (32). A limitation of this algorithm is that not too many parameters can be optimized because of computational constraints and because of the inevitable occurrence of correlations between parameters when their number is increased. The big advantage of the method is in its simplicity and speed of calculation (when the number of parameters is small) which allow calibration without previous upscaling.

The parameters considered during the calibration were:
- the horizontal conductivity (K_h) of the aquifers;
- the vertical conductivity (K_v) of the aquitards;
- the river bed resistance of each surface water type;
- groundwater recharge (by means of one multiplication factor applied to the whole field).

PEST requires the modeller to set a maximum and minimum value for each parameter. The ranges used in the calibration of the Zeeland model are shown in Table 18.

Table 18. Maxima and minima of the parameter ranges used in the PEST calibration of the Zeeland model.

Parameter	Minimum	Maximum
K_h aquifers	1/3*initial value	3*initial value
K_v aquitards	1/5* initial value	5*initial value
Resistance river beds	1/10*initial value	10*initial value
Groundwater recharge	9/10*initial value	11/10*initial value

To allow for more flexibility in the parametrization, the model domain was subdivided into five regions during the calibration:
- Schouwen-Duiveland/Goeree-Oveflakkee
- Walcheren/Noord-Beveland
- Tholen/St. Philipsland
- Zuid-Beveland
- Zeeuws-Vlaanderen.

The calibration was performed separately for each of these regions.

If the model output at a certain measurement location is not sensitive to a parameter, this parameter cannot be calibrated because the measurements do not contain information about these parameters. To determine which parameters belong to this category, the SENSAN software program developed by Doherty in 2005 was used.

PEST was first run in the parameter estimation mode, which resulted in PEST proposing large changes to some of the parameters. In some cases (when the uncertainty is high) such large changes can be legitimized. However, sometimes, the same effects can be obtained by changing other correlated parameters. The changes are then spread over more parameters, so that large changes in to a limited number of specific parameters are not needed anymore. After running PEST in the estimation mode, the output was used to run PESTs regularisation mode. In the regularisation mode the aimed minimization of the misfit was complemented with the request to limit as much as possible the changes to the parameters.

Calibration results. After a successful calibration the median of the residuals should be approximately zero; otherwise there is a systematic error ('bias') in the output, which means that there is an systematic under- or overestimation of the equivalent freshwater heads. The results presented in table 19 show that such a systematic error is not present in any of the regions of the Zeeland model.

The average absolute residuals tell something about the extent to which the model is capable to simulate the measured equivalent freshwater heads in absolute terms. The smaller these values the better the modelled values approach the measured values.

Although rarely discussed in model calibration reports, J_{meas} is also an important calibration result. In J_{meas} not only the residuals are considered but also the reliability of the measurements. When the average absolute residual is equal at the end of a calibration, a calibrated model that reproduces especially well the less certain measurements is less valid than a model that reproduces especially well the more certain measurements. Therefore, a strong decrease in J_{meas} indicates that the validity of the model has increased due to the calibration, even if the reduction in the average absolute residual is minimal. Table 19 shows that the calibration has strongly reduced the value of J_{meas}.

Table 19. Tabular summary of the calibration results of the Zeeland model.

Region	Median value residuals	Average absolute residuals	J_{meas} (m^2)
Schouwen-Duiveland/Goeree-Oveflakkee	-0.06→0.06	0.38→0.35	21709→13221
Walcheren/Noord-Beveland	0.18→0.17	0.33→0.31	7349→4909
Tholen/St. Philipsland	-0.03→0.004	0.42→0.31	7762→3835
Zuid-Beveland	0.16→0.03	0.27→0.20	4380→2409
Zeeuws-Vlaanderen.	0.18→-0.009	0.29→0.24	8318→6393

Appendix C: Dynamic equilibrium?

Figure showing the development of chloride concentrations over time; cross-section x=25 000 m. Note that freshwater lenses are still increasing after 250 years.

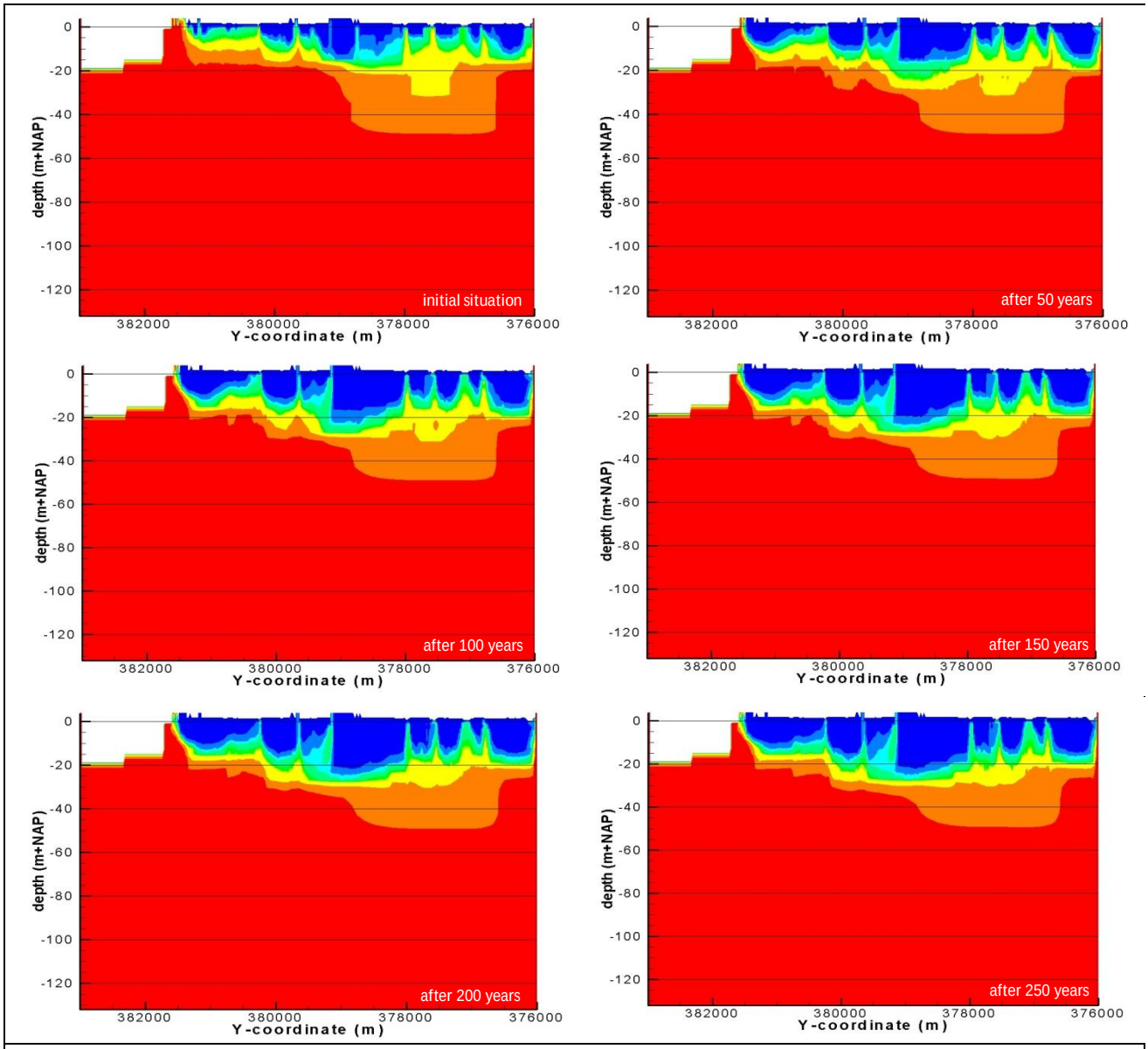

Appendix D: Calculation q_z

$$q_z = -K_z\left(\frac{\delta\phi_f}{\delta z} + \frac{\rho_i - \rho_f}{\rho_f}\right) = -K_z\left(\frac{\delta\phi_f}{\delta z} + \frac{\rho_S - \rho_f}{\rho_f} * \frac{C_i}{C_S}\right) \quad (33)$$

$$q_z(A) = -1.00E^{-4} * \left(\frac{1.335 - 1.675}{20} + \frac{1025 - 1000}{1000} * \frac{14617}{18630}\right) =$$
$$= -1.00E^{-4} * (-1.70E^{-2} + 1.96E^{-2}) =$$
$$= -1.00E^{-4} * 2.60E^{-3} =$$
$$= -2.60E^{-7} m/d$$

$$q_z(B) = -1.00E^{-4} * \left(\frac{0.8813 - 1.2780}{20} + \frac{1025 - 1000}{1000} * \frac{14199}{18630}\right) =$$
$$= -1.00E^{-4} * (-1.98E^{-2} + 1.91E^{-2}) =$$
$$= -1.00E^{-4} * 7.00E^{-4} =$$
$$= 7.00E^{-8} m/d$$

Appendix E: Effect GHB-transmissivity on horizontal velocities

Plots depicting the difference in effective pore groundwater flow velocities in the direction of the x-coordinate axis between a model run wherein a GHB-transmissivity of 2000m^2/d and the reference run wherein a GHB-transmissivity of 500m^2/d is used.

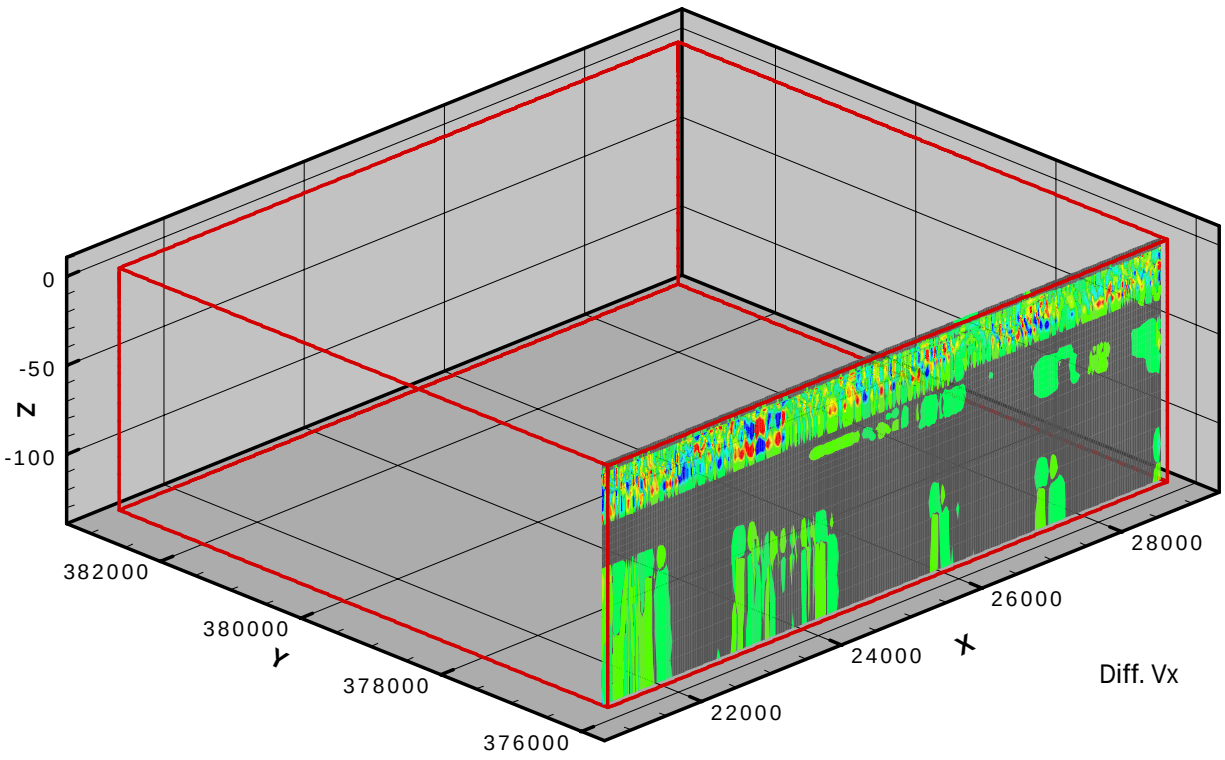

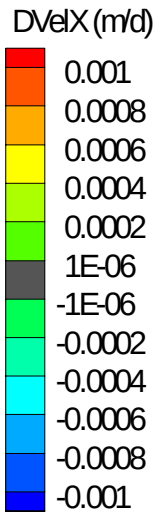

Appendix F: Probe of concentrations (river concentrations)

Concentrations per layer at point X=[27156;380511] for run WD035 (reference) and WD057 (with river concentrations 30% higher)

WD057_CONC_LAYER1.IDF	-1.000000	WD035_CONC_LAYER1.IDF	-1.000000
WD057_CONC_LAYER2.IDF	-1.000000	WD035_CONC_LAYER2.IDF	-1.000000
WD057_CONC_LAYER3.IDF	136.8000	WD035_CONC_LAYER3.IDF	101.5000
WD057_CONC_LAYER4.IDF	343.6000	WD035_CONC_LAYER4.IDF	211.7000
WD057_CONC_LAYER5.IDF	353.3000	WD035_CONC_LAYER5.IDF	252.0000
WD057_CONC_LAYER6.IDF	460.8000	WD035_CONC_LAYER6.IDF	343.8000
WD057_CONC_LAYER7.IDF	578.9000	WD035_CONC_LAYER7.IDF	436.8000
WD057_CONC_LAYER8.IDF	718.6000	WD035_CONC_LAYER8.IDF	544.5000
WD057_CONC_LAYER9.IDF	880.9000	WD035_CONC_LAYER9.IDF	668.0000
WD057_CONC_LAYER10.IDF	1082.100	WD035_CONC_LAYER10.IDF	807.1000
WD057_CONC_LAYER11.IDF	1116.700	WD035_CONC_LAYER11.IDF	846.7000
WD057_CONC_LAYER12.IDF	1157.100	WD035_CONC_LAYER12.IDF	868.6000
WD057_CONC_LAYER13.IDF	1182.600	WD035_CONC_LAYER13.IDF	883.0000
WD057_CONC_LAYER14.IDF	1179.300	WD035_CONC_LAYER14.IDF	883.9000
WD057_CONC_LAYER15.IDF	1165.700	WD035_CONC_LAYER15.IDF	869.9000
WD057_CONC_LAYER16.IDF	1124.500	WD035_CONC_LAYER16.IDF	829.0000
WD057_CONC_LAYER17.IDF	1149.300	WD035_CONC_LAYER17.IDF	910.0000
WD057_CONC_LAYER18.IDF	1175.200	WD035_CONC_LAYER18.IDF	857.8000
WD057_CONC_LAYER19.IDF	1144.500	WD035_CONC_LAYER19.IDF	821.7000
WD057_CONC_LAYER20.IDF	2741.200	WD035_CONC_LAYER20.IDF	1869.400
WD057_CONC_LAYER21.IDF	3114.800	WD035_CONC_LAYER21.IDF	2606.500
WD057_CONC_LAYER22.IDF	3783.200	WD035_CONC_LAYER22.IDF	3350.100
WD057_CONC_LAYER23.IDF	9824.700	WD035_CONC_LAYER23.IDF	10462.60
WD057_CONC_LAYER24.IDF	13221.60	WD035_CONC_LAYER24.IDF	13304.00
WD057_CONC_LAYER25.IDF	14839.80	WD035_CONC_LAYER25.IDF	14873.90
WD057_CONC_LAYER26.IDF	15059.50	WD035_CONC_LAYER26.IDF	15061.10
WD057_CONC_LAYER27.IDF	15091.50	WD035_CONC_LAYER27.IDF	15091.80
WD057_CONC_LAYER28.IDF	15092.00	WD035_CONC_LAYER28.IDF	15092.00
WD057_CONC_LAYER29.IDF	15092.00	WD035_CONC_LAYER29.IDF	15092.00
WD057_CONC_LAYER30.IDF	15092.00	WD035_CONC_LAYER30.IDF	15092.00
WD057_CONC_LAYER31.IDF	15092.00	WD035_CONC_LAYER31.IDF	15092.00
WD057_CONC_LAYER32.IDF	15092.00	WD035_CONC_LAYER32.IDF	15092.00
WD057_CONC_LAYER33.IDF	15092.00	WD035_CONC_LAYER33.IDF	15092.00
WD057_CONC_LAYER34.IDF	15092.00	WD035_CONC_LAYER34.IDF	15092.00
WD057_CONC_LAYER35.IDF	15092.00	WD035_CONC_LAYER35.IDF	15092.00
WD057_CONC_LAYER36.IDF	15092.00	WD035_CONC_LAYER36.IDF	15092.00
WD057_CONC_LAYER37.IDF	15092.00	WD035_CONC_LAYER37.IDF	15092.00
WD057_CONC_LAYER38.IDF	15092.00	WD035_CONC_LAYER38.IDF	15092.00
WD057_CONC_LAYER39.IDF	15092.00	WD035_CONC_LAYER39.IDF	15092.00
WD057_CONC_LAYER40.IDF	15092.00	WD035_CONC_LAYER40.IDF	15092.00

NB: location is below a RIV-cell, flux is downward in layers 1 to 15 and upward in all other.

Appendix G: Probe of concentrations (flow time steps)

Concentrations per layer at point X=[24111;377207] for run WD038 (one flow time step per stress period of one year), WD039 (12 flow time steps per stress period of one year) and WD035 (reference, 36 flow time steps per stress period of one year).

WD038_CONC_LAYER1.IDF	-1.000000	WD039_CONC_LAYER1.IDF	-1.000000	WD035_CONC_LAYER1.IDF	-1.000000
WD038_CONC_LAYER2.IDF	-1.000000	WD039_CONC_LAYER2.IDF	-1.000000	WD035_CONC_LAYER2.IDF	-1.000000
WD038_CONC_LAYER3.IDF	-1.000000	WD039_CONC_LAYER3.IDF	-1.000000	WD035_CONC_LAYER3.IDF	-1.000000
WD038_CONC_LAYER4.IDF	23.10000	WD039_CONC_LAYER4.IDF	21.20000	WD035_CONC_LAYER4.IDF	21.10000
WD038_CONC_LAYER5.IDF	35.00000	WD039_CONC_LAYER5.IDF	31.20000	WD035_CONC_LAYER5.IDF	28.20000
WD038_CONC_LAYER6.IDF	54.60000	WD039_CONC_LAYER6.IDF	89.50000	WD035_CONC_LAYER6.IDF	91.60000
WD038_CONC_LAYER7.IDF	602.1000	WD039_CONC_LAYER7.IDF	294.6000	WD035_CONC_LAYER7.IDF	303.3000
WD038_CONC_LAYER8.IDF	769.8000	WD039_CONC_LAYER8.IDF	334.8000	WD035_CONC_LAYER8.IDF	344.6000
WD038_CONC_LAYER9.IDF	822.6000	WD039_CONC_LAYER9.IDF	332.4000	WD035_CONC_LAYER9.IDF	350.3000
WD038_CONC_LAYER10.IDF	842.3000	WD039_CONC_LAYER10.IDF	325.6000	WD035_CONC_LAYER10.IDF	347.1000
WD038_CONC_LAYER11.IDF	862.6000	WD039_CONC_LAYER11.IDF	312.4000	WD035_CONC_LAYER11.IDF	344.5000
WD038_CONC_LAYER12.IDF	875.9000	WD039_CONC_LAYER12.IDF	288.9000	WD035_CONC_LAYER12.IDF	317.3000
WD038_CONC_LAYER13.IDF	938.0000	WD039_CONC_LAYER13.IDF	289.0000	WD035_CONC_LAYER13.IDF	334.8000
WD038_CONC_LAYER14.IDF	1064.000	WD039_CONC_LAYER14.IDF	295.0000	WD035_CONC_LAYER14.IDF	320.6000
WD038_CONC_LAYER15.IDF	1248.000	WD039_CONC_LAYER15.IDF	317.5000	WD035_CONC_LAYER15.IDF	349.4000
WD038_CONC_LAYER16.IDF	1472.700	WD039_CONC_LAYER16.IDF	353.5000	WD035_CONC_LAYER16.IDF	417.7000
WD038_CONC_LAYER17.IDF	1714.700	WD039_CONC_LAYER17.IDF	386.2000	WD035_CONC_LAYER17.IDF	411.9000
WD038_CONC_LAYER18.IDF	1831.500	WD039_CONC_LAYER18.IDF	449.0000	WD035_CONC_LAYER18.IDF	433.8000
WD038_CONC_LAYER19.IDF	2048.200	WD039_CONC_LAYER19.IDF	541.7000	WD035_CONC_LAYER19.IDF	537.2000
WD038_CONC_LAYER20.IDF	2228.700	WD039_CONC_LAYER20.IDF	662.6000	WD035_CONC_LAYER20.IDF	655.1000
WD038_CONC_LAYER21.IDF	2369.500	WD039_CONC_LAYER21.IDF	700.4000	WD035_CONC_LAYER21.IDF	673.8000
WD038_CONC_LAYER22.IDF	2722.200	WD039_CONC_LAYER22.IDF	1076.000	WD035_CONC_LAYER22.IDF	886.3000
WD038_CONC_LAYER23.IDF	3497.000	WD039_CONC_LAYER23.IDF	3289.700	WD035_CONC_LAYER23.IDF	2421.000
WD038_CONC_LAYER24.IDF	3723.900	WD039_CONC_LAYER24.IDF	3688.300	WD035_CONC_LAYER24.IDF	3395.200
WD038_CONC_LAYER25.IDF	3836.600	WD039_CONC_LAYER25.IDF	3832.200	WD035_CONC_LAYER25.IDF	3818.700
WD038_CONC_LAYER26.IDF	4201.700	WD039_CONC_LAYER26.IDF	4201.400	WD035_CONC_LAYER26.IDF	4200.700
WD038_CONC_LAYER27.IDF	6041.300	WD039_CONC_LAYER27.IDF	6041.300	WD035_CONC_LAYER27.IDF	6041.300
WD038_CONC_LAYER28.IDF	6413.100	WD039_CONC_LAYER28.IDF	6412.800	WD035_CONC_LAYER28.IDF	6413.600
WD038_CONC_LAYER29.IDF	6666.100	WD039_CONC_LAYER29.IDF	6665.700	WD035_CONC_LAYER29.IDF	6666.200
WD038_CONC_LAYER30.IDF	8167.300	WD039_CONC_LAYER30.IDF	8167.300	WD035_CONC_LAYER30.IDF	8167.200
WD038_CONC_LAYER31.IDF	12117.60	WD039_CONC_LAYER31.IDF	12117.60	WD035_CONC_LAYER31.IDF	12117.60
WD038_CONC_LAYER32.IDF	12858.60	WD039_CONC_LAYER32.IDF	12858.50	WD035_CONC_LAYER32.IDF	12858.60
WD038_CONC_LAYER33.IDF	12956.70	WD039_CONC_LAYER33.IDF	12956.60	WD035_CONC_LAYER33.IDF	12957.30
WD038_CONC_LAYER34.IDF	13617.40	WD039_CONC_LAYER34.IDF	13617.40	WD035_CONC_LAYER34.IDF	13618.80
WD038_CONC_LAYER35.IDF	13639.70	WD039_CONC_LAYER35.IDF	13639.70	WD035_CONC_LAYER35.IDF	13639.70
WD038_CONC_LAYER36.IDF	13639.70	WD039_CONC_LAYER36.IDF	13639.70	WD035_CONC_LAYER36.IDF	13639.70
WD038_CONC_LAYER37.IDF	13639.70	WD039_CONC_LAYER37.IDF	13639.70	WD035_CONC_LAYER37.IDF	13639.70
WD038_CONC_LAYER38.IDF	13639.70	WD039_CONC_LAYER38.IDF	13639.70	WD035_CONC_LAYER38.IDF	13639.70
WD038_CONC_LAYER39.IDF	13639.70	WD039_CONC_LAYER39.IDF	13639.70	WD035_CONC_LAYER39.IDF	13639.70
WD038_CONC_LAYER40.IDF	13639.70	WD039_CONC_LAYER40.IDF	13639.70	WD035_CONC_LAYER40.IDF	13639.70

Appendix H: Overview runs

Run	Sens. analysis	nsps	nfts/sp	part.	Tr. GHBs (m2/d)	c sea floor (d)	c riv bed (d)	Conc. (mgCl-/l)	Disp. (l/t)	CFL-factor	RCH (mm/y)	Poro.	Discr (m2)	Runtime
wD001 to wD034	Exploratory runs													
wD035	Reference run	300	36	4	500/0	208	2	946	0,05/0,005	4	186	0,3	25*25	26h19min
wD035b	Discr. drainage system	300	36	4	500/0	208	2	946	0,05/0,005	4	186	0,3	100*100	25h14min
wD036	CFL-factor	100	36	4	500/0	208	2	946	0,05/0,005	2	186	0,3	25*25	29h3min
wD037	CFL-factor	100	36	4	500/0	208	2	946	0,05/0,005	0,8	186	0,3	25*25	42h16min
wD038	Flow time steps	100	1	4	500/0	208	2	946	0,05/0,005	4	186	0,3	25*25	13h43min
wD039	Flow time steps	100	12	4	500/0	208	2	946	0,05/0,005	4	186	0,3	25*25	16h02min
wD040	Flow time steps	100	73	4	500/0	208	2	946	0,05/0,005	4	186	0,3	25*25	37h55min
wD041	Advection particles	100	36	1	500/0	208	2	946	0,05/0,005	4	186	0,3	25*25	29h24min
wD042	Advection particles	100	36	8	500/0	208	2	946	0,05/0,005	4	186	0,3	25*25	32h16min
wD043	Advection particles	100	36	27	500/0	208	2	946	0,05/0,005	4	186	0,3	25*25	85h52min
wD044	Inversions	500	1	4	500/0	208	2	946	0,05/0,005	4	186	0,3	25*25	106h52min
wD045	GHB-transmissivity	100	36	4	2000/0	208	2	946	0,05/0,005	4	186	0,3	25*25	38h06min
wD046	GHB-transmissivity	100	36	4	100/0	208	2	946	0,05/0,005	4	186	0,3	25*25	22h17min
wD047	GHB-transmissivity	100	36	4	0/0	208	2	946	0,05/0,005	4	186	0,3	25*25	22h23min
wD048	Groundwater recharge	100	36	4	500/0	208	2	946	0,05/0,005	4	140	0,3	25*25	26h26min
wD049	Groundwater recharge	100	36	4	500/0	208	2	946	0,05/0,005	4	233	0,3	25*25	26h09min
wD050	Groundwater recharge	100	36	4	500/0	208	2	946	0,05/0,005	4	167	0,3	25*25	26h04min
wD051	Groundwater recharge	100	36	4	500/0	208	2	946	0,05/0,005	4	205	0,3	25*25	23h39min
wD052	Sea floor resistance	100	36	4	500/0	1,25	2	946	0,05/0,005	4	186	0,3	25*25	38h24min
wD053	Sea floor resistance	100	36	4	500/0	12,5	2	946	0,05/0,005	4	186	0,3	25*25	27h17min
wD054	River bed resistance	100	36	4	500/0	208	0,5	946	0,05/0,005	4	186	0,3	25*25	33h50min
wD055	River bed resistance	100	36	4	500/0	208	4	946	0,05/0,005	4	186	0,3	25*25	24h08min
wD056	Concentration rivers	100	36	4	500/0	208	2	662,2	0,05/0,005	4	186	0,3	25*25	24h52min
wD057	Concentration rivers	100	36	4	500/0	208	2	1261,3	0,05/0,005	4	186	0,3	25*25	24h51min
wD058	Dispersion	100	36	4	500/0	208	2	946	0,5/0,05	4	186	0,3	25*25	40h47min
wD059	Dispersion	100	36	4	500/0	208	2	946	0,005/0,0005	4	186	0,3	25*25	24h58min
wD060	Porosity	100	36	4	500/0	208	2	946	0,05/0,005	4	186	0,2	25*25	33h36min
wD061	Porosity	100	36	4	500/0	208	2	946	0,05/0,005	4	186	0,4	25*25	24h21min
wD062	Porosity	100	36	4	500/0	208	2	946	0,05/0,005	4	186	0,5	25*25	21h22min

REFERENCES

Badon Ghijben, W. and J. Drabbe (1889). "Nota in verband met de voorgenomen putboring nabij Amsterdam." Tijdschrift voor het Koninklijk Instituut voor Ingenieurs **8**(22): 8-22.

Bear, J. (1979). Hydraulics of groundwater. New York, McGraw-Hill.

Bear, J. and A. Verruijt (1987). Modeling groundwater flow and pollution. Dordrecht, The Netherlands, D. Reidel.

Berendsen, H. J. A. (2005). Fysische geografie van Nederland, deel 4: Landschappelijk Nederland. De fysisch-geografische regio's. Assen, The Netherlands, Van Gorcum.

Bot, B. (2011). Grondwaterzakboekje. Rotterdam, Bot Raadgevend Ingenieur.

Buma, J. (2010). Plan Waterdunen: nulmeting grondwater. Deltares conceptrapport. Utrecht, Deltares.

Chilakapati, A. (1998). "A characteristic-conservative model for Darcian advection." Advances in Water Resources **22**(6): 597-609.

Chow, V. T. (1964). Handbook of Applied Hydrology. New York, N.Y., McGraw-Hill.

Clement, T. P. (2011). "Complexities in hindcasting models - when should we say enough is enough?" Groundwater **49**(5): 620-629.

CMA (N.D.). Geleidbaarheidssensor 0382 - Gebruikershandleiding, Centrum voor Microcomputer Applicaties.

Cobaner, M., R. Yurtal, et al. (2012). "Three dimensional simulation of seawater intrusion in coastal aquifers." Journal of Hydrology(464-465): 262-280.

Connors, D. N. and D. R. Kester (1974). "Effect of major ion variations in the marine environment on the specific gravity-conductivity-chlorinity-salinity relationship." Marine Chemistry(2): 301-314.

Courtens, C., A. Vandenbohede, et al. (2011). SCALDWIN: Analyse van de grensoverschrijdende verzilting van het grondwater in Oos-, West- en Zeeuws Vlaanderen. Utrecht, Deltares, Universiteit Gent.

Dam, J. C. (1996). Salt water intrusion: analysis, research needs and opportunities. 14th Salt Water Intrusion Meeting (SWIM96) - Rapporter och meddelanden. Sweden, Malmö, SGU - Geological Survey of Sweden.

Diersch, H.-J. G. (2005). FEFLOW: Fintie element subsurface flow and transport simulation system. . Berlin, Germany, WASY GmbH Institute for Water Resources Planning and Systems Research.

Diersch, H.-J. G., D. Prochnow, et al. (1984). "Finite-element analysis of dispersion-affected saltwater upconing below a pumping well." Applied Mathematical Modelling(8): 305-3012.

Eeman, S. d., A. Leijnse, et al. (2011). "Analysis of the thickness of a freshwater lens and of the transition zone between this lens and upwelling saline water." Adv. Water Resour.(34): 191-302.

Frolkovic, P. (2001). "Flux-based method of characteristics for contaminant transport in flowing groundwater." Computing and Visualization in Science(5): 73-83.

Gelhar, L. W., C. Welty, et al. (1992). "A critical review of data on field-scale dispersion in aquifers." Water Resources Research **28**(7): 1955-1974.

Genuchten, M. T. v. and P. J. Wieringa (1986). Solute dispersion coefficients and retardation factors. Methods of soil analysis, Part 1. Physical and mineralogical methods. Madison, US, American Society of Agronomy - Soil Science Society of America.

Geodan (2012). Actueel Hoogtebestand Nederland, Het Waterschapshuis.

Google (2013). "Google Maps." Retrieved 19-08-2013, 2013.

Grift, B. v. d. and J. Griffioen (2008). "Modelling assessment of regional groundwater contamination due to historic smelter emissions of heavy metals." Journal of Contaminant Hydrology(96): 48-68.

Guo, W. and C. D. Langevin (2002). User's guide to SEAWAT: a computer program for simulation of three-dimensional variable-density ground-water flow. US, US Geological Survey Open-File Report 01-434.

Harbaugh, A. W., E. R. Banta, et al. (2000). MODFLOW-2000, The U.S. geological survey modular ground-water model - user guide to modularization concepts and the ground-water flow process. Reston,. Virginia, U.S. Geological Survey.

Herzberg, A. (1901). "Die Wasserversorgung einiger Nordseebaden." Zeitung fur Gasbeleuchtung und Wasserversorgung(44): 815-819 & 842-844.

Holzbecher, E. (1998). Modelling density-driven flow in porous media. Berlin, Germany, Springer-Verlag.

Hoogvliet, M., G. H. P. Oude Essink, et al. (2008). Koploper Klimaat Werkpakket Watervoorziening. Utrecht, Deltares**:** 59.

HydroGeoLogic Inc (2002). MODHMS - modflow-based hydrogeological modeling system: documentation and user's guide. Herndon, Virginia.

Instituto Geologico y Minero de Espana (2004). Groundwater and saline intrusion. SWIM, Cartagena, Instituto Geológico y Minero de Espana.

Jakovovic, D., A. D. Werner, et al. (2011). "Numerical modelling of saltwater upconing: Comparison with experimental laboratory observations." Journal of Hydrology(402): 261-273.

Janssen, G. M. C. M. and G. H. P. Oude Essink (2012). SCALDWIN: Analyse grensoverschrijdende verzilting grondwater in het podergebied van de provincies Oost-Vlaanderen, West-Vlaanderen en Zeeland. Fase 2, Deelopdracht 4: Detailmodellering Waterdunen. Deltares conceptrapport. Utrecht, Deltares.

Jousma, G. and H. T. L. Massop (1996). Intreeweerstanden waterlopen. inventarisatie en analyse. Delft, TNO.

Konikow, L. F. (2011). "The secret to successful solute-transport." GroundWater **49**(2): 144-159.

Konikow, L. F. and J. D. Bredehoeft (1978). Chapter 2. Computer model of two-dimensional solute transport and dispersion in groundwater: U. S. Geological Survey Techniques of Water-Resources Investigations, USGS.

Konikow, L. F., D. J. Goode, et al. (1996). A three-dimensional method-of-characteristics solute-transport model (MOC3D) - U.S. Geological Survey Water-Resources Investigations Report. US**:** 96.

Langevin, C. D. and W. Guo (2006). "MODFLOW/MT3DMS-based simulation of variable-density ground water flow and transport." Groundwater **44**(3): 339-351.

Langevin, C. D., W. B. Shoemaker, et al. (2003). MODFLOW-2000, The US Geological survey Modular Groundwater Model-Documentation of the SEAWAT-2000 Version with the Variable-Density Flow Process (VDF) and the Integrated MT3DMS Transport Process (IMT), US Geological Survey.

Langevin, C. D., E. Swain, et al. (2005). "Simulation of integrated surface-water/ground-water flow and slinity for a coastal wetland and adjacent estuary." Journal of Hydrology(314): 212-234.

Leake, S. A. and D. V. Claar (1999). Procedures and computer programs for telescopic mesh refinement using MODFLOW. Tucson, Arizona, U.S, U.S. Geological Survey.

Lebbe, L. C. (1999). "Parameter identification in fresh-saltwater flow based on borehole resistivities and freshwater head data." Adv. Water Resour. **22**(8): 791-806.

Louw, P. G. B. d., S. d. Eeman, et al. (2011). "Shallow rainwater lenses in deltaic areas with saline seepage." Hydrol. Earth Syst. Sci. Discuss.(15): 3659-3678.

Lusczynski, N. J. (1961). "Head and flow of ground-water of veraible density." Journal of Geophysical Research(66): 4247-4256.

Massop, H. T. L. (2002). Landelijke karakterisering buisdrainage.

Massop, H. T. L. and J. W. J. v. d. Gaast (2006). Intreeweerstand, nader beschouwd. Wageningen, Alterra.

McDonald, M. G. and A. W. Harbaugh (1988). A modular three-dimensional finite-difference ground-water flow model, U.S. Geol. Surv. Tech. Water Resour Invest.

Meinardi, C. R. (1983). "Fresh and brackish ground-water under coastal areas and islands." GeoJournal **7**(5): 413-425.

Morway, E. D., R. G. Niswonger, et al. (2012). "Modeling Variable Solute Subsurface Solute with MODFLOW-UZF and MT3DMS." Groundwater **51**(2): 237-251.

Oreskes, N. (1994). "Verification, validation, and confirmation of numerical models in the Earth Sciences." Science **263**(5147): 641-646.

Oreskes, N. and K. Belitz (2001). Philosophical issues in model assessment. Model validation: perspectives in hydrological science. M. G. Anderson and P. D. Bates. US, John Wiley & Sons, Ltd.

Oude Essink, G. H. P. (1996a). Impact of sea level rise on Dutch groundwater regimes. 14th Salt Water Intrusion Meeting (SWIM96) - Rapporter och meddelanden. Sweden, Malmö, SGU - Geological Survey of Sweden.

Oude Essink, G. H. P. (1996b). MOC3D adapted to simulate 3D density-dependent groundwater flow. MODFLOW'98 Conference. Golden, Colorado, USA**:** 291-303.

Oude Essink, G. H. P. (1996c). Impact of sea level rise on groundwater flow regimes - a sensitivity analysis for The Netherlands. Delft Studies in Integrated Water Management. Delft, Delft University of Technology. **PhD**.

Oude Essink, G. H. P. (2001a). Density dependent groundwater flow. Salt water intrusion and heat transport. Utrecht, Utrecht University.

Oude Essink, G. H. P. (2001b). "Salt water intrusion in a three-dimensional groundwater system in the Netherlands: A numerical study." Transp. Porous Media **43**(1): 137-158.

Oude Essink, G. H. P., E. S. v. Baaren, et al. (2008). Beschouwing van de effecten van een zout Volkerak-Zoommeer op het grondwatersysteem. Utrecht, TNO**:** 83.

Oude Essink, G. H. P. and R. H. Boekelman (1996). Problems with large-scale modeling of salt water intrusion. 14th Salt Water Intrusion Meeting (SWIM96) - Rapporter och meddelanden. Sweden, Malmö, SGU - Geological Survey of Sweden.

Oude Essink, G. H. P., E. S. Van Baaren, et al. (2010). "Effects of climate change on coastal groundwater systems. A modelling study in teh Netherlands. ." Water Resources Research(46).

Oude Essink, G. H. P. and J. Verkaik (2010). NHI zoet-zout: grondwater in het Nederlandse kustgebied. Utrecht, Deltares**:** 9.

Pauw, P. (2011). Overview of common field measurements applicable in the research on freshwater lenses in coastal areas. Utrecht/Wageningen, Deltares - Wageningen UR.

Pauw, P., P. G. B. d. Louw, et al. (2012). "Groundwater salinization in the Wadden Sea area of The Netherlands; quantifying the effects of climate change, sea level rise and anthropogenic interferences." Journal of Geosciences **91**(3): 373-383.

Post, V. E. A. (2004). Groundwater salinization processes in the coastal area of The Netherlands due to trangressions during the Holocene. Amsterdam, Free University of Amsterdam. **Ph.D.**

Project Waterdunen (2013). "Project Waterdunen." Retrieved 14-08-2013, 2013.

Reilly, T. E. and A. S. Goodman (1985). "Quantitative analysis of saltwater - freshwater relationships in groundwater systems. A historical perspective." Journal of Hydrology(80): 125-160.

Scheidegger, A. E. (1958). "The physics of flow through porous media." Soil Science **86**(6).

Sommeijer, M. (2013). Identfying suitable measures to enlarge fresh groundwater reserves on a regional scale. Utrecht - Wageningen, Deltares/ WUR.

Stuyfzand, P. J. (1993). PhD Thesis Hydrochemistry and hydrology of the coastal dune area of the Western Netherlands. Amsterdam, Vrije Universiteit Amsterdam**:** 366.

TNO-DINOloket (2008). "REGIS II - model." Retrieved January - August 2013.

U.S. Geological Survey (2013). "Online Guide to MODFLOW." Retrieved 18-08-2013, 2013.

Van Baaren, E. S., G. H. P. Oude Essink, et al. (2011). Verzoeting verzilting grondwater in de Provincie Zeeland, Rapportage 3D regionaal zoet-zout grondwater model. Deltares conceptrapport. Utrecht, Deltares.

Van Meir, N. and L. C. Lebbe (2003). "Deriving TDS values in coarse sediments from long normal and electric logs." Groundwater **41**(1): 33-40.

Vandenbohede, A. (2004). Solute transport in heterogeneous aquifers - parameter indication and its use in groundwater pollution and salt water intrusion problems. Geology and Soil Sciences. Gent, Gent University. **Ph.D.**

Vandenbohede, A. (2008). Visual MOCDENS3D - Visualisation and processing software for MOCDENS3D, a 3D density dependent groundwater flow and solute model. Ghent, Ghent University - Research unit groundwater modelling.

Vandenbohede, A., E. v. Houtte, et al. (2009). "Sustainable groundwater extraction in coastal areas: A Belgian example." Environ. Geol.(57): 735-747.

Verruijt, A. (1980). "The rotation of a vertical interface in aporous medium." Water Resources Research **16**(1): 239-240.

Voss, C. I. and A. M. Provost (2008). SUTRA, a model for saturated-unsaturated variable-density groundwater flow with solute or energy trasnport. Reston, Viriginia, US Geological Survey.

Wetterskyp Fryslân (2005). Bodemdaling Barradeel II Inrichtingsplan. Utrecht, Arcadis & TNO.